CENTRAL SCOTIAN SLOPE STABILITY: THE POSSIBLE ROLE OF GAS HYDRATES

Christopher Robert LeBlanc

Submitted in Partial Fulfilment of the Requirements
for the Degree of Bachelor of Science, Honours
Department of Earth Sciences
Dalhousie University, Halifax, Nova Scotia
April 30, 2002

Dalhousie University

Department of Earth Sciences
Halifax, Nova Scotia
Canada B3H 3J5
(902) 494-2358
FAX (902) 494-6889

DATE April 29, 2002

AUTHOR Christopher Robert LeBlanc

TITLE "Central Scotian Slope Stability: the possible role of gas hydrates"

Degree B.Sc. Convocation May Year 2002

Permission is herewith granted to Dalhousie University to circulate and to have copied for non-commercial purposes, at its discretion, the above title upon the request of individuals or institutions.

Chris LBlanc
Signature of Author

Abstract

Gas hydrates are ice−like solids in which large quantities of methane are trapped in a solid phase as a result of suitable pressure and temperature conditions in the presence of an excess supply of methane gas. They are a potential fuel source, possible greenhouse gas contributor, and a geohazard concern due to their potential effect on slope stability. Gas hydrates may cause sediment failures by releasing methane gas and water when they dissociate (melt), causing *in situ* sediment pore pressures to increase. The purpose of this study is to search for the presence of gas hydrate in an area of known sediment instability on the continental slope east of Nova Scotia (Verrill Canyon area), using a geophysical approach. This area displays several sediment failures, between 15 and 12 ka. Geotechnical infinite slope stability analysis has shown that the area is inherently statically stable and that excess pore pressures were necessary to effect failure. Increased pore pressure probably resulted from one or more of: ground accelerations due to earthquakes or isostatic readjustments following glaciation, shallow gas charging, dissociation of gas hydrates, or rapid sedimentation during glaciation and deglaciation. Dissociation of gas hydrate is one of the proposed potential mechanisms. A drop in sea level or increase in bottom water temperatures as during glaciation / deglaciation may cause dissociation of gas hydrate, which would free methane and water; causing an increase in pore pressure. The presence of failures and pockmarks near the theoretical minimum stable depth (500 metres below sea level) suggest the presence of gas hydrate. Hydrates in some locations can be detected on seismic reflection profiles by the presence of a bottom simulating reflector, which probably corresponds to the acoustic impedance contrast at the transition between gas hydrate and free gas. Gas hydrate can also be detected by using wide−angle seismics (such as an ocean bottom seismometer, or OBS) to detect an unusually high velocity within the hydrate stability zone, or velocity inversion below the hydrate stability zone. Examination of 14 high resolution single channel seismic reflection lines in the study area has not revealed any BSRs. An OBS was deployed where gas hydrates are most likely to be present (850 metres below sea level). A velocity model was produced from the OBS data, that displays anomalously high velocities coincident with the theoretical gas hydrate stability zone. It is therefore proposed that gas hydrate is possibly present in the sediment, but there is no indication of an underlying free gas zone (because there is no evidence of anomalously low velocities). This implies that the sediment failures near 500 metres below sea level may have possibly been induced by increased pore pressure, at least partially resulting from the dissociation of gas hydrate.

Table of Contents

Chapter 1: Introduction....1

1.1 Relationship Between Slope Stability and Gas Hydrates....1

1.2 Thesis objectives....2

1.3 Location of Study....4

1.4 Glacial History....6

Chapter 2: Sediment Stability....12

2.1 Classification of Sediment Failures....12

2.2 Factors influencing slope stability....14

2.3 Triggers....21

Chapter 3: Methane Gas hydrates....23

3.1 Global Importance....23

3.1.1 Definition and distribution of hydrates....23

3.1.2 Greenhouse gas potential....25

3.1.3 Potential fuel resource....26

3.2 Hydrate Properties....27

3.2.1 Chemical Composition, Clathrate Lattice....27

3.2.2 Hydrate Stability....27

3.2.3 Physical Properties....29

3.2.4 Acoustic Properties....31

3.2.5 Formation Styles and Mechanisms....32

Chapter 4: Data Acquisition and Analytical Methods....36

4.1 Wide−Angle Equipment Used Onboard Cruise HUD2001−028....36

4.1.1 Wide−Angle Seismic Data Analysis Procedure.....39
4.2 Towed Array Equipment Used on Cruise HUD2001−048A.....44
4.2.1 Single Channel Seismic Data Analysis Procedure.....45
Chapter 5: Results.....47
5.1 Gas Hydrate Stability Model.....47
5.2 Multibeam Bathymetry.....50
5.3 Single Channel Reflection Seismic Data.....52
5.4 Wide−Angle Velocity Modelling.....56
5.4.1 Velocity Structure.....63
Chapter 6: Discussion.....67
Chapter 7: Conclusions and future work.....73
7.1 Conclusion.....73
7.2 Future work.....73

Table of Figures

Figure 1.1: Location map.....5

Figure 1.2: Diagram of the evolution of the Wisconsinian glacier.....7

Figure 1.3: Diagram illustrating the ice advance and retreat pattern.....10

Figure 2.1: Map of failures in the study area.....13

Figure 2.2: Example of a slump.....14

Figure 2.3: Summary of forces involved in infinite slope analysis.....15

Figure 3.1: Global distribution of known and inferred gas hydrates.....23

Figure 3.2: Map of gas hydrate thickness for the Atlantic region.....24

Figure 3.3: Empirical pressure temperature plot of gas hydrates seen in nature.....28

Figure 3.4: Illustration of the formation mechanism described by Paull et al.....33

Figure 4.1: An OBS ready for deployment on the deck of CCGS Hudson.....37

Figure 4.2: Detailed map of single channel reflection lines.....38

Figure 4.3: Seismic section of wide−angle data, channel.....39

Figure 4.4: Frequency spectrum of OBS channel 2 data.....43

Figure 5.1: Phase diagram for the OBS location.....49

Figure 5.2: Multibeam bathymetry image of the study area.....50

Figure 5.3: Map of Verrill Canyon area.....52

Figure 5.4: Single channel reflection line 29.....55

Figure 5.5: Seismic section and minimum velocity model.....57

Figure 5.6: Seismic section and maximum velocity model.....58

Figure 5.7: 2 layer refraction velocity model.....60

Figure 5.8: Horizon (reflection) velocity model.....62

Figure 5.9: Regional velocity depth plot.....64

Figure 5.10: Local velocity depth plot.....64

Figure 5.11: Plot of sediment velocity versus hydrate percentage of pore space.....66

Figure 6.1: Local velocity plot.....69

Table of Tables

Table 1.1: Horizon information.....11

Table 3.1: Gas hydrate properties.....30

Table 5.1: Horizon velocity and depth summary.....63

Acknowledgements

I would like to extend great thanks to Dr. Keith Louden for giving me the chance to do a very interesting thesis and supporting me with excellent resources and feedback. I would also like to thank Dr. David Mosher for his guidance, and motivation in helping me create a quality report. Dr. David Piper is a pioneer in the field of hydrate research and slope stability on the eastern continental margin of Canada, and without him this thesis would be impossible. Thanks to everyone at the Bedford Institute of Oceanography, and the scientific staff and crew of the CCGS Hudson during cruise 2001−028. I would also like to thank everyone at Dalhousie that has helped me: Dr. Marcos Zentilli, Simon Newton, and the entire Earth Science department, aswell as Dr. Thomas Funck and Helen Lau in the Dalhousie Oceanography Seismic Group. Many thanks to C&C technologies for sharing the multibeam bathymetry data, and BP Canada for a generous scholarship.

CHAPTER 1: INTRODUCTION

1.1 Relationship Between Slope Stability and Gas Hydrates

Slope stability is an important consideration for the safe operation of the oil and gas industry on the Scotian margin. It is believed that the sediments on the Scotian slope are statically stable, unless they occur on steep gradients or have high pore pressure (Mosher et al., 1994). High pore pressure may be the result of many causes, including migration of shallow petrogenic gas, residual pore pressure in rapidly deposited glacial sediments, dissociation of gas hydrates, and earthquake ground accelerations, to name a few.

Methane gas near saturation will form an ice like solid, under pressure – temperature conditions that exist below approximately 500 metres below sea level in the study area (described in section 1.3). This compound is known as a "methane gas hydrate". Sloan (1998) states that "Each volume of hydrate can contain 184 volumes of gas (at standard temperature and pressure)". The stability of methane gas hydrates has a strong influence on pore pressure and thus the stability of the sediments in which it forms.

Gas hydrates are also important to other topics such as global warming and as a potential fuel resource. The relationship between slope stability and the possible existence of gas hydrates is the focus of this paper. The presence of gas hydrates on the Scotian slope has not been proven, but the geologic setting; including the presence of hydrocarbon reserves, is ideal. This hypothesis is further supported by circumstantial evidence, such as pockmarks, BSRs (bottom simulating reflectors), and head scarp locations (Piper, 2001).

Methane gas hydrates occur in permafrost and oceanic regions. Oceanic gas hydrates can form in sediments that are in waters deeper than approximately 300 m (relatively high temperature, high pressure). Permafrost gas hydrates form near the surface in cold permafrost regions, the shallowest currently discovered are stable at 150 metres below the sediment surface (low temperature, low pressure) (Kvenvolden, 2000). Permafrost hydrates exist under very different pressure–temperature conditions than oceanic hydrates do, and therefore will not be discussed in this paper.

Gas hydrates may also be a major fuel source. The most common estimates for the volume of the world's gas hydrate resource indicate the volume of methane is approximately twice the equivalent volume of all other fossil fuel resources (including coal). However, there is a large variation between estimates, by as much as 3 orders of magnitude, because there is a great deal of speculation about the distribution and concentration of gas hydrates (Sloan, 1998).

1.2 Thesis objectives

There is indirect evidence of possible gas hydrate occurrences in the study area (defined in section 1.3), from the following data: Sidescan sonar imagery shows abundant pock marks at 700 to 1100 mbsl (Piper, 2001). A BSR (bottom simulating reflector, believed to represent the large negative reflection coefficient that can be seen at a sharp interface between gas hydrate and the underlying sediment, which "simulates" the shape of the seafloor) has been found within approximately 90 km of the study area (D. Piper and D. Mosher, personal communication, 2001). Sediment failures appear to occur at depths that approximately coincide with the minimum stable depth of gas hydrate (Piper, 2001; Mosher et al., 2002).

The primary purpose of this study is to examine the study area for the possible presence of gas hydrate, and its possible link to slope stability. If there is a link between the two, it should be possible to support the existence of gas hydrates by indirect methods. It is unlikely that the existence of gas hydrate will be *proven* in the study area without drilling, due to the difficulty in detection of low concentrations of gas hydrate by seismic methods. However, the results of this study should indicate whether or not gas hydrates are present.

Multibeam bathymetry will be used to locate head scarps, and evidence of any other features that may indicate the presence of gas hydrate. The depth of these features will be compared to the theoretical gas hydrate stability zone (GHSZ) to determine if the headscarps are possibly hydrate related. It has been documented in other regions, such as the US Atlantic continental margin, that the locations of head scarps for slumps and debris flows match the intersection of the GHSZ with the sea floor (Booth et al., 1994; Dillon and Max, 2000). Failures occurring near this region may have been caused primarily by gas hydrate dissociation, therefore this study will focus on these features.

Sediment which has failed on "decollement surfaces" may be related to overpressures caused by gas hydrate dissociation. Comparing the depth to these failure horizons, with a theoretical model for the base of gas hydrate stability may indicate if the failure could have been related to gas hydrates. This will be analysed with single channel seismic reflection data collected on the CCGS Hudson cruise 2001−048A. Regions of high gas hydrate concentration have been discovered by the presence of a BSR, but previous seismic studies of the study area have not revealed any BSRs.

High resolution wide−angle seismic data collected aboard CCGS Hudson cruise

2001−028 will be analysed to develop a velocity vs. depth model. Any anomalously high velocities or velocity gradients in the shallow sediment should be apparent from these data, and may indicate the presence of gas hydrate, which typically has a much higher velocity than hydrate−free sediment. A high velocity gradient in the hydrate stability zone that is underlain by a relatively normal velocity gradient would be a strong indicator for gas hydrates (Sloan, 1998; Lee et al., 1993B). The depths to any velocity anomalies can be compared with the theoretical hydrate stability model to determine if gas hydrate would be stable at the depth observed. The velocity profile of the sediment will also be compared with a regional gradient, obtained from sonic logs in deep−water wells, to determine the difference between the regional velocity gradient and any anomalies.

1.3 Location of Study

The Central Scotian Slope is part of the passive continental margin off the coast of Nova Scotia (Figure 1.1). The shelf break occurs at 100 − 120 metres below sea level (mbsl), and the slope extends from this depth to the continental rise at 2000−2500 mbsl, with a mean gradient of 3° (from the shelf break to 1000 metres depth) (Piper, 2001). The morphology of the area is mainly smooth, caused by progradation of sediment during the Pliocene and Quaternary (Gauley, 2001). The area was a major depocenter during the Pliocene (Piper, 2001). Glacial till is dominant in the shallow sediment on the shelf, but has a lateral facies change from till to silt to clay, in water depths greater than 500 mbsl (Gauley, 2001).

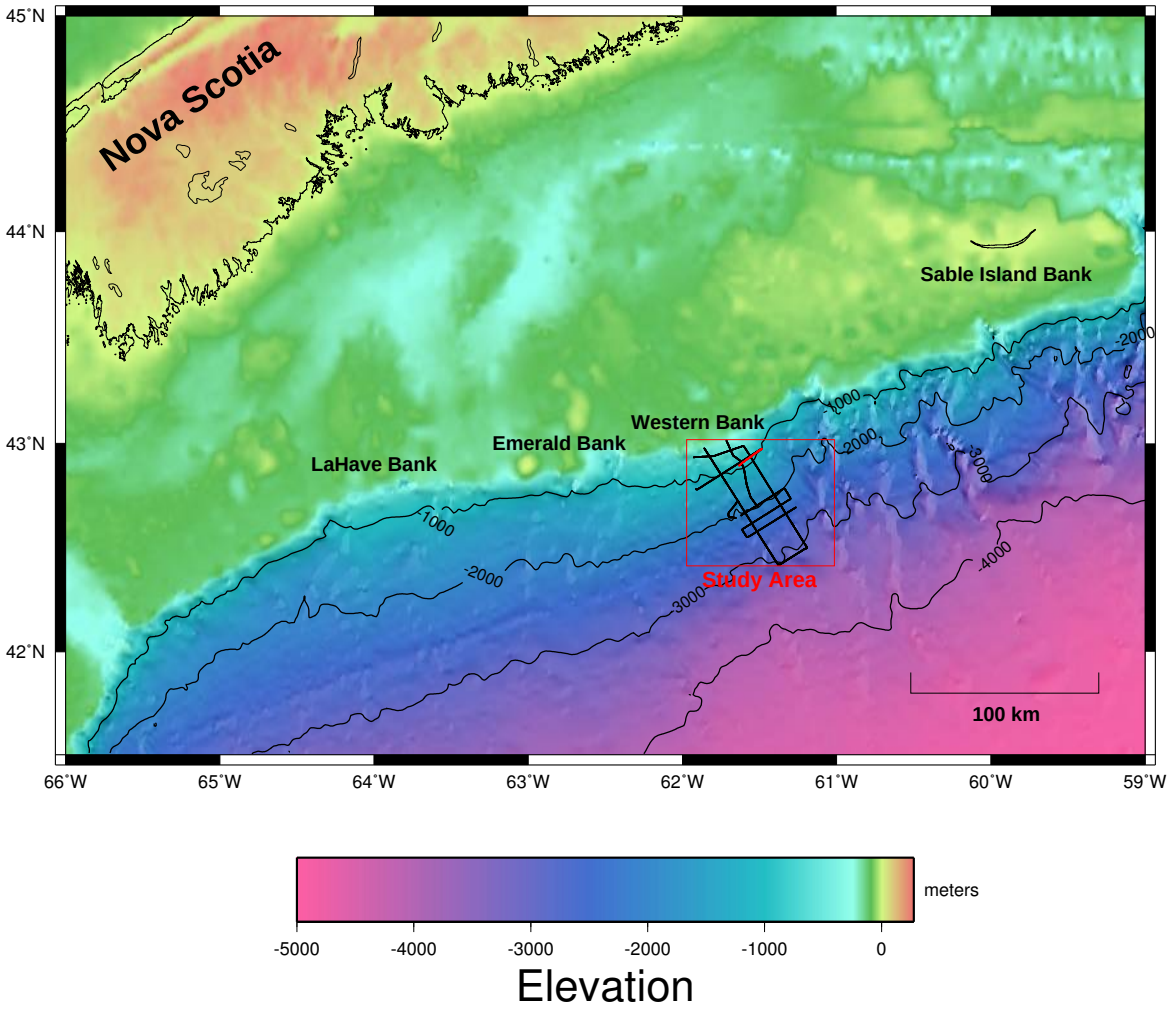

Figure 1.1: Location map, illustrating the location study area (red box), single channel reflection lines (thick black lines), and OBS line (thick red line).

The upper slope has "relict iceberg furrows", and shallow gullies (20 m deep, by 500 m wide) that extend to a depth of 600 mbsl (Piper, 2001). There are large rotational slumps on the upper slope that head at depths of 500–600 mbsl, which are the likely sources for turbidites on the continental rise (Piper, 2001). These features are important to this paper because they occur at sufficient depth to be gas hydrate related, and the failures seem to show similar character to each other.

There is evidence of pockmarks in water depths of mainly 500 – 1100 mbsl,

though they are present to depths as great as 2200 mbsl. The zone deeper than approximately 500 mbsl is the range in which hydrates are theoretically stable (Piper, 2001). There is no upper pressure limit on hydrate stability, but hydrates are less common on the continental rise and abyssal plains due to a lack of methane available in the shallow sediment (Max, 2000).

Piper notes that the relationship of pockmarks to deeper structures is not known (Piper, 2001). Most of the pockmarks in the study area are 10 to 30 metres in diameter, and are thought to represent gas escape features. There are also large scale pockmark features, that are approximately 10 metres in depth, and an order of magnitude larger than the pockmarks mentioned previously. These may represent fluid escape collapse structures (Mosher et al., 2002). There is too little data to propose a link between pockmarks and gas hydrates at this time.

1.4 Glacial History

The oldest strata discussed in this paper is Pliocene, as the reflection data does not penetrate much deeper than this age of sediment. The Pliocene strata has many shallow channels, and as mentioned before, the area is believed to have been an important Pliocene depocenter (Piper, 2001). The base of the Quaternary strata is heavily gullied, while the lower and middle Quaternary appear to be draped muddy sediment (Piper, 2001).

The recent geological history of the study area is dominated by glacial influence (75 ka to 12.5 ka). The Wisconsinian glaciation lasted from approximately 75 k.y.a to 10.8 ka (Stea et al., 1998). The Wisconsinian glaciation had five phases, the Caledonian, Mid−Wisconsinian, Escuminac, Scotian, and Chignecto, identified on the basis of glacial

flour events, and are summarised in Figure 1.2. The Collins Pond phase lasted from 12.5 ka to 10.8 ka, but is restricted to inland locations that would not likely have affected sedimentation of the Western Bank (Stea et al., 1998).

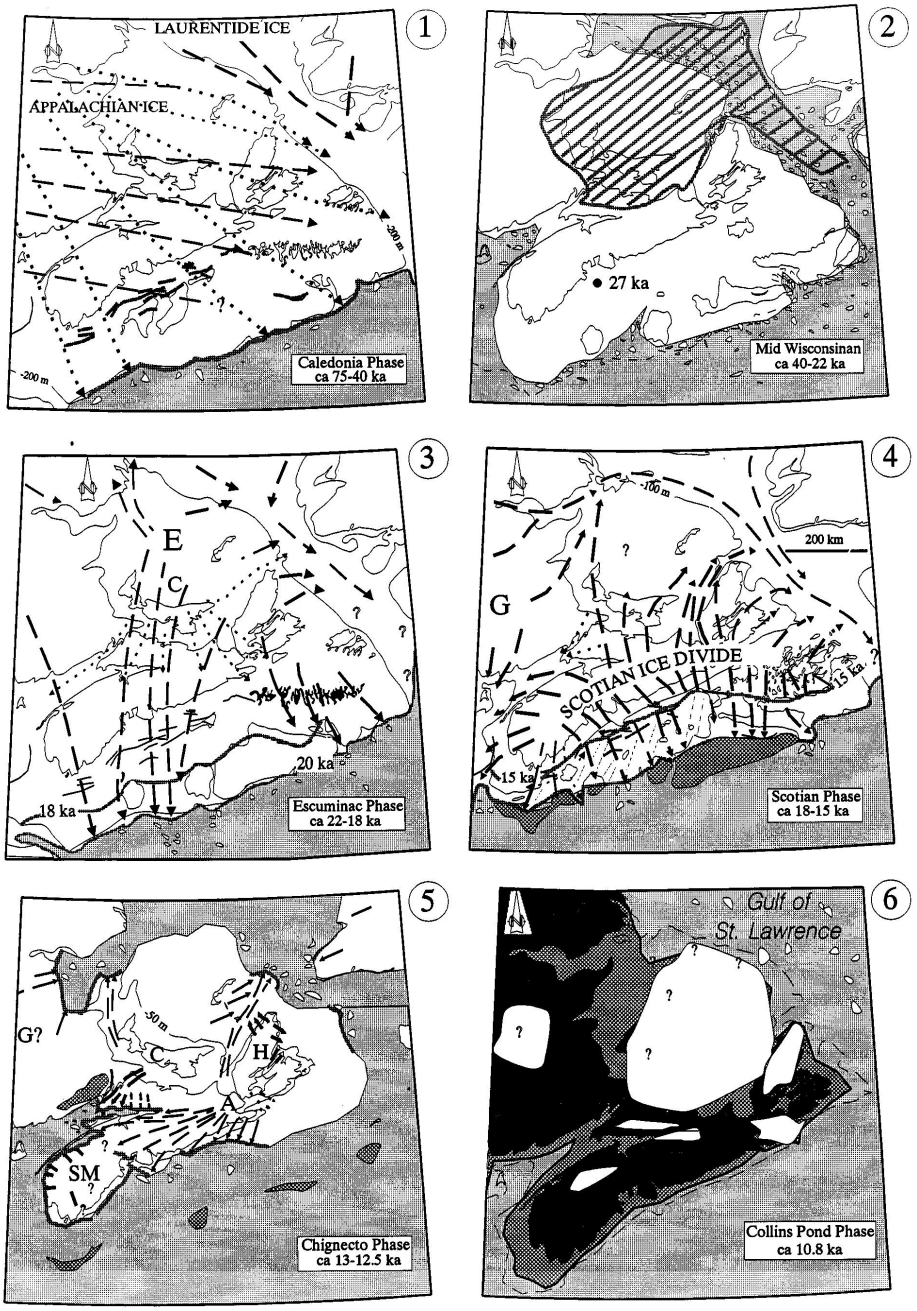

Figure 1.2: Diagram of the evolution of the Wisconsinian glacier from 75 ka to 10.8 ka. White = ice, dotted = ocean, cross hatch = emergent land, diagonal lines = possible ice shelf. Phase (1) Caledonian, (2) Mid–Wisconsinian, (3) Escuminac, (4) Scotian, (5) Chignecto, (6) Collins Pond (or Younger Dryas readvance) (after Stea et al, 1998).

The Caledonian phase occurred from the early to middle Wisconsinian time. An ice sheet originating from an upland Appalachian source extended to the shelf edge. This created diamicton sediments (or ice−proximal sediment) that interfinger with glaciomarine strata (Stea et al., 1998). During the Mid−Wisconsinian, the glacier retreated to the inner Scotian shelf. However, the position of the glacier appears to have remained in the same approximate location during the Wisconsinian and Mid−Wisconsinian, with respect to the study area (Fig. 1.2).

During the Escuminac phase, the source changed to the Magdalen shelf, and transported a large volume of red−bed sediment towards the outer shelf and slope. This Carboniferous red sediment has been correlated with Lawrencetown till (Gauley, 2001). This sediment has been dated and is approximately coincident with the last glacial maximum (Gauley, 2001). This glacier retreated at approximately 18 ka (Stea et al., 1998).

The source of the glacier then shifted to the "Scotian divide", as illustrated in part 4 of Figure 1.2. The glacier receded from 15 to 13 ka. A short lived ice sheet then formed, with its source near Chignecto. The glacier did not extend far onto the shelf, perhaps half way in the central region (Fig. 1.2). There was a period of rapid warming at 12.5 ka, which caused the glacier to rapidly receded. The glacier formed several isolated sheets (part 6, Fig. 1.2). A sealevel lowstand of −65 m was recorded on the inner shelf, and dated at 11.7 ka). Cooling during the Collins Pond phase reactivated the isolated remnant glaciers as seen in Figure 1.2, at 10.8 ka (Stea et al, 1998). However, this phase can be ignored for the purpose of the geological history of the Western Bank, as it probably has little impact on the sediments of the Scotian slope.

There are features identified on seismic reflection profiles on the Scotian slope termed "till tongues", which are interpreted as indicative of the advance of an ice sheet across the Scotian shelf (Piper, 2001). Till tongues are visible in seismic records to a depth of 500 m, which is on the upper slope (Gauley, 2001). These tongues are wedge shaped, acoustically incoherent units (Mosher, 1989). Mosher interprets these units as coarse ice−proximal sediment, as opposed to diamicton. These features will be referred to as till tongues for simplicity, despite the possible inaccuracy of this term. Extrapolation of sedimentation rates by Mosher has indicated that the lower till tongue has an age of 70 ka (Mosher, 1989). This strongly indicates that the the ice sheet reached the upper slope (Gauley, 2001), and is cited as confirmation of the extent of the ice sheet (Stea et al., 1998).

Figure 1.3 is a summary of the glacial activity, and the percentage of hematite coated quartz grains (distinctive red−bed sediment, transported from the Magdalen shelf) for the last 35 ka from carbon−14 dating. It also describes the oxygen isotope record for the past 20 ka. It is noted that ice rafting during periods of glacial recession correlate well with periods of increased hematite coated grain percentage (Stea et al., 1998).

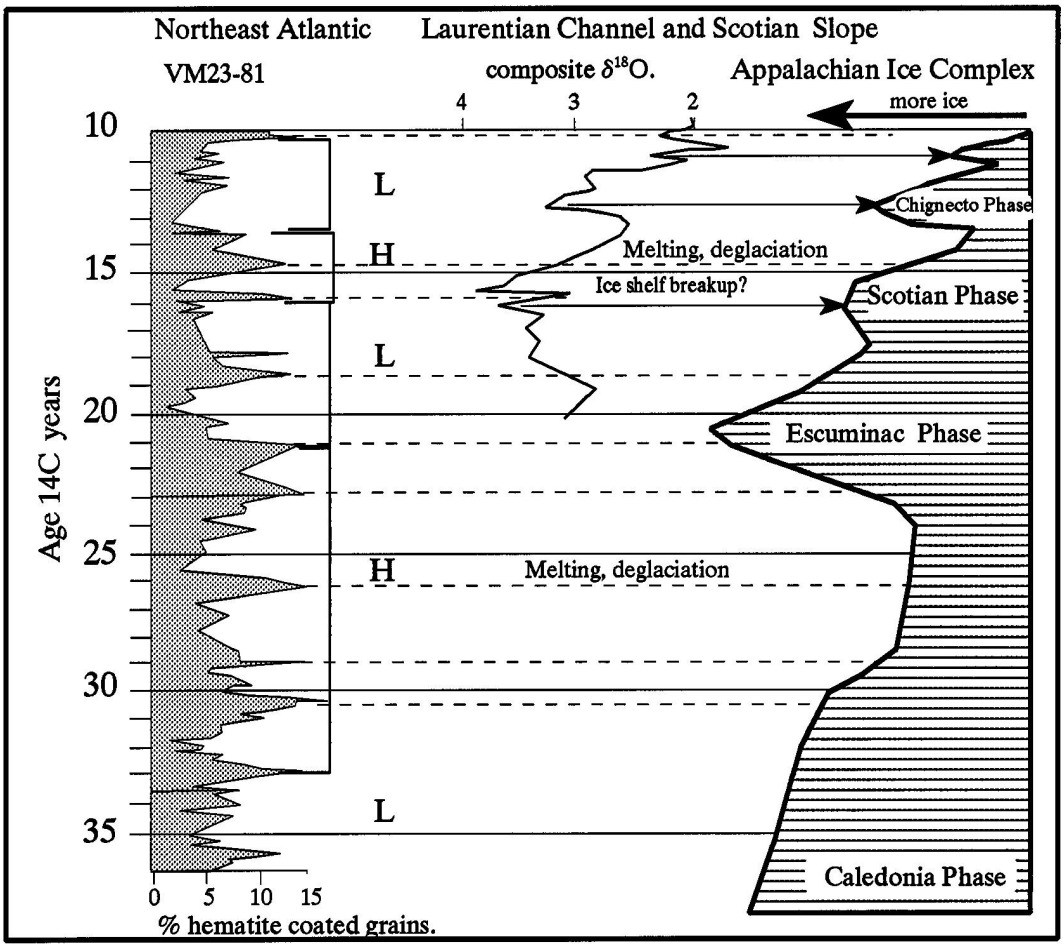

Figure 1.3: Diagram illustrating the ice advance and retreat pattern, and hematite coated grain sediment percentage (red–bed) for 35 ka to present. The oxygen isotope record for the past 20 ka is included (after Stea et al, 1998).

Seismic horizons were picked on a single channel reflection line from 1985 (in Appendix B) by Piper. A summary of the horizons, and the corresponding ages are listed in Table 1.1 reproduced from Piper and Normark (1989). The carmine reflector (0.45 Ma) marks the onset of glacial sedimentation, and is mentioned in later chapters.

It appears that all the factors needed for the formation of natural gas hydrate (appropriate pressure, temperature, and source of methane) are present off the Western Bank, and there is circumstantial evidence suggesting the possibility of gas hydrates (Piper, 2001). It is hoped that this study can shed new information on this subject.

Reflector name	Regional reflector	Probable age
Light Red	A	
Light Yellow		
Brown		
Carmine	B	middle Pleistocene (0.45 Ma)
Flesh (Gold)		
Rose		
Grey	C	basal Pleistocene (1.6 Ma)
Magenta		
Blue		
Red	D	
Lavender	E	middle Pliocene
Orange		
Pink		basal Pliocene
Canary	F	early Miocene (deep water); Miocene/Eocene unconformity (shallow water)

Table 1.1: Summary of reflectors, used for seismic stratigraphy (after Piper and Normark., 1989).

CHAPTER 2: SEDIMENT STABILITY

2.1 Classification of Sediment Failures

The study of submarine mass−movement is still in its infancy (Locat and Lee, 2000). There is ambiguity in some of the terminology used. Where possible, this paper will attempt to use terms defined by Mulder and Cochonat (1996). The mass movements of interest on the Central Scotian Slope can be categorised into three main categories, gravity driven flows (slumps, slides and creep), laminar fluid motion (plastic flows), and turbulent flows (turbidity currents). Turbulent flows appear to develop from either gravity driven or plastic flows (Mulder and Cochonat, 1996). The post−failure mechanics of mass movements are beyond the scope of this study, therefore turbulent and plastic flow failure deposits that may exist in the study area will not be examined.

Creep is described by Gauley (2001), but there is little distinct evidence of creep features from the seismic lines in this study. The creep occurred subsequent to the deposition of the teal horizon, which is probably too shallow in the sediment to be influenced by overpressures related to hydrate dissociation.

The main failure features of interest are in or near the "eastern disturbed area" (Fig. 2.1), which contains two slump deposits that appear to have failed at 15 ka, and 12 ka (Piper, 2001). From Figure 1.3, it can be seen that both failures occurred during glacial retreat. There are similar failures in the "western disturbed area", but the eastern zone is less complicated, with no failures occurring after 12 ka (Piper, 2001). The upper slope failures are described as rotational failures, that have a failure plane associated with "a period of time that experienced rapid sedimentation as the ice sheet retreated landward" (Gauley, 2001).

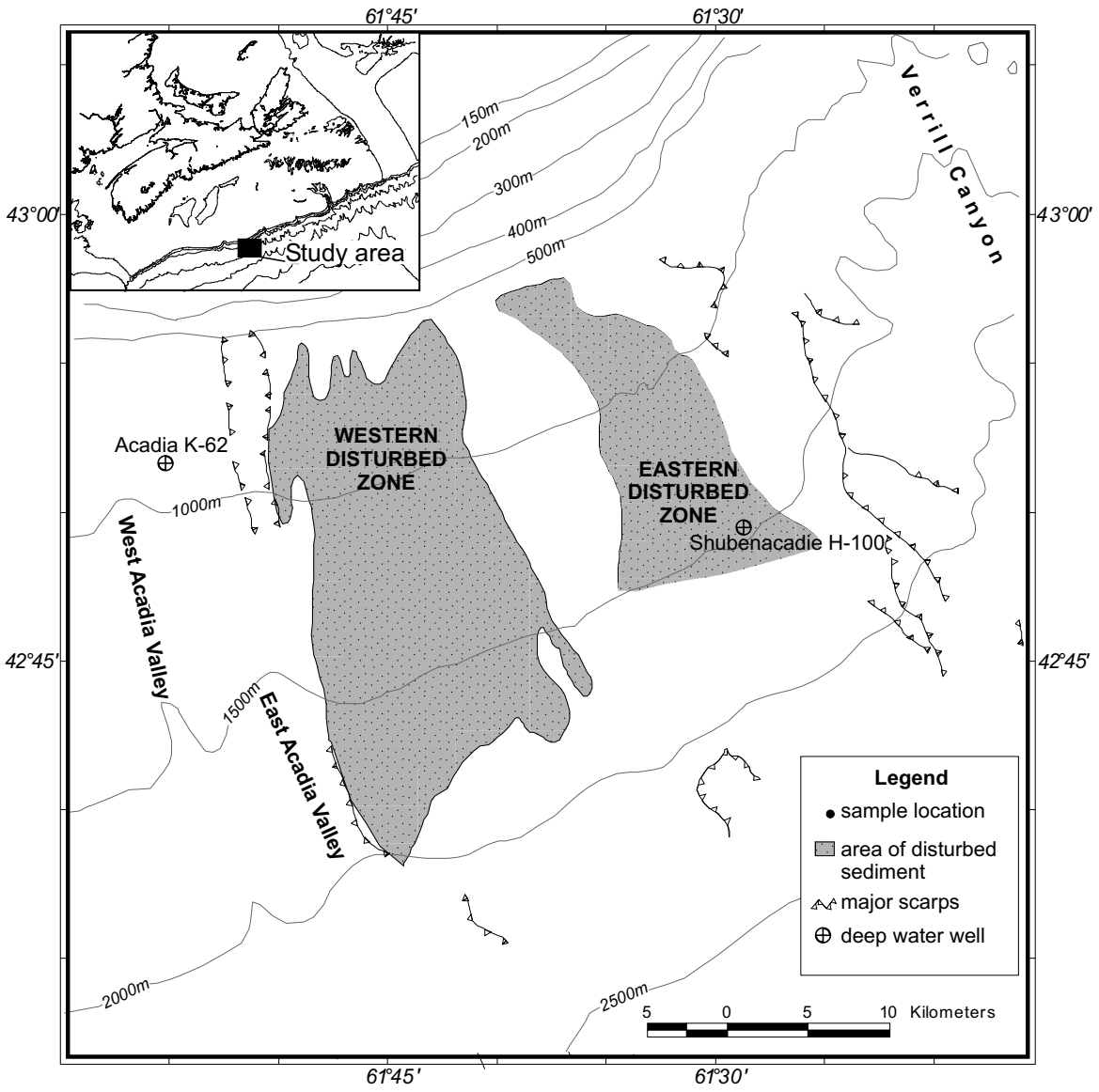

Figure 2.1: Map of failures in the study area, displaying the debris flows from the eastern and western disturbed areas (the source for these flows are the upper slope failures) (Mosher D.C., personal communication, 2002).

Pockmarks are seen in the study area, as well as gassy cores, and acoustic effects indicative of gas. The pockmarks are interpreted as gas escape craters. However, the relationship of pockmarks to underlying structures is not known (Piper, 2001). The zone falling between 500 and 1100 mbsl is within the GHSZ (Piper, 2001). It is possible that these pockmarks are related to gas hydrate processes. Another explanation is that the pockmarks are gas escape craters which are unrelated to gas hydrates, but it is not known

why this gas would not form gas hydrate if it is in the stability zone.

2.2 Factors influencing slope stability

Slumps are defined as rotational failures, while slides are translational. Both kinds of failures consist of an acoustically coherent sediment block, which is bound by failure planes on all sides. The slip plane (or basal decollement, basal shear plane, or glide plane) in a slide must eventually intersect the surface of the slope and therefore will probably not follow the strata entirely. Failures that have an intermediate geometry are called "mixed slides" (Mulder and Cochonat, 1996). The middle and lower slope failures in the study appear to be predominately bedding slides and mixed slides, as they have a small circular scar, and a huge planar body (Mulder and Cochonat, 1996). Figure 2.1 shows the locations of the eastern and western disturbed areas, and other smaller failures. The eastern and western disturbed areas are rotational failures, where the other smaller failures further down slope are predominately bedding plane slides (or mixed slides) (Piper, 2001).

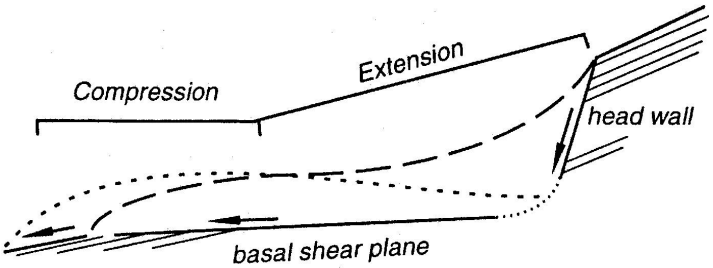

Figure 2.2: Example of a slump, showing regions of compression and extension. Note that the basal shear plane does not follow the strata (reproduced from Mello and Pratson, 1999).

A slide failure will typically exhibit extensional features near the top of the failure, and compressional features near the bottom (Fig. 2.2). Extensional features may include normal faults, while compressional features may include folding or thrust

faulting (Mello and Pratson, 1999).

Sediment failure will occur when the sum of the downslope forces exceeds the sum of the forces resisting downslope motion (Locat and Lee, 2000). The downslope force is gravity acting on the mass of the sediment (F=MA). The shear strength of a sediment is the resisting force. Earthquakes, waveloading, tides, sediment loading, gas and glacial loading are factors which can increase pore pressure, thereby decreasing the strength of the sediment. External trigger mechanisms (such as earthquakes) are involved is mass movement, and will be discussed in section 2.2.

Infinite slope analysis is a relatively simple method of evaluating the stability of a slope, in which the planar failure surface (ie: bedding planes in a translational slide) is parallel to the planar seafloor surface. This technique is a poor approximation in areas that do not meet the criteria (such as canyon walls), but it is a good approximation for most of the study area.

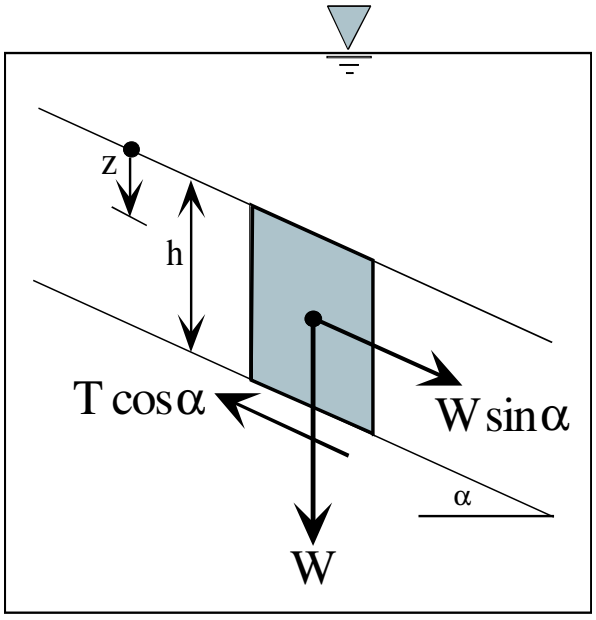

Figure 2.3: Summary of forces involved in infinite slope analysis (reproduced from Hampton et al., 1996).

$$\tau = \gamma' z \sin\alpha \quad (2.1)$$

Infinite slope analysis is based on formulae 2.1 and 2.2 (Hampton et al., 1996). In Formula 2.1, τ is the shear stress acting downslope, γ' is the submerged density of the sediment, and z is the depth below the sea–water interface. The shear strength of the sediment (ie: the force resisting downslope movement) is given by the Mohr–Coulomb failure criterion:

$$\tau_f = c' + (\sigma - u)\tan\phi' \quad (2.2)$$

Where τ_f is the shear strength, c' is the effective cohesion, ϕ' is the friction angle, σ is the stress acting normal to the failure surface, and u is the pore water pressure. This equation states that the shear strength of a cohesionless sediment decreases as the pore pressure increases. Dividing τ_f by τ gives the *factor of safety, F*. An F of greater than 1 implies a statically stable slope, while an F of 1 or less implies an unstable slope.

Pore pressure in excess of hydrostatic pressure, called *overpressure* or *excess pressure*, may be caused by several factors. Excess pore pressure from high sedimentation rates appears to be the most commonly cited explanation for high pore pressures, especially in glaciated areas. This is applicable to the Scotian slope, which has undergone glaciation, and rapid sedimentation. Sediment which is deposited under low sedimentation rates has time to expel pore water during burial. Rapidly deposited sediment retains much higher pore pressures due to the inability for the pore water to migrate out of the sediment (Mosher et al., 1994).

Overpressures can also result from the dissociation of gas hydrates. Gas hydrates exist under a specific pressure – temperature regime and will dissociate if they are not in

the GHSZ (Sloan, 1998). A drop in pressure, from a relative sea level fall, or from a rise in seawater temperature (at the seafloor) can cause gas hydrates to dissociate. This dissociation liberates methane gas and water, which can increase the pore pressure, and decrease the shear strength of the sediment (Popenoe et al., 1993). This is most likely to occur during a glacial lowstand, or during deglaciation, when relative sea level is low, and the bottom waters are warmer (Piper, 2001). A change in the P–T conditions is most likely to affect the upper slope hydrates, which are more susceptible to changes in pressure and temperature (Paull et al., 2000). Gas hydrate dissociation will always occur at the base of the gas hydrate stability zone, therefore increased pore pressure will always occur in this region as well. Therefore sediment failures that occur far above the BGHSZ, such as the middle and lower slope failures, were probably not influenced by gas hydrate dissociation.

Excess pore pressure can also be caused by the generation of shallow gas, which is not associated with gas hydrates. Very shallow biogenic gas production from the decay of organic matter may create methane gas, but would not have been at a sufficient depth to influence the mass movements of interest on the slope, which have up to 80 m high vertical scarps (Mosher, 1987). Methane could also have migrated upward from a thermogenic or petrogenic source. Piper (2001) describes the sediments as gassy, on the basis of acoustic and core properties. The source for the gas seen in the study area is not known, but Piper (2001) speculates that thermogenic gas is more probable. Methane in gas form or dissolved in pore water would be expected to form gas hydrate if it travelled into the GHSZ (Dillon and Max, 2000). Thus, overpressure from gas charging (biogenic and thermogenic/petrogenic) may be a more important factor in sediments outside the

GHSZ.

The generation of excess pore pressures created by rapid glacial sedimentation and gas hydrate dissociation are hard to distinguish. Rapid glacial sedimentation occurs during deglaciation, when the sea level is likely at a low level, and meltwater is transporting and depositing large volumes of sediment (Piper, 2001). This is also the same time that gas hydrates would be expected to dissociate (Piper, 2001); therefore it is difficult to distinguish (based on time) what caused sediment failure. The approach taken in this paper is that if gas hydrates exist on the slope today, then they probably existed during the time of sediment failures. If they were present during glaciation, then they could have dissociated and caused a corresponding increase in sediment pore pressure during deglaciation. Moran et al. (2001) discuss warming events related to Dansgaard–Oeschger (or D/O) events, and warm freshwater coming from the Laurentian Channel during the glacial retreat at 14 ka. From Figure 1.3, it is clear that the failures occurred during periods of glacial retreat (15 and 12 ka). Moran et al. (2001) state that failures in this region are as old as mid Pliocene, and thus pre–date glaciation. This seems to support the model of gas hydrate increasing pore pressure, and partially inducing failure. The impact of glacial loading is also important to pore pressure, and is discussed later.

Gas hydrated sediments have a higher shear strength relative to non–hydrated sediment, due to the strength of the hydrate cementing the sediment, as well as the decrease in porosity and permeability of the sediments (Paull et al., 2000). The porosity and permeability of the sediments is decreased because dissolved methane and water are extracted to form gas hydrates (Paull et al., 2000). Decomposition of hydrate will cause a decrease in sediment strength. If the sediments are already saturated in methane, the

decomposition of the hydrate will release both water and methane into the pore spaces. This will result in a pressure increase in well sealed sediments, or a volume increase in sediments that allow fluid flow. The resulting increase in one or both of pressure and volume has the potential to weaken the sediment (Paull et al., 2000).

Slope gradients have an important impact on the stability of slope sediments. From Formula 2.1 it can be seen that as the slope gradient increases, so does the shear stress, due to gravity. However, this factor does not appear to be the most important in the study area. Slope stability analysis has shown that the regional 2° to 3° (local gradients can be much steeper) gradients are stable under static conditions (no seismic triggering) (Mosher et al., 1994). Therefore it can be assumed that the cause of the failures was something other than the slope gradient, either a factor greatly reducing the shear strength (such as a pore pressure increase), or an external trigger mechanism (such as an earthquake), but more likely a combination of the two.

Sediment lithology is also an important aspect of slope stability analysis. Not only is the pore pressure higher during the rapid sedimentation that occurs during deglaciation, the lithology is also quite different. The strength of the matrix is the "main sediment support mechanism" (Mulder and Cochonat, 1996). Granular sediments typically have much less shear strength than a cohesive sediment. Perfectly granular, uncemented sediments have no cohesion, and therefore c' in the Mohr–Coulomb equation is zero. Grain to grain friction is thus the main resisting force in such sediments. However, it is noted that concentrations of clays as low as 5% can induce cohesive strength (Mulder and Cochonat, 1996). Analysis of failure horizons with sediment cores has revealed that failures appear to be "localised at horizons with

abundant sand beds" (Campbell, 2000; Piper, 2001).

An increase in the thickness of a sediment column will increase the normal stress (load) on the sediment, and therefore may cause a failure. The main reason sediment does not fail as it is progrades is that is becomes consolidated. This is a process of dewatering, and compaction. Consolidation increases the shear strength of the sediment. The increase in shear strength with depth is referred to as the shear strength gradient (Mulder and Moran, 1995). Sediment that has an unusually low shear strength in relation to its depth of burial is called *apparently underconsolidated*, while sediment that has unusually high shear strength given its depth of burial is called *apparently overconsolidated* (Mulder and Moran, 1995).

The theory of glacial loading causing mass-failure has been proposed as the "dominant mechanism for slope instability on glaciated margins" by Mulder and Moran (1995). The theory states that during a glacial sea level lowstand, an ice sheet may extend to the outer continental shelf, and may rest directly on the seafloor (Mulder and Moran, 1995). As the sediment is loaded, the vertical stress increases, through an increase in pore pressure, increasing the susceptibility to failure (Mulder and Moran, 1995).

Although ice-loading may be a critical factor for slope stability, it is unclear which (if any) mechanism is dominant: ice-loading, rapid sedimentation, earthquake ground accelerations, or excess pore pressure due to gas or gas hydrate dissociation. Glacial loading does not appear to be considered a significant factor in sediment failure analysis by Gauley (2001), and is briefly mentioned by Piper (2001). Piper (2001) notes that there is no geological evidence to support this process, therefore rapid sedimentation, earthquakes ground accelerations, and gas hydrate dissociation (and gas charging) will be

considered as the main mechanisms that create overpressures in the upper slope failures seen in the study area. The middle and lower slope failures may also be influenced by salt tectonics, but there is no indication of salt tectonism near the upper slope.

2.3 Triggers

The term *triggers* appears to be used interchangeably with the processes that cause slope failure. This study will differentiate between the processes that cause increased stress (or decreased strength) and the *external triggers* which may cause the failure to occur (some failures may not involve external triggers). Locat and Lee (2000) describe 10 *triggers* that can cause slope failure: 1) oversteepening, 2) seismic loading (earthquakes), 3) storm−wave loading, 4) rapid accumulation and underconsolidation, 5) gas charging, 6) gas hydrate dissociation, 7) tidal drawdown, 8) seepage, 9) glacial loading and 10) volcanic island processes. Of these processes this study will consider 4 processes as external triggers: seismic loading (earthquakes), storm wave loading, low tides, and glacial loading. The study area is located in water that is too deep to be impacted by storm−wave loading and tidal variation (even during a lowstand), and are not considered further (Piper, 2001). This leaves seismic loading, and glacial loading as external triggers (and salt tectonics for the lower slope failures, which are not discussed in relation to gas hydrate dissociation).

The most obvious, and most commonly−cited external triggering mechanism is an earthquake. As in the 1929 Grand Banks mass−movement, in which an earthquake initiated a large failure, it is clear that earthquakes play an important role in slope failures (Piper, 2001). Earthquakes can be produced from two sources (for the purposes of this study); interplate seismicity, or from isostatic adjustment in response to glacial loading

and unloading (Fjeldskaar, 2000). The recurrence interval of plate motion seismicity would not vary during glaciation, but the glacial seismicity would be largest during ice–loading and isostatic rebound (Fjeldskaar, 2000).

The current seismic activity of the continental margin is somewhat high, relative to most other passive margins (Piper, 2001). The recurrence interval for an earthquake equal to the 1929 Grand Banks event is 10 to 100 ka, based on geological data. Keen et al. (1990) note that earthquakes were more frequent in the Pleistocene. This information therefore indicates that an earthquake that would trigger a failure during deglaciation would likely be caused by glacial seismicity.

Slope stability analysis studies by Mosher et al. (1994) shows that there are both large and small scale failures in the study area. The paper states that excess pore pressure may make sediment susceptible to failures, but is unlikely to trigger failure on the smooth sediment of the Verrill Canyon area (Mosher et al., 1994). Mosher et al. conclude that sediment failure was likely triggered by seismic activity, in addition to elevated pore pressures. The article also states that large, distant earthquakes are unlikely to be the external trigger mechanism for large scale failures in the study area. It is more likely that smaller scale, and more frequent earthquakes in the study area were probably the external trigger. An earthquake of magnitude 5.0 or greater within 40 km of the site, or a magnitude 3.0 earthquake at the study area would be required to produce slope failure (Mosher et al., 1994).

CHAPTER 3: METHANE GAS HYDRATES

3.1 Global Importance

3.1.1 Definition and distribution of hydrates

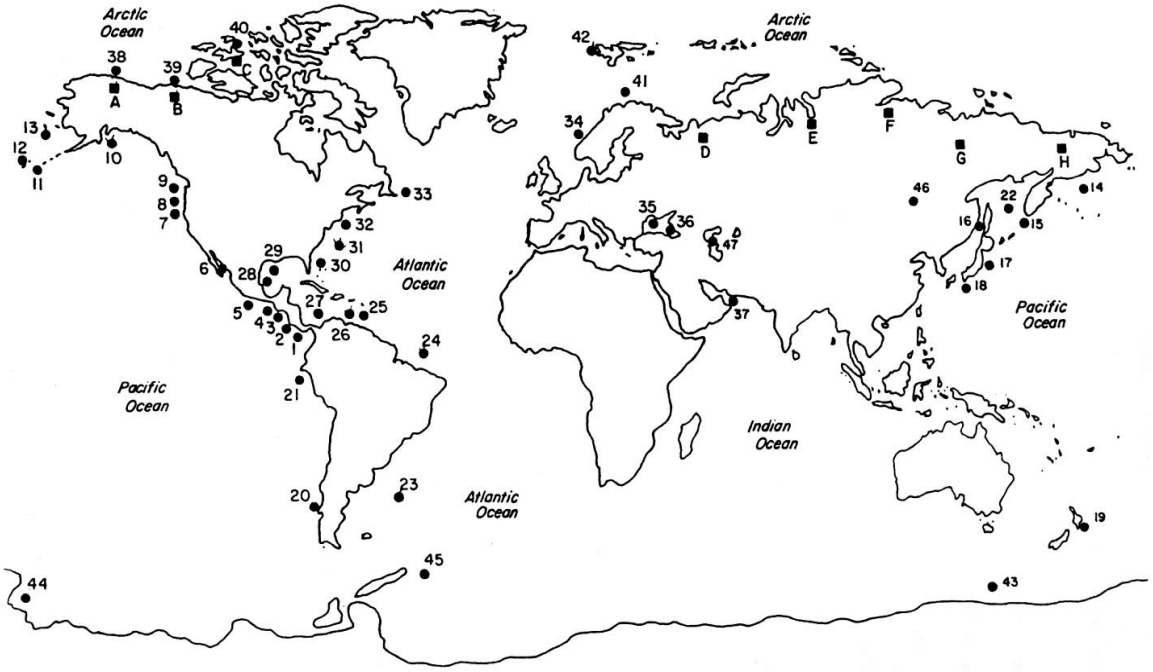

Figure 3.1: Global distribution of known and inferred gas hydrates, black circles depict oceanic hydrate, black squares indicate permafrost hydrate locations (reproduced from Sloan, 1998). Note that the Scotian slope is is bounded by two hydrate locations (32 and 33).

Gas hydrates are naturally occurring ice–like solids that form under specific pressure–temperature regimes. Gas hydrates belong to the clathrate class of molecules. A clathrate compound is composed of an asymmetric spherical lattice "cage" of host molecules, which surrounds a guest molecule. Methane gas hydrates have a lattice of water molecules, surrounding a single methane molecule (Sloan, 1998). The chemistry of hydrates will be discussed later in this chapter.

Gas hydrates appear to be a common occurrence, and tend to form wherever water and methane (with sufficient methane flux) coexist under low temperatures and elevated pressure regimes, as depicted in Figure 3.1 (Sloan, 1998). It is a relatively new

field of research and there are vast areas that are unsurveyed for hydrates, therefore the true extent of oceanic gas hydrate is likely to be far greater than seen in Figure 3.1.

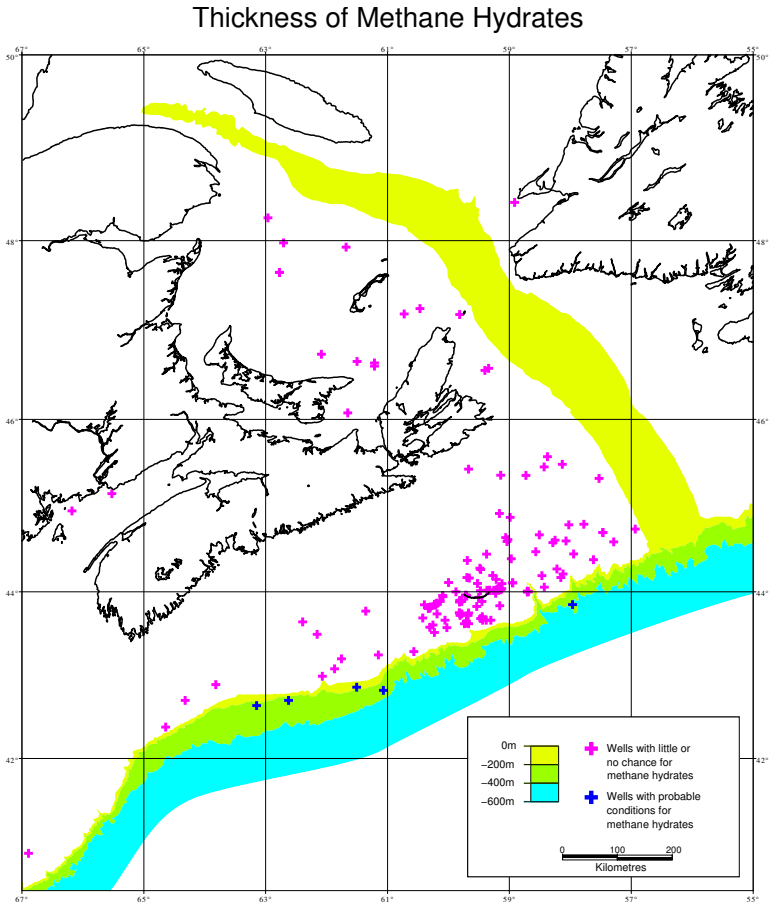

Figure 3.2: Map of gas hydrate thickness for the Atlantic region (after Majorowicz, 2002).

A BSR occurrence has been found recently on the central Scotian Slope (within 90 km of the study area) from industry seismic data but the data remain confidential (D. Piper and D. Mosher, Personal Communication, 2001). The approximate thickness of the gas hydrate stability zone is displayed in Figure 3.2. The estimates for the thickness of the GHSZ in chapter 5 are similar to the estimates in Figure 3.2 (after Majorowicz, 2002).

The approximate total volume of oceanic gas hydrate has been estimated to range

from $3.1x10^{15}$ m^3 to $7.6x10^{18}$ m^3 (Sloan, 1998). A value of $21x10^{15}$ m^3 has become the current consensus (Kvenvolden, 2000). The estimated volume of permafrost hydrates is typically 1 to 2 orders of magnitude smaller than the volume of oceanic hydrates, and therefore makes a small contribution to global hydrate volume, relative to oceanic hydrate (Sloan, 1998).

3.1.2 Greenhouse gas potential

The large volume of methane sequestered in hydrates is an important factor to consider in terms of global climate and ocean chemistry (Kvenvolden, 2000). The stability of oceanic gas hydrate depends greatly on its pressure and temperature regime. A decrease in sea level (and associated decrease in hydrostatic pressure), or a bottom water temperature increase could cause a large volume of hydrate on the continental slopes to dissociate and release methane gas into the ocean, and perhaps into the atmosphere (Haq, 2000).

Haq (2000) notes that climatic warming occurs in parallel with a rapid increase in methane and carbon dioxide, which is thought to have possibly come from gas hydrate dissociation. The mechanisms of methane flux into the atmosphere from hydrate dissociation are poorly understood, but it appears that a climate feedback loop may exist. Haq (2000) proposes that during glaciation, a sea level lowstand promotes hydrate dissociation, and sediment failures, which release large amounts of methane into the atmosphere, and may cause warming of global climate due to the greenhouse effect. This would account for the abrupt terminations of glacial cycles. It is not clear whether initial warming is caused by hydrate dissociation, or if warming causes the dissociation. It is important to note that hydrate dissociation is likely not the main cause for the initiation

of deglaciation, but it probably assists as a positive feedback mechanism (Haq, 2000).

3.1.3 Potential fuel resource

The estimated volume of global hydrate ($21x10^{15}$ m^3) is approximately twice that of the total fossil fuel reserve (Sloan, 1998). If 1% of the estimated hydrate resource were extracted for fuel, it would yield approximately 2,000 TCF (trillion cubic feet) of methane. This is equal to an 80 year supply for the United States, at a consumption rate of 25 TCF per year (Current US consumption is equivalent to 22 TCF per year) (Max, 2000). Clearly gas hydrates are a massive unconventional potential fuel resource.

Methane is an excellent fuel for combustion, due to its high H:C ratio (hydrogen:carbon). The products of combustion are CO_2 and H_2O. Methane releases the least amount of CO_2 per mole of any fossil fuel. Methane therefore appears to be a possible replacement for other fuels, due to its abundance, and increased concern for greenhouse gas emissions (Max, 2000). Methane is also an excellent fuel for fuel cells, which may play an increasing role in the future of electricity generation.

Max (2000) discusses the production of gas hydrate, which is likely to be costly, when compared to other fossil fuels, due to the inaccessibility of the resource and its distributed nature (Fig. 3.1). It is therefore likely that countries that have little fossil fuels will be the first to attempt to mine gas hydrates. Countries such as Japan, that lack large deposits of conventional fossil fuels, are likely to be the first to develop the gas hydrate resource, as it will likely be economically feasible before it is elsewhere in the world. Japan's independence from the current fossil fuel monopoly is also seen as a political imperative. It appears that the widely distributed nature of gas hydrates may result in more evenly distributed fuel resources around the world (Max, 2000).

3.2 Hydrate Properties

3.2.1 Chemical Composition, Clathrate Lattice

Clathrates can form spontaneously under specific pressure–temperature regimes, if there is a host molecule which can crystallise to form an open lattice, and a guest molecule which can fit inside the open lattice. Many different molecules can act as guest and host molecules in a clathrate, including hosts of urea, phenol, water, clay minerals, zeolites, graphite, and many others. Guest molecules include hydrocarbons, HCl, SO_2, CO_2, halogens, noble gasses, sulphur, etc. (Pellenbarg and Max, 2000). There are over 130 compounds identified which can form clathrates with water. However, the only clathrate of interest in this paper is *methane gas hydrate* which has H_2O (water) as a host, and CH_4 (methane) as a guest molecule. For simplicity, It will be assumed that any gas hydrate deposits that may exist in the study area are methane gas hydrates.

Methane gas hydrates form with several different crystal lattice structures. All natural gas hydrates form structures of either sI (body–centred cubic), sII (diamond cubic), or sH (hexagonal), commonly referred to as types I, II, and H (Sloan, 1998). Type I hydrate is the most common, with type II and H occurring only rarely . Type II and possibly type H hydrates are seen in the Gulf of Mexico. These hydrates are believed to have a thermogenic origin, which is far less common than a biogenic origin (Kvenvolden in Max, 2000). Methane gas hydrates (type I) account for over 99% of gas hydrate occurrences (Dillon and Max, 2000).

3.2.2 Hydrate Stability

The stability of gas hydrate is an important factor in the stability of slope sediments. The pressure – temperature relationship of gas hydrate is plotted in Figure

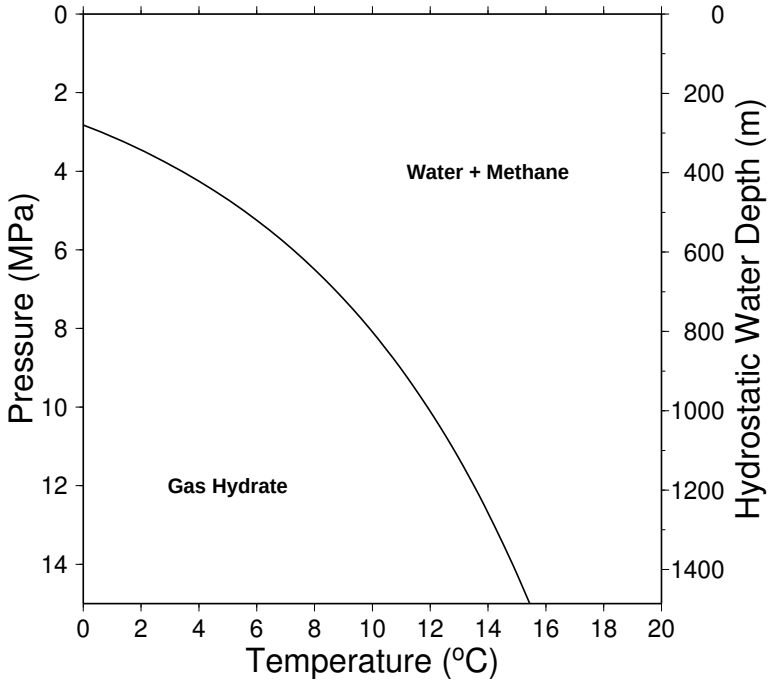

Figure 3.3: Empirical pressure temperature plot of gas hydrates seen in nature. The curve is derived from Formula 3.1. Hydrate is stable below the curve, and unstable above it.

3.3. It is apparent that it has a non−linear relationship. Several empirical equations have been proposed to approximate this relationship. Peltzer and Brewer (2000) state that the best equation to date appears to be a second order polynomial proposed by Brown et al. (1996):

$$T = 11.729 + 20.5[\log_{10}(z)] - 2.2[\log_{10}(z)]^2 \quad (3.1)$$

$$z = \frac{1000P}{\rho g} \quad (3.2)$$

Where T is temperature in degrees Celsius, and z is water depth in kilometres (not accounting for atmospheric pressure). The hydrostatic depth relationship is described by Formula 3.2, where z is depth in km, P is pressure in MPa, ρ is the density of water in kg/m^3, g is the gravity constant in m/s^2, and a conversion factor of 1000 is used. This relationship assumes that water density does not change with depth, which is incorrect

(Peltzer and Brewer, 2000). However, for the purposes of this study, it is a close enough approximation.

From Formula 3.1, the intersection of the gas hydrate stability zone with the seafloor can easily be calculated. It is simply the intersection of the bottom water temperature with the curve on Figure 3.3. The pressure is proportional to the water depth, which is then calculated (using Formula 3.2). This has been done for the study area, and reveals that gas hydrates should exist at and below approximately 500 mbsl, using an average bottom water temperature of 5 °C (440 mbsl when 4.1 °C is used). These calculations will be discussed in greater detail in chapter 5.

Calculations of the depth to the base of the gas hydrate stability zone (BGHSZ) are much more difficult to obtain. The pressure gradient in sediment is higher than that of water, and other factors (especially overpressures) make estimation of pressure problematic. However, measurements which assume a hydrostatic pressure gradient in sediment can be useful for making a first approximation of depth to the BGHSZ. *In situ* measurement of pore pressure is helpful in calculations which aim to have a greater degree of accuracy. The geothermal gradient is likely to be linear in undisturbed sediments, and therefore should be a straightforward calculation in most cases (Peltzer and Brewer, 2000; Sloan, 1998). From the multibeam bathymetry image (displayed in chapter 5), it can be seen that the OBS was placed on undisturbed sediment, therefore the geothermal gradient calculations should be acceptable.

3.2.3 Physical Properties

Sloan (1998) has shown that there is relatively little variation between the types of hydrate. The properties of hydrate are summarised in Table 3.1, after Pellenbarg and

Max (2000). Laboratory experiments by Stern et al. (2000) have shown that the strength of hydrate + ice versus pure ice at low temperatures (< 200 °K) is relatively similar. However, the difference in strength at temperatures near 260 °K is substantial. The hydrate and ice mixture is several times stronger than ice. Stern et al. (2000), citing their work in progress, suggest that pure hydrate is even stronger under the same conditions.

The main result of the formation of hydrate in a sediment is to strengthen it. This increase in strength changes the physical and acoustic properties of the sediment. Both compressional wave, and shear wave velocities (Vp and Vs respectively) will increase with increasing hydrate concentration (Lee and Collett, 2001). Vp may increase from around 1.6 km/s in normal sediment, to 2.5 km/s or higher in hydrated sediment. It is noted that Vs can rise by orders of magnitude in hydrated sediment, and dramatically increase the sediments ability to transmit shear waves (Miles, 2000).

Property	Ice	Hydrate
Dielectric constant at 273 °K	94	~58
NMR rigid lattice 2nd moment of H_2O protons (G2)	32	33±2
Water molecule reorientation time at 273 °K (μsec)	21	~10
Diffusional jump time of water molecules at 273 °K (μsec)	2.7	>200
Isothermal Young's modulus at 268 °K (109 Pa)	9.5	~8.4
Speed of longitudinal sound at 273 °K		
Velocity (km/sec)	3.8	3.8*
Velocity ratio Vp/Vs at 272 °K	1.88	1.95
Poisson's ratio	0.33	~0.33
Bulk modulus (272 °K)	8.8	5.6
Shear modulus (272 °K)	3.9	2.5
Bulk density (gm/cm^3)	0.92	0.91
Adiabatic bulk compressibility at 273 °K 10−11 Pa	12	14
Thermal conductivity at 263 °K (W/m−K)	2.25	0.49±0.02
Heat of fusion (kJ/mol)	6	54−57

Table 3.1: Summary of properties of ice and gas hydrate. Note the similarity of most properties (from Pellenbarg and Max, 2000). The velocity of hydrate (*) is discussed in Sloan (1998), and is estimated at 3.8 km/s.

3.2.4 Acoustic Properties

The main method of detecting gas hydrated sediments is to locate a BSR, or bottom simulating reflector. The BSR is believed to correspond to the interface between the hydrated sediments in the GHSZ, and the free gas (or hydrate free sediments) below the base of the GHSZ (Sloan, 1998; Miles, 2000). There is also thought that it may represent the top of the free gas layer, which is discussed later in this chapter. Some locations do not have a sharp contact between hydrate and free gas. Therefore it is important to know whether the bottom of the hydrate or the top of the free gas layer causes the BSR feature. The high velocity of the hydrate, and low velocity of the free gas (or hydrate free sediments) results in a negative reflection coefficient. Hydrates are more sensitive to temperature changes than pressure changes, and therefore the BGHSZ follows isotherms of the sediment, which approximate the shape of the sea floor. Sediments containing gas hydrate typically show decreased seismic attenuation compared to hydrate free sediment, while the free gas zone beneath the hydrate shows increased attenuation and gassy "bright spots" (Pecher and Holbrook, 2000).

The lack of a BSR does not necessarily indicate that gas hydrates are not present. Chapman (2001) states that highly reflective sediments can mask the BSR. The sediments of the Verrill Canyon area are also highly reflective, and may possibly be masking a BSR. It is also believed that the lack of free gas beneath the BGHSZ is the dominant factor responsible for the lack of a BSR on seismic reflection lines (Pecher and Holbrook, 2000).

Despite extensive examination of the single channel reflection seismic lines used in this study, no BSRs have been found in the Verrill Canyon area (other than shallow

artifacts which have been interpreted as side echoes). Therefore other geophysical methods will be used to determine if gas hydrates are present. A high resolution Ocean Bottom Seismometer (OBS) was deployed to gather information about the velocity structure of the sediments in approximately 850 m water depth, near the western flank of the Verrill Canyon. An anomalously high velocity in the theoretical GHSZ may indicate the presence of hydrate, while the lack of an anomalously high velocity may indicate that little or no hydrate is present at the OBS location. A limitation of this study is that only one OBS was used. Certainly the velocity structure of the entire study area cannot be summarised on the basis of one instrument. However, other indirect evidence (the theoretical depth at which hydrate may be stable, sediment failures and pockmarks) indicates that the OBS location is ideal to examine the possible existence of upper slope gas hydrates.

3.2.5 Formation Styles and Mechanisms

Hydrates form as either disseminated, nodular, layered, or massive (with increasing proportion of hydrate to sediment). The first informal model of hydrate formation assumed that hydrates formed as disseminated deposits, then grew to nodular, layered and massive deposits (Sloan, 1998). The form of hydrate is also dictated by the grain size and porosity of the sediments. Coarse grained sediments tend to have pore fillings and disseminated grains of hydrate, while finer grained sediment typically have nodules and veins (Dillon and Max, 2000). This theory describes the state in which the hydrate forms, but does not explain the processes that cause hydrate to grow. Three main theories have emerged for the formation of hydrate. Kvenvolden and Barnard (1983) suggest that the hydrate may form in place from the *in situ* generation of biogenic

gas. This has been disputed by the presence of hydrate deposits that have very high hydrate concentrations, which cannot be accounted for by *in situ* biogenic methane generation alone.

The generation of hydrate from the migration of free gas from below into the hydrate stability zone has been proposed by Paull et al (1994). This theory does not presume the gas to be necessarily biogenic in origin, it may come from biogenic (bacterial methanogenesis), thermogenic (abiological), or from the gas produced from dissociated gas hydrates. Paull describes a mechanism as follows: as sediment is deposited, the base of the gas hydrate stability field moves upward (with the isotherms), and dissociates hydrate, freeing methane gas which can form more hydrate in a shallower location.

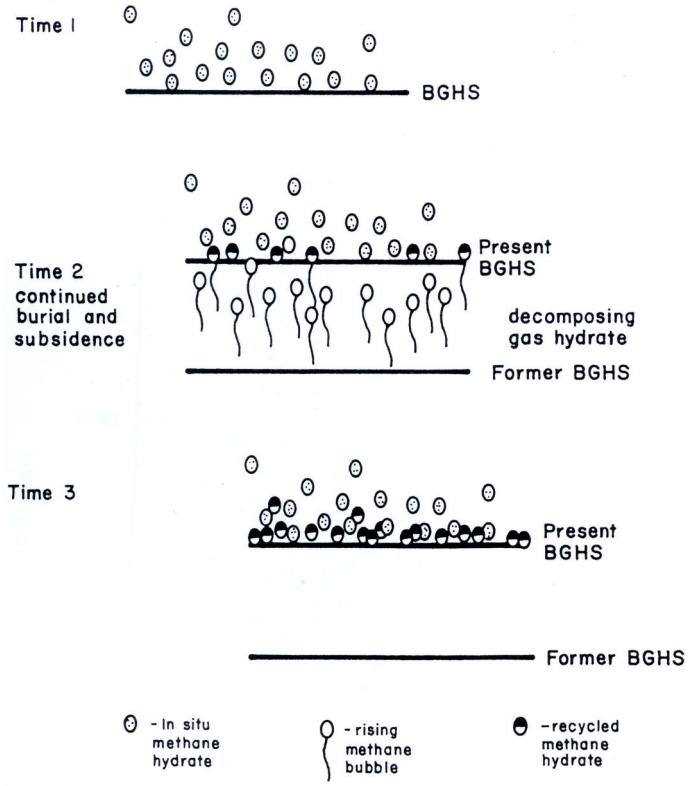

Figure 3.4: Illustration of the formation mechanism described by Paull et al, showing three stages in the formation of hydrate. Note that the position of the BGHS (or BGHSZ) moves upwards with time (after Paull et al, 1994).

Hyndman and Davis (1992) propose another mechanism for the formation of gas hydrate, it states that hydrate may form from the dissolution of methane gas in water as it ascends through the sediment. The saturation of water decreases with decreasing pressure, resulting in the water being saturated in methane as it passes through into the hydrate stability zone which causes hydrate to form. This theory accounts for massive hydrate deposits which do not have a free gas zone beneath (methane may be dissolved in pore water under the GHSZ). Sloan (1998) states that it is not clear which of these processes is dominant in nature, and that more research is required.

A BSR is thought to either represent the top of the free gas layer, or the acoustic impedance seen at the contact between sediments containing hydrate and free gas. Xu and Ruppel (1999) discuss the importance of the mass fraction and flux of methane in relation to gas hydrate deposits. The mass fraction of methane must be in excess of the local methane solubility for gas hydrate to accumulate. The methane flux must exceed a critical level for the base of hydrate occurrence to be equal to the BGHSZ. It is noted that the methane flux is closely related to the total fluid flux. The critical flux depends on the water depth, heatflow, and fluid flux. It is noted that most systems appear to be dominated by advection rather than diffusion.

High methane flux is required to create a strong BSR, despite there being controversy regarding what a BSR represents. Hydrated sediments, and a free gas layer can be separated by a layer of sediment that contains neither. If a BSR represents the top of the free gas zone, this situation would account for BSRs that are seen at far greater depths than the BGHSZ. This would also explain many hydrate occurrences that do not have an underlying free gas layer, and lack a BSR (Xu and Ruppel, 1999).

However, if a BSR marks the impedance contrast between gas hydrate and hydrate free sediment (not necessarily a free gas zone), this would explain why some BSRs are seen in depths far shallower than the BGHSZ. A low methane flux rate would cause the hydrate to form shallower in the sediment, and may cause the bottom of the hydrate layer to be more poorly defined than it would be in a high flux environment. This would likely result in less of an impedance, and therefore a weaker BSR (Xu and Ruppel, 1999).

CHAPTER 4: DATA ACQUISITION AND ANALYTICAL METHODS

4.1 Wide−Angle Equipment Used Onboard Cruise HUD2001−028

CCGS Hudson cruise 2001−028 operated from June 20th to July 11th, 2001. The main purpose of the cruise was to better determine the structure and evolution of the continental margin and sedimentary basins of the eastern Canadian margin off the coast of Nova Scotia. The study of shallow sediment velocity structure was a secondary objective. Three large profile lines were run, which varied in length from 300 to 500 km. OBSs were placed at regular intervals to collect data on deep structures. OBS number 6 on line 2 was equipped to record deep refraction data from a 6300 in^3 airgun array, as well as high resolution reflection / refraction data from a 40 in^3 sleeve gun source. The velocity information gathered from the OBS is a major focus of this thesis. Heat probe data was planned, but cancelled due to time constraints.

Each OBS consists of three buoyant glass spheres (or floats) encased in yellow plastic, a pressure casing, steel weights (anchors), a radio direction transmitter, strobe light, and acoustic pinger. The instruments include a hydrophone, and three geophones mounted in the x, y and z orientations (1 vertical, and 2 horizontal). The data collected from the hydrophone and geophones are stored on 4 separate channels and recorded on a 1 Gb hard drive contained inside the pressure casing, along with other electronics. The raw data is recorded in DREA format, and later converted to SEGY format. The SEGY format includes offset information for the airgun shots, which is derived from the ship's navigational data.

Communication with the OBS is performed using an acoustic pinger, which operates at 12.5 kHz. The OBS can be released off the sea floor by sending the proper

acoustic signal to the OBS from the ship. If this fails, the OBS will self–release after a specified amount of time. The OBS is released from the seafloor by disconnecting a steel weight, which causes the buoyant OBS to rise to the surface.

Figure 4.1: An OBS ready for deployment on the deck of CCGS Hudson.

The OBSs were deployed in a sequential order, dropping each weighted OBS to the seafloor. Positioning of each OBS was determined and recorded using the ship's differential GPS system. The position of the OBS was recorded both on deployment and on recovery. Following the deployment of the OBSs, the ship proceeded over the OBSs it had launched, firing an airgun array consisting of 12 airguns totalling 6300 in^3. The data collected using the 6300 in^3 source has a resolution that is too low to be useful for hydrate research. After completion of the airgun line, the OBSs were retrieved in the order they were launched.

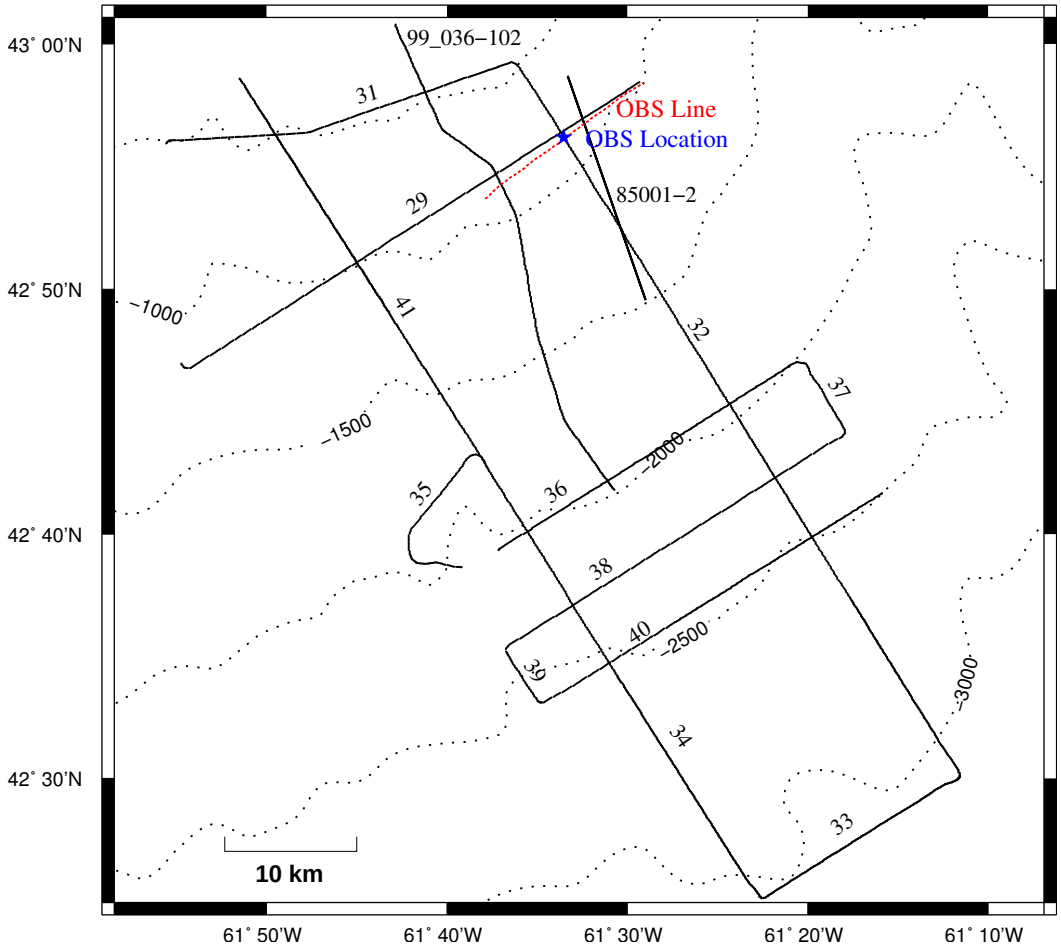

Figure 4.2: Detailed map of single channel reflection lines (solid black lines), wide–angle OBS line (dashed red line, from cruise 2001–028), and OBS location (blue star). Lines 29 to 41 are from cruise HUD2001–048A, while lines 99_036–102 and 85001–2 are from cruises 1999–036 and 1985–001–2 respectively. Bathymetry contours are dotted lines at a 500 m interval.

Before retrieval of the 6th OBS on line 2, a 10 nm long high resolution line was performed, line 2–1. This line was perpendicular to the large profile line, over OBS 6. One 40 in^3 sleeve gun was used as the seismic source, firing once every 4 seconds. The average frequency is 50 Hz, resulting in an approximate wavelength of 35 m, and a resolution of 9 m (¼ wavelength). There were no problems with the operation of the sleeve gun and data were collected on all channels.

4.1.1 Wide–Angle Seismic Data Analysis Procedure

The data collected from the OBS is plotted as trace number vs. travel time, for the *x* and *y* axes respectively. This is later plotted as offset from the OBS in km vs. travel time. This plot (Fig. 4.3) shows a normal moveout, which is a hyperbolic reflection geometry. As the shots are fired from the ship, the distance from the shot to the OBS increases, approaching the horizontal distance (offset) between the shot and the OBS (which accounts for the hyperbolic shape). The sediments appear reflective , which is confirmed by the single channel data. Both reflections, and refractions are visible on the plot. The seafloor occurs at approximately 580 ms (at zero offset). The direct wave travels from the source (near the ocean surface) to the receiver (on the seafloor), and corresponds to approximately 860 metres depth. Reflectors below the seafloor arrival

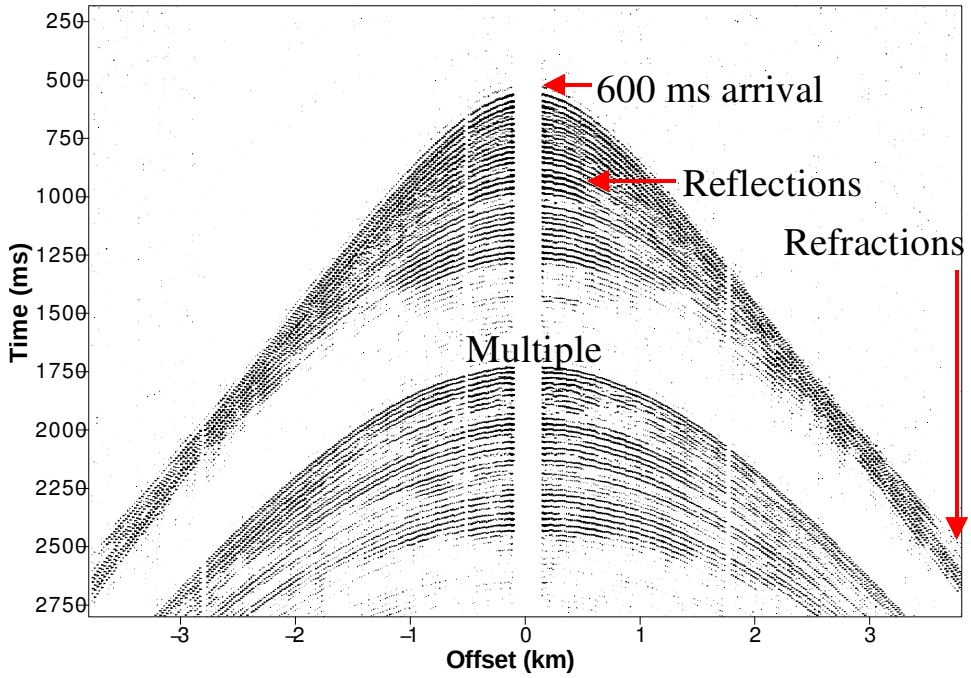

Figure 4.3: Seismic section of wide–angle data, channel 1. The hyperbolic features are reflections, while the linear features are refractions. This is a plot of travel time (ms) versus offset (km).

undergo two−way travel time, because the acoustic signal must travel through the sediment, reflect , and propagate to the OBS. Useable data for this analysis is present to 900 ms below the seafloor arrival, and is followed by the bottom multiple, which occurs at around 1750 ms below the seafloor arrival (at zero offset) which is approximately 3 times the seafloor arrival time (due to 3 way travel time). The four channels (hydrophone, z, x, and y geophones) were all plotted, but the vertical geophone (channel 2) displayed the best results, especially for analysis of the shallowest reflections (plots from all channels are displayed in appendix A).

The velocity of the sediments can be determined by fitting travel time curves from a velocity−depth model, to the observed reflectors and refractors. The geometry of each reflector and refractor will differ, depending on the properties of each layer (such as the velocity gradient). Accurately fitting travel time curves to both the reflectors and refractors for each layer, will yield a more representative model than by fitting either the reflectors or refractors alone. Both the reflectors and refractors were modelled in this study, but primary emphasis was given to reflectors.

$$t_c = t_r - t_0 = (t_0^2 + x^2/V_w^2)^{1/2} - t_0 = (z^2/V_w^2 + x^2/V_w^2)^{1/2} - z/V_w \quad (4.1)$$

$$t_0 = z/V_w \quad (4.2)$$

The OBS data were displayed using normal moveout correction (NMO correction, defined in Formula 4.1), where t_r is the uncorrected travel time, t_c is the corrected travel time, z is the water depth, V_w is the velocity of water, and x is the offset (Reynolds, 1997). A velocity of 1480 m/s was used for a reducing velocity (average velocity of seawater). NMO correction has the effect of flattening the layer which has the same velocity as the reducing velocity, in this case the water layer. NMO correction

is used to differentiate between reflectors and refractors that have similar velocities. It is especially useful for the shallow reflectors, which may be difficult to identify in the non–NMO corrected plot.

The data displays a "ringy" nature. A reflection that should occur as one arrival is displayed as several repetitive arrivals. The ringing in the data is probably a result of a problem with the OBS instrument, or ringing in the sleeve gun (though it is apparent in all the recievers, possibly implying a problem with the sleeve gun). The ringy nature of the data has posed a problem. It is important that a "pick" not be an artifact (in this case a reverberation); this would yield inaccurate results. The ringy data has also posed a problem in observing the shallow reflectors, because the direct wave from the source is of much higher amplitude than the shallow reflectors, which are masked by the artifacts from the direct wave. Spiking deconvolution has been applied in an attempt to merge the several parallel arrivals into one arrival. The deconvolution did succeed in merging some of the arrivals, but it decreased the signal of the shallow reflectors, which have a small amplitude relative to the direct wave. For this reason, deconvolution was not used in the processing of the data.

The data was filtered using a trapezoidal bandpass frequency filter. The frequency spectrum of the data, and the filtered plots are displayed in Figure 4.4. This technique filters the data between a specified range. From the frequency spectrum, it is clear that there are 3 main *peaks*, which can be separated out from the rest of the data. The attempt was to filter out the lower frequency data, which is likely masking much of the higher frequency data. The result of the filtering was successful, the higher frequency data resulted in better definition of shallow reflectors, while the low frequency

data defined the deeper structure. However, the ringy signature of the data is more apparent in the high frequency filter, which makes it difficult to determine which reflectors have a large amplitude. The apparent number of reflectors seem to increase greatly in the higher frequency data. Therefore both the unfiltered and high frequency filters were used in the analysis, depending on the requirements of the situation.

Velocity modelling of the OBS data was performed using software developed at Dalhousie, which uses RAYINV to generate the ray traces (Zelt, 1992). The velocity model was developed by creating slightly dipping layers (to simulate the dip of the sediment layers, as discussed in section 5.3) with differing velocities, and examining the travel time curves that these layers produce. The travel time curves are red lines, overlain on the seismic section. The fit of the travel time curves to the actual reflectors and refractors is judged visually. Travel times are calculated by ray tracing in which the geometry of the travel time curves are calculated based on the velocity and depth characteristics of the velocity model. The first layers to be modelled are the shallowest, followed by progressively deeper reflectors. This process is known as forward modelling. This is an iterative process, and can be time consuming.

Two methods were used to determine the velocity structure of the sediments. The sediments were modelled with a simple 2 layer sediment (and water layer) model, containing 2 different gradients. This model was adjusted to fit the refractor, with the curvature of the refractor describing the velocity gradient. The reflections were modelled using the seismic horizons picked on the single channel reflection seismic lines. The travel time (below the seafloor) for the single channel data should be equal to the travel time for the OBS data (because both undergo two−way travel time). The model was first

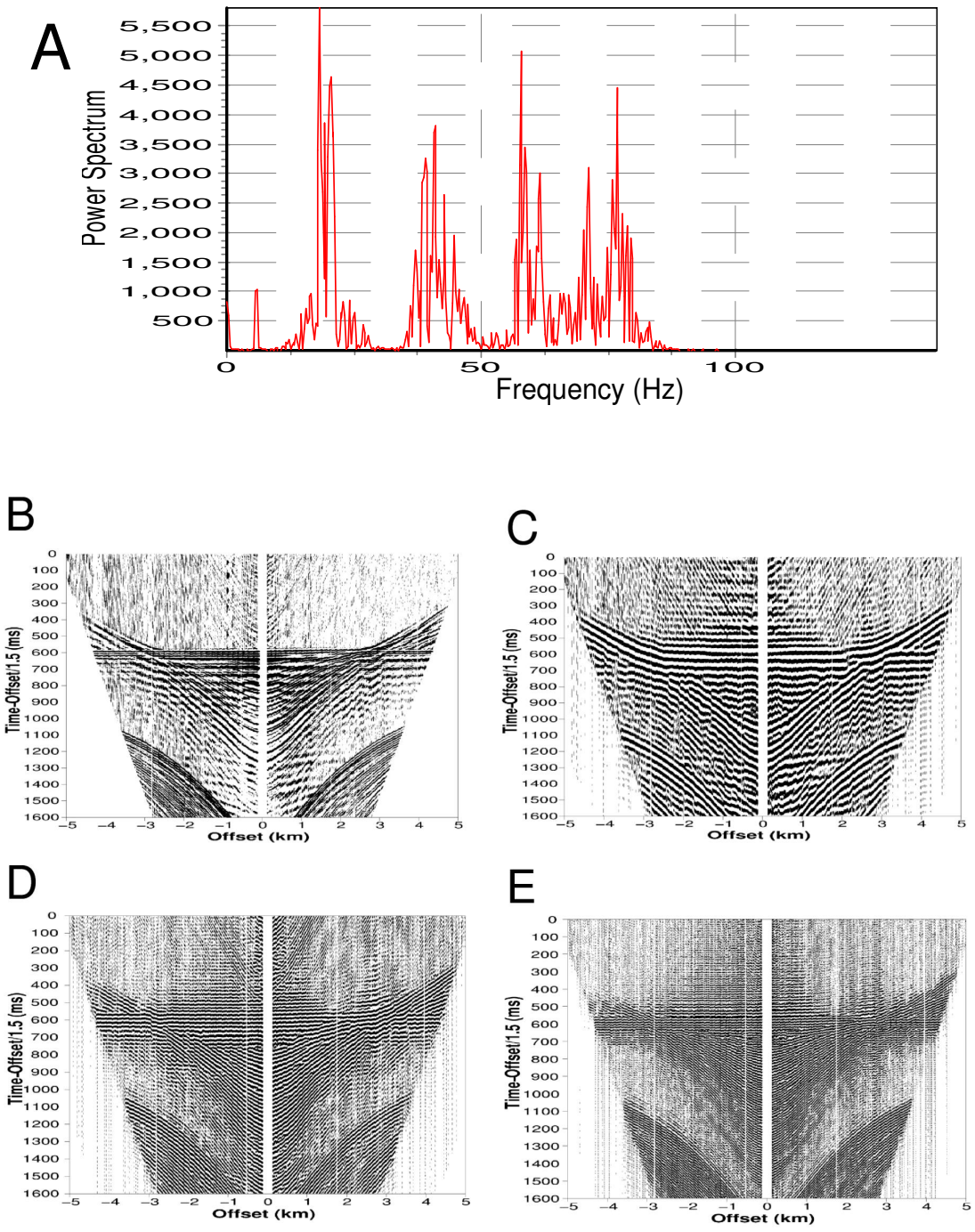

Figure 4.4: (A) Frequency spectrum of OBS channel 2 data, at shotpoint 825 (zero offset). Note the large spikes at approximately 15, 40, 60, and 80 Hz, (B) Unfiltered OBS data (NMO corrected), (C) Channel 2 filtered to include data between 0 – 30 Hz, (D) Channel 2 filtered to include 30 –55 HZ, and (E) Channel 2 filtered to include 50 – 100 Hz.

constructed to fit the refractions, then refined to fit the reflections. The range of velocities near 200 mbsf was estimated by determining the range of velocities that were within ± 15 ms at maximum offset. This analysis yields information about the error involved in this analysis, which is discussed in chapter 5.

4.2 Towed Array Equipment Used on Cruise HUD2001−048A

The single channel reflection data used in this study, was collected on cruise HUD2001−048A; conducted from August 28th to September 5th, 2001. Detailed information on the equipment and techniques can be found in the cruise report (Mosher, 2001). Two 40 in^3 sleeve guns were used as the sources, which were towed behind the ship. The guns were mounted on a metal frame, 0.8 m apart, and 0.54 m below the beam. The frame was secured to a Norwegian float. The airguns were 2.54 metres below sea level while the ship was stationary, but were likely less than 2 metres below the surface while the ship was underway due to surfing. The rate of fire of the sleeve guns was usually once every 4 seconds, but sometimes 3 or 5 seconds in certain water depths (Mosher, 2001). Two single channel hydrophone arrays were used as receivers. The 22.5 metre Benthos array consists of 25 hydrophones, at 36 inch (0.91 m) spacing intervals.

This array was towed 200 m behind the ship. The received signal was digitised at a sample interval 500 μs, over a window size of 2048 ms, with a low cut and high cut of 35 and 1000 Hz respectively. The second array was a 10 metre Geoforce GF30, which consists of 21 hydrophones, at 0.3 metre intervals. It was towed parallel to the sleeve gun array, on the starboard quarter. The Benthos data were the only single channel data presented in this report.

Delay times for the water column were controlled by the PMITS system, which omits collection of data in the water column for profiles in deep water. The seismic data was displayed on an EPC 9800 Thermal Graphic Recorder, and recorded in SEGY format on Exabyte tapes, using the AGC_DIG data logger. Calm seas helped in the acquisition of good quality data.

4.2.1 Single Channel Seismic Data Analysis Procedure

The raw SEGY data collected from the single channel reflection seismic cruise was stored on Exabyte tapes. The data files (records) were merged and parsed. The navigation data was merged with the shot data, and stored as a separate .utm file using UTM coordinates of zone 20, and datum NAD 83. The delays that were introduced with the PMITS system (to minimise file size) were corrected. This file was saved in the SEGY format. The final SEGY file and the georeferencing file (.utm) was imported into Kingdom 2d/3d seismic software package. The delay of each seismic line was adjusted to a common value, so the lines would display equal travel times at the intersections between the lines.

Picking of horizons was performed, starting with the seafloor. The automated picking routines of Kingdom 2d/3d are not intended for data of this high resolution. Therefore manual picking was performed for much of the data. The initial horizon picking was later completed by Simon Newton at the Bedford Institute of Oceanography, Geological Survey of Canada (Atlantic), the results of which are displayed Figure 5.4.

The reflection seismics give an excellent window on the structure of the subsurface, and are a good companion to the multibeam bathymetry data. The seismic data is too widespread to obtain an accurate 3 dimensional model of failures, whereas the

multibeam bathymetry yields a complete view only of the sediment surface. Using both tools can help to determine the features and extent of sediment failures.

CHAPTER 5: RESULTS

5.1 Gas Hydrate Stability Model

The thickness of the gas hydrate stability zone is an important part of this thesis. It dictates where to examine the OBS data for indications of anomalous velocities, or lack thereof. It also indicates where to examine the single channel reflection data for the presence of a BSR, and where a BSR may be out of place. A change in the geothermal gradient of 10 °C/km can result in a 90 metre difference in the depth to the BGHSZ, therefore accurate measurements are essential to obtaining a representative depth to the BGHSZ.

A stability model can be produced for a location where the seafloor temperature, geothermal gradient, and depth to the seafloor are known. The pressure–temperature conditions of the sediment can be plotted on the same graph as the empirical gas hydrate phase boundary discussed in chapter 3, derived from Peltzer and Brewer (2000). If the pressure–temperature (P–T) regime of the sediment is in the hydrate stability field, gas hydrate will be stable (assuming all other conditions, such as methane concentration and flux are met). The point at which the P–T regime of the sediment crosses the hydrate phase boundary is where hydrate becomes unstable in the sediment. The equation for the phase boundary given in Peltzer and Brewer is given by equation 3.1 in chapter 3 (2000). This equation is compared to several other proposed equations for the phase boundary, and appears to be the most accurate.

Gas hydrate is quickly dissolved in sea water. Only regions with very high methane flux have hydrate in contact with sea water at the ocean floor, such as Hydrate Ridge off of British Columbia (Chapman, 2001). Therefore, the zone of hydrate stability

is between the lower phase boundary (the methane gas – hydrate contact), and the seafloor.

The depth and water temperature data is taken from NOAA CTD data, collected in 1995 (NOAA World Ocean Database, 1998). The measurement stops at 756 metres water depth. The seafloor temperature is extrapolated from these data, to be approximately 4.2 °C. The geothermal gradient of 41 °C/km was measured from the Acadia K–62 deep water well (Reiter and Jessop, 1985). A change in the geothermal gradient has a large affect on the depth to the BGHSZ, therefore an accurate measurement is key to obtaining an accurate result. The accuracy of the geothermal gradient measurement has been debated (the heatflow values appear to be too high) by Issler and Beaumont (1986). Therefore a range from 30 °C/km to 50 °C/km was also used, but the range of 30 °C/km to 40 °C/km is the most likely. A more accurate geothermal gradient measurement would be required to accurately determine the thickness of the GHSZ.

The most straightforward method of determining the thickness of the GHSZ is to plot the phase boundary and local P–T conditions, and determine the difference in pressure between the seafloor and the BGHSZ. This pressure difference corresponds to the thickness of the sediment in which hydrate is stable. For a depth approximation, it is assumed that the sediment follows a hydrostatic pressure regime. For sediments deep below the seafloor, or in sediments where elevated pore pressures are known or expected, a more accurate pressure–depth relationship should be used.

This stability model (Fig. 5.1) indicates that the BGHSZ should occur at approximately 200 mbsf for a 41 °C/km geothermal gradient (approximately 160 and 300

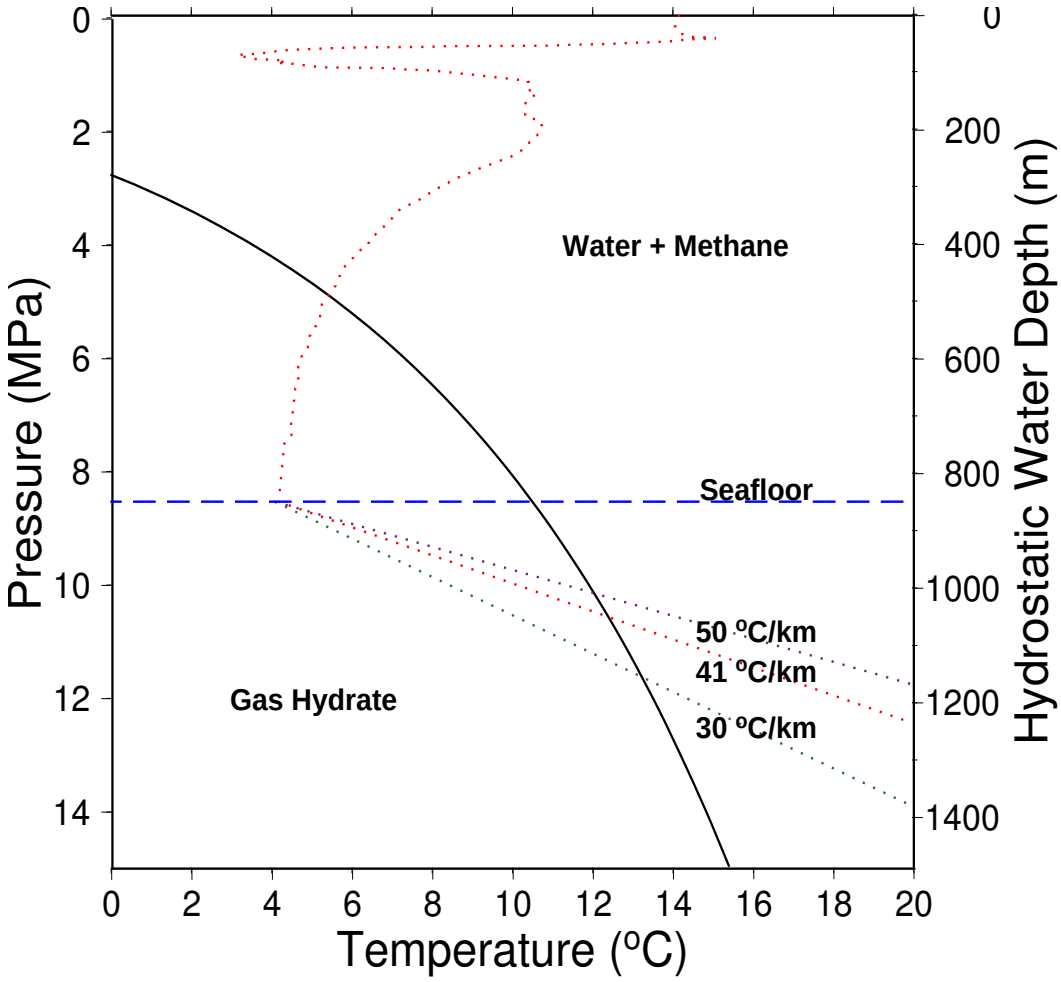

Figure 5.1: Phase diagram for the OBS location, using a 41 °C/km geothermal gradient, and 4.2 °C seafloor temperature (The 30 °C/km and 50 °C/km geotherms are included for comparison). The dashed blue line represents the seafloor, the dotted red line is the hydrothermal / geothermal trend, and the solid black line is the gas hydrate phase boundary (phase boundary after Peltzer and Brewer, 2000).

mbsf for the 50 °C/km and 30 °C/km respectively). It is assumed that the geothermal gradient at the well site is the same for the OBS location, due to the relatively close proximity of the well to the OBS site (Figure 5.3).

There is a BSR feature within 90 km of the study area, which has been identified on industry seismic data. The depth to the BGHSZ was estimated for the BSR feature, using the same parameters used for the OBS location. The depth to the theoretical BGHSZ is similar to the BSR depth. This indicates that the stability calculations for the

OBS location are accurate enough for the purposes of this study.

5.2 Multibeam Bathymetry

The multibeam bathymetry image (Fig. 5.2) is a visual representation of the morphology of the study area. The dataset is a relatively new acquisition to the Bedford Institute of Oceanography, and has revolutionised the interpretation of seafloor features. It has been shaded, to highlight small features. The colour corresponds to depth,

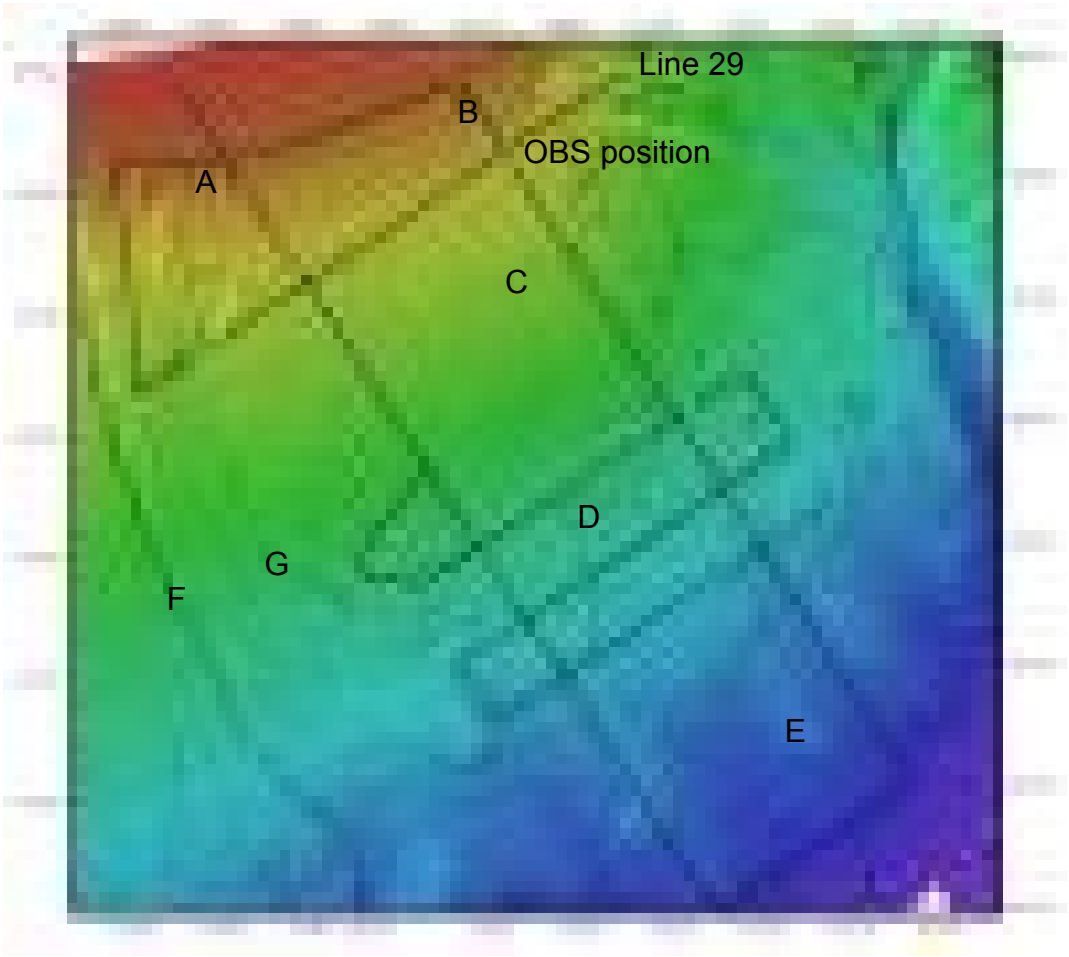

Figure 5.2: Multibeam bathymetry image of the study area. The black lines are the single channel reflection lines, while the blue circles are the OBS locations. The upper OBS location is the only one used for this report. A and B are the head scarps of the upper slope failures, and the source of the western and eastern disturbed zones respectively. C is a midslope failure, D is a lower slope failure, and E is a doming structure. F and G are the West and East Acadia valleys respectively (courtesy of Marathon Oil, Murphy Oil Company Limited, PanCanadian Petroleum Limited, and Norsk Hydro. Collected by C&C Technologies).

although the colour scale can not be displayed due to data confidentiality. The image has been downsampled from the full resolution (the full resolution image is restricted). However, many interesting features are still quite obvious. The doming structures of the salt diapirs show up well on the lower part of the image (E). The East and West Acadia valleys are clearly displayed (F and G). Large scarps are visible on the flanks of the Verrill Canyon, and smaller scarps are visible throughout the study area, which correlate well to the failures of the eastern and western "disturbed areas".

It is useful to compare the failure map (Fig. 5.3) to the multibeam bathymetry image (Fig. 5.2). There are several smaller features that are visible on the multibeam image, which are not depicted on the failure map. Correlations between what were previously thought of as distinct features, have been made in the study area. An example of this is the head scarp on the mid−slope of the study area, which appears to be possibly one failure.

The upper slope failures are quite important to this study. These failures appear to head at approximately 500 metres water depth, and they all display the same approximate head wall height. Reflection line 31 (Appendix B) appears to be the only seismic line that comes close to these failures. It is possible that these failures originated as a result of hydrate dissociation at its uppermost extent, where gas hydrate potentially tapers out (Piper, 2001).

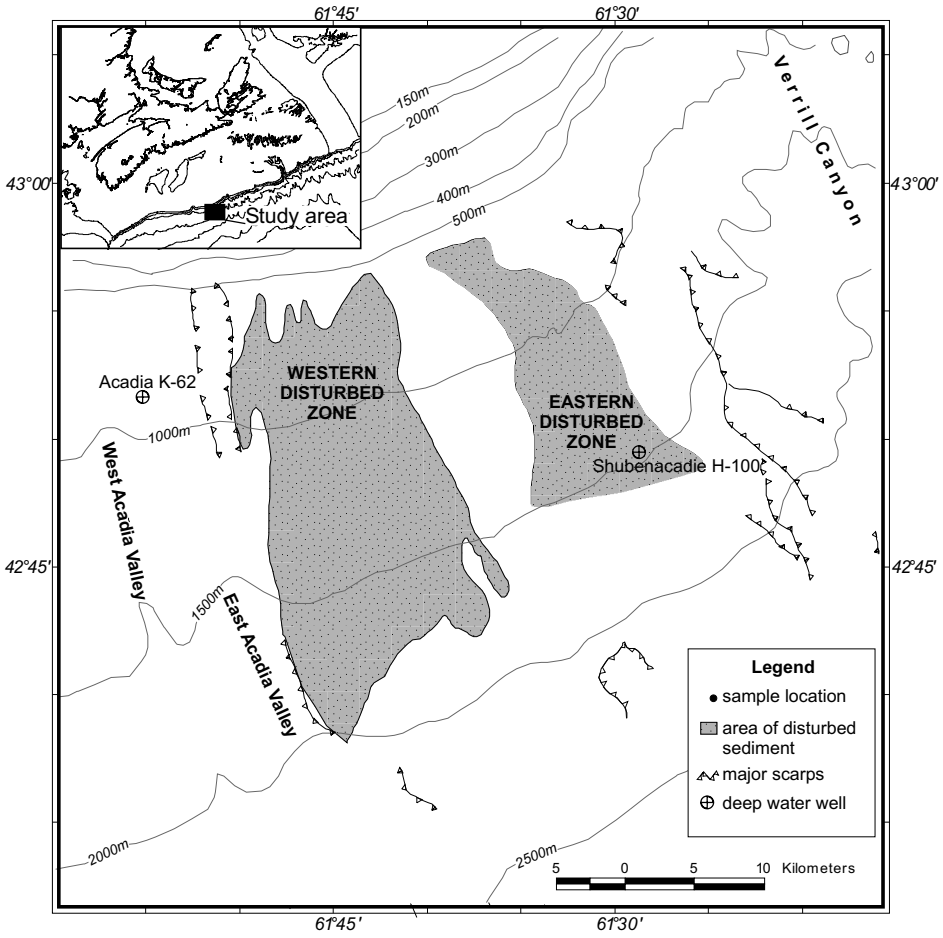

Figure 5.3: Map of Verrill Canyon area, the shaded areas are the western and eastern disturbed zone. Major head scarps are indicated. The dashed line indicates the extent of the till tongue , while the grey areas indicate debris flows that originated from the upper slope failures (Mosher D.C., personal communication, 2002).

The multibeam bathymetry data is an excellent tool in studying the morphology of the failures, but it is only one tool of many that must be employed to get a complete view of the processes responsible for producing the observed features.

5.3 Single Channel Reflection Seismic Data

There are several important pieces of information that can be acquired from the single channel reflection seismic data. The most obvious would be the presence of a BSR which would indicate the presence of gas hydrates. Thorough examination of the seismic lines has not revealed any BSRs. However, the lack of a BSR does not

necessarily prove the absence of gas hydrate. The lack of a BSR in hydrated sediments would likely indicate the lack of a free gas zone beneath the hydrate (Xu and Ruppel, 1999). The hydrophones (non−acceleration cancelling) do not record the low frequencies necessary for identification of the phase inversion (Mosher D.C., personal communication, 2002). The seismic lines do not appear to show blanking associated with high concentrations of gas hydrate, and bright spots associated with free gas are absent from these data. The single channel reflection seismic lines studied in this report are illustrated in appendix B. The horizons have been omitted, as they are currently being digitised and revised for other studies at the Bedford Institute of Oceanography, Geological Survey of Canada (Atlantic).

A second important piece of information is the structure of the failures, that may have been influenced by gas hydrate dissociation. The depth to the failures likely indicates the horizon on which the sediment failed. If the horizon is close to the BGHSZ, it may indicate that elevated pore pressures from gas hydrate dissociation could have been partially responsible for the failure. The maximum height of head scarps on the lower and middle slope failures is 80 m, which is far shallower than the BGHSZ at these depths (the BGHSZ is approximately 350 mbsf for water depths of 1500 m). Lines 32, 34, and 41 (Appendix B) are dip lines that show the structure of the middle and lower slope failures.

The failures on the middle and lower slope are excluded from this study, because the influence of gas hydrate dissociation on pore pressure would be lower than on the upper slope, and salt tectonism makes determining the cause of failure more complicated. The seismic lines do not cross the upper slope failures (Fig. 5.2), so analysis of the slump

features cannot be performed from the single channel reflection seismic data.

Line 29 (Fig. 5.4) is a strike line that is nearly parallel to the OBS shotline (Appendix A). It is the most useful reflection line for this study, because it can be assumed that the stratigraphy is nearly identical to the OBS site. The horizon data is important because it gives additional information about the sediment, such as age lithology, and depositional environment. The carmine horizon is important because it marks the onset of glaciation, approximately 0.45 ma (Piper and Normark, 1989). The wide−angle data indicates a abnormally high velocity near the carmine horizon, as is discussed in the next section of this chapter.

Figure 5.4 depicts the entire seismic section of line 29. This seismic line is located approximately 410 metres distance upslope from the OBS location, and therefore the horizons should be very similar. Shotpoint 1000 is very close to the intersection of lines 29 and 32, and to the OBS location. A higher detail region of the seismic section shows that the strata to the left of the OBS location is quite flat, and therefore can be described by a model with slightly dipping layers.

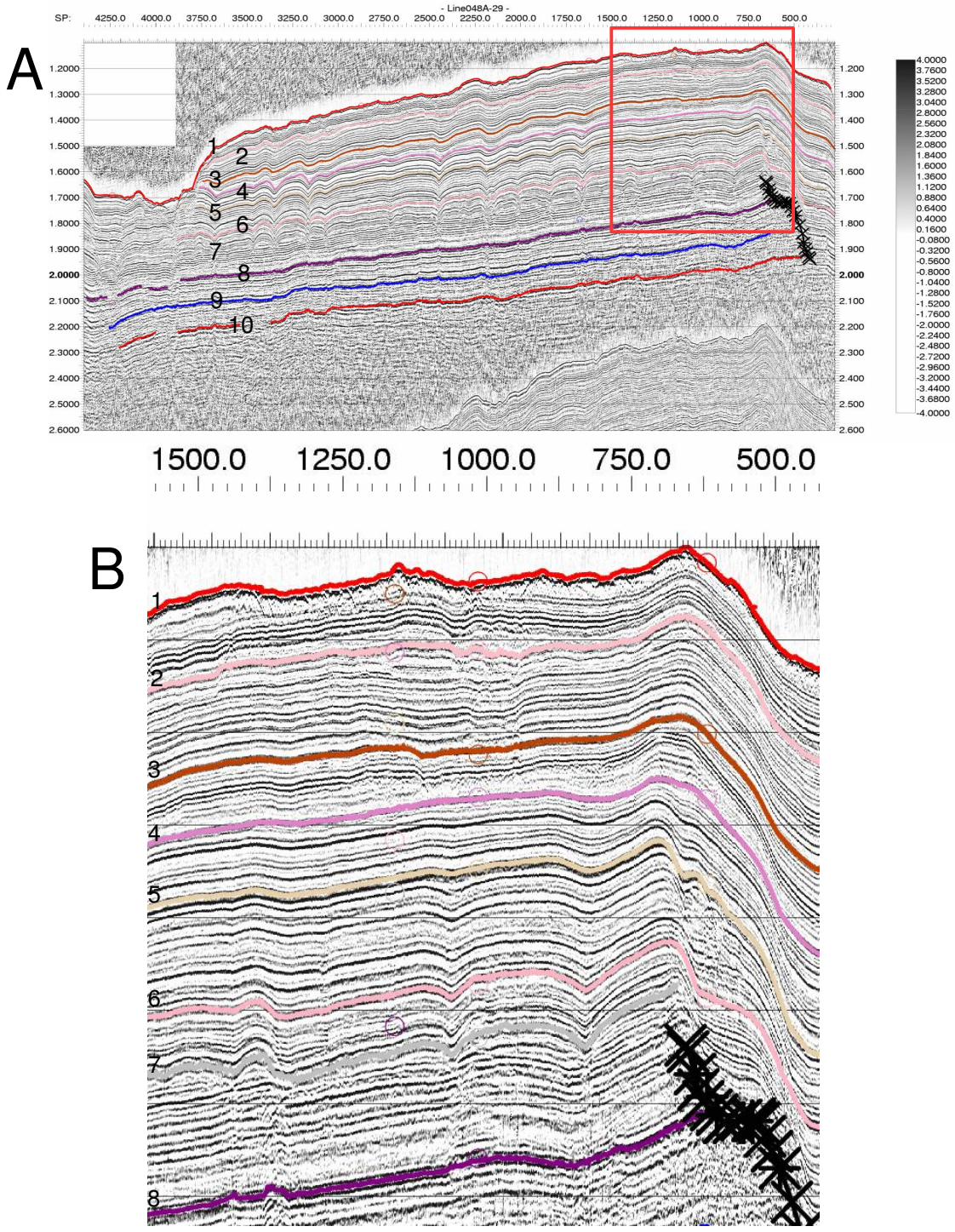

Figure 5.4: (A) Single channel reflection line 29 from Hudson cruise 2000–048A. An *automatic gain control* (agc) filter has been applied. The plot is travel time vs. shotpoint. The horizons are 1 seafloor, 2 light red, 3 brown, 4 carmine, 5 flesh, 6 rose, 7 grey, 8 magenta, 9 blue, and 10 red. The strong feature beneath the red horizon is a multiple. (B) Region of seismic plot that is of importance to the wide–angle data (zoomed section from red box in part A, OBS position is near shotpoint 1000). Note that the strata on the left side shotpoint 1000 is much flatter than the faulted sediment on the right side.

5.4 Wide−Angle Velocity Modelling

Error analysis conducted on the OBS data has been performed on the upper 200 metres of sediment. Two models were produced, which display travel time curves that fit both the reflectors and refractors to approximately ±35 ms at maximum offset (the difference between the red travel time curves in Figure 5.5 and the reflector / refractor that was modelled at maximum offset). The final velocity model fits the refractors / reflectors at least as well as the error checking model. The minimum velocity model (the minimum velocity for approximately 200 mbsf) shows a velocity gradient that increases from 1550 m/s at seafloor to 1770 m/s at approximately 200 mbsf (Fig. 5.5). The maximum velocity model (for approximately 200 mbsf) displays a linear velocity gradient from 1550 m/s at the seafloor to 1840 m/s at approximately 200 mbsf (Fig. 5.6). These models imply an error of approximately ±35 m/s in velocity estimates near 200 mbsf, though perhaps greater in deeper sediment.

The increase in velocity of a hydrated sediment is dependent on the concentration of hydrate (low concentrations will yield lower velocities, relative to high concentrations). Therefore determining the velocity of the shallow sediments is of great importance to this study. The analysis indicates that velocities outside of this range would probably not fit this model, and are therefore probably not seen in the sediment. Velocities in deeper sediment have a larger velocity range, due to the cumulative influence of overlying sediment velocities.

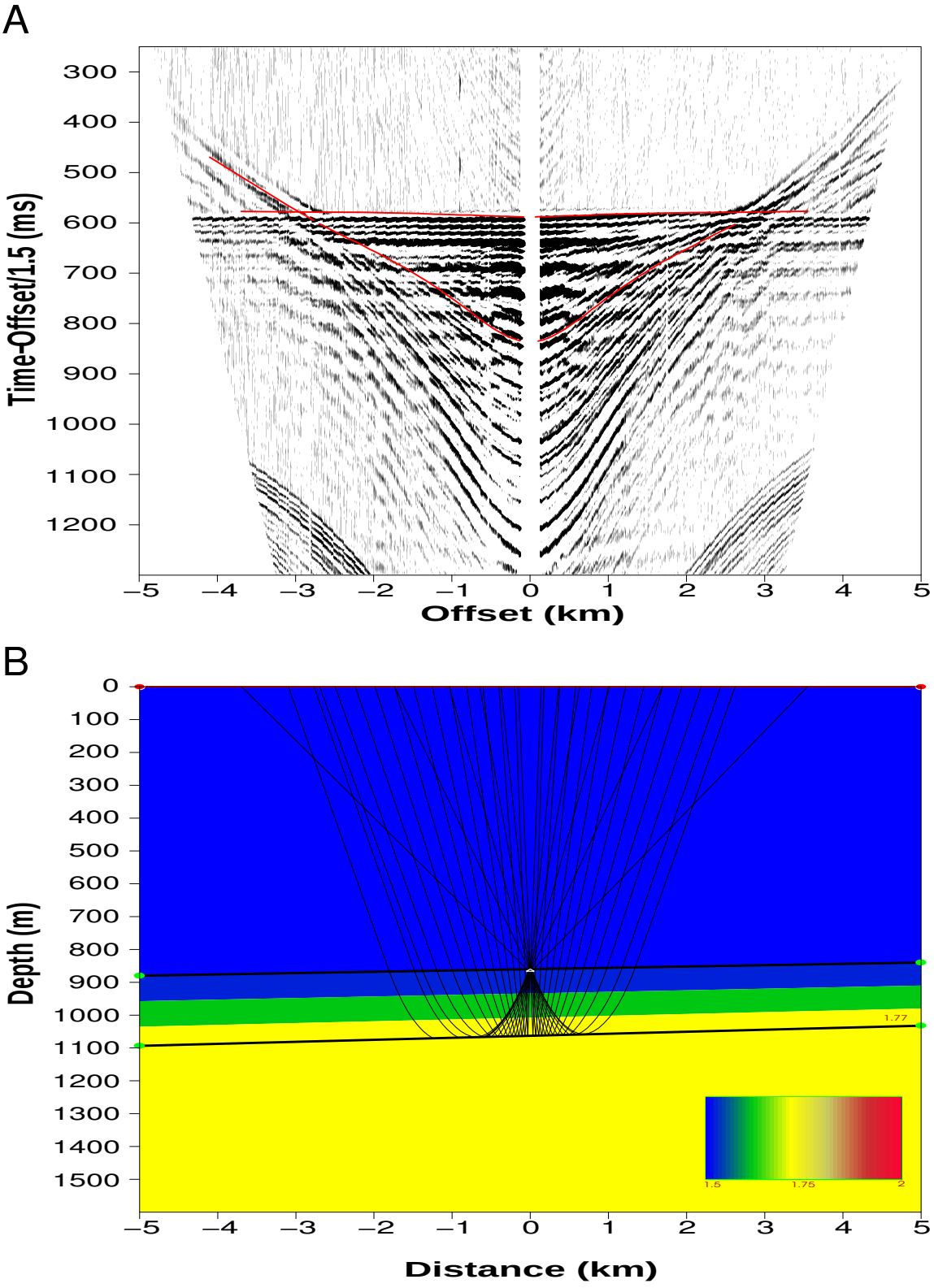

Figure 5.5: (A) Seismic section, and travel time overlay (red) of minimum velocity model. (B) The velocity model indicates that 1770 m/s is the minimum velocity that fits the data at 200 mbsf.

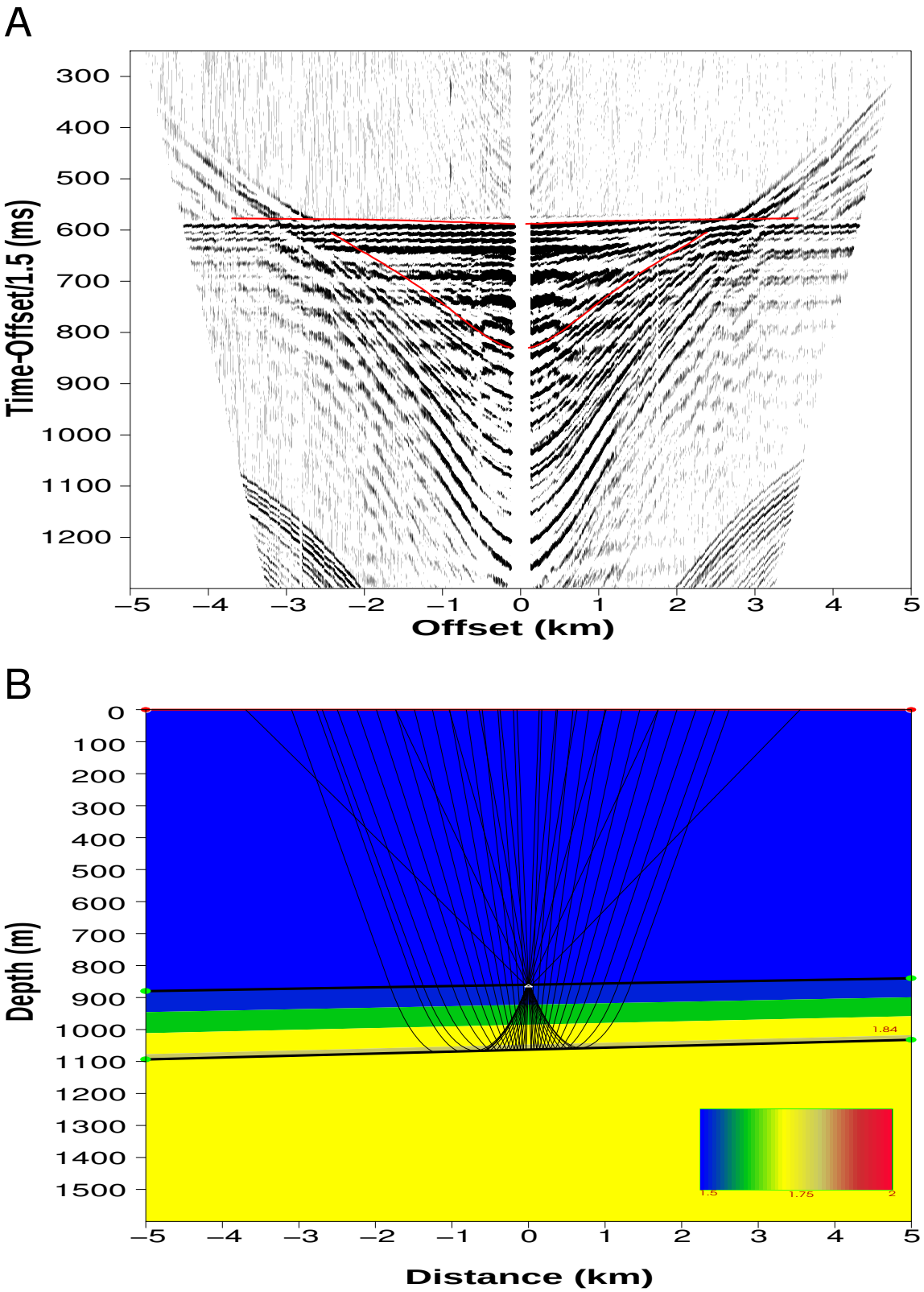

Figure 5.6: (A) Seismic plot, and travel time overlay (red) of maximum velocity model. (B) The maximum velocity model indicating that 1840 m/s is the maximum velocity that fits the data at 200 mbsf.

The *refraction* model (Fig. 5.7) uses a simple 2 layer velocity model, because the data does not extend to great enough offset to model deeper refractors. The resulting model displays a high gradient up to approximately 200 mbsf (1550 m/s at the seafloor to 1800 m/s at approximately 200 mbsf), which is then underlain by a lower velocity gradient (1800 m/s at approximately 200 mbsf to 2100 m/s at 550 mbsf). The western side of the OBS was studied, but the refractor is also matched on the eastern side. The travel time curve matches the refractor to within ±5 ms on the western side (Fig. 5.7). The refractor data is important because it can be compared to the reflection model, it also asserts that there cannot be a low velocity zone in the sediment depth analysed.

The model was developed using velocity gradients to describe many small layers. The ringy nature of the data made it difficult to describe any horizons in the very shallow sediment. A gradient from approximately 1550 m/s to the first reflector / refractor that can be accurately modelled, describes the shallow sediment. The strata west of the OBS location appears to be sufficiently flat to allow the use of a simple velocity model, which has flat layers (Fig. 5.4).

The seismic horizons that were picked in the single channel reflection seismic data were used to describe the layers in the velocity model. The difference in travel time between the seafloor horizon and the lower horizons were calculated (interval travel time). A velocity model (the *reflection* or *horizon* model) was developed which used the "interval travel time" described, as both seismic data should share the same interval travel time. The resulting velocity model should adequately describe the sediments. The seismic horizons that were picked in the single channel reflection seismics do not necessarily represent the strongest acoustic reflectors, but they should be apparent on the

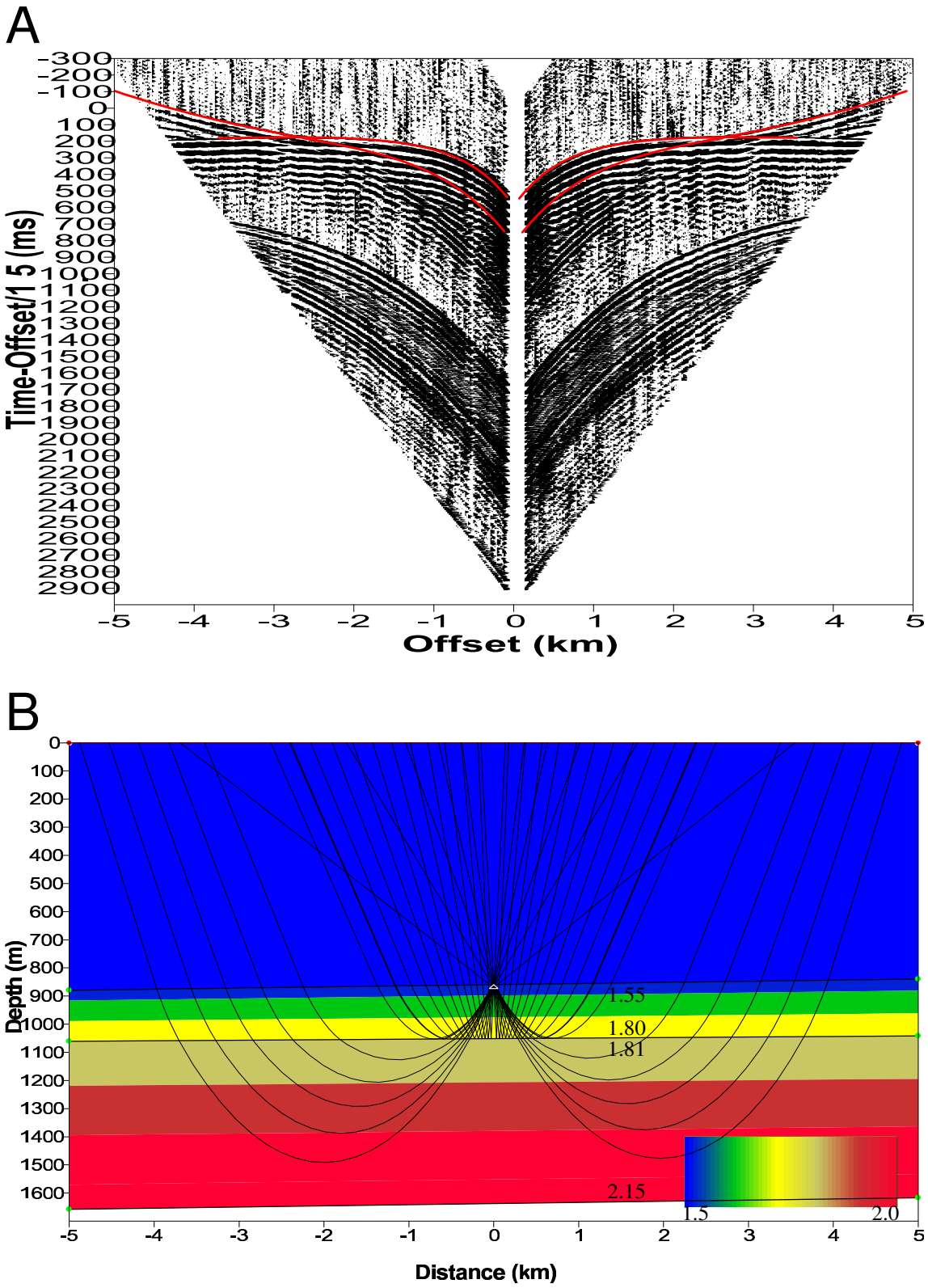

Figure 5.7: (A) Plot of OBS data – 2 layer refraction model, using a reduction velocity of 1550 m/s, with travel time curves overlain. (B) The velocity model with velocities indicated, and ray paths displayed.

OBS data. Using the horizons as layers in the velocity modelling will likely yield information about the velocity of the sediment which the horizons represent. The velocity information about specific horizons can be applied to other areas that have been correlated with horizon picking, making this technique quite valuable. There is a high degree of similarity between the *high amplitude* velocity model and the *horizon* velocity model, therefore only the *horizon* model will be discussed.

The reflection model (Fig. 5.8) is the basis for the velocity estimates used in this report. The reflections were fit in this model, in addition to the refractors. This should yield more reliable results. The travel time curves fit well on both sides of the OBS data, but were fit to the western side of the OBS due to faulting on the right (eastern) side. The refractions are the bending rays in part B of Figure 5.8, while the linear rays that reflect off boundaries are reflections. The refractions do not terminate in the seismic section (they would terminate if there was a low velocity zone), therefore there is probably not a low velocity zone beneath approximately 200 mbsf. Table 5.1 summarises the velocity and depth information from the reflection model, derived from the OBS data at 0 m offset.

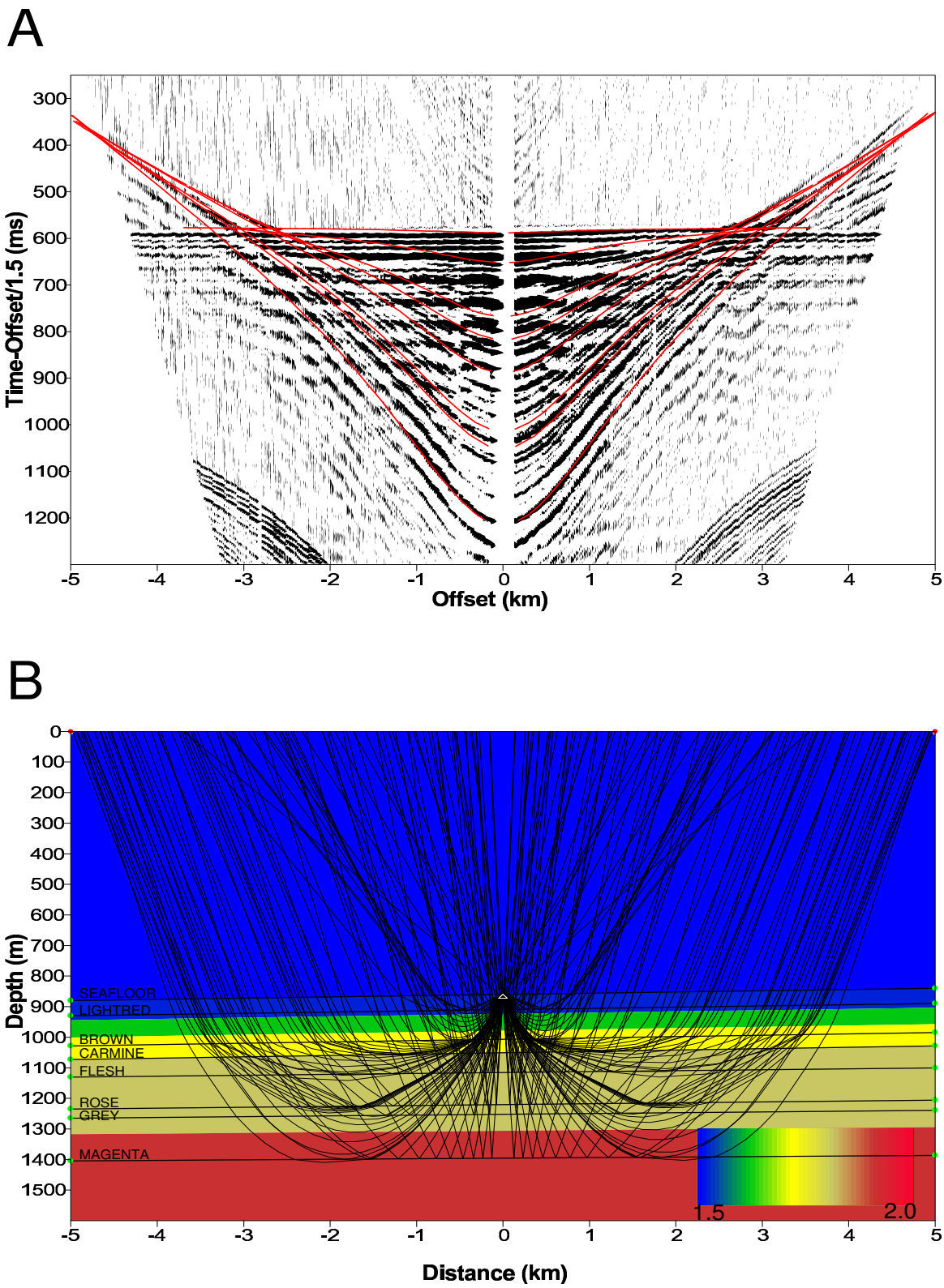

Figure 5.8: (A) NMO corrected OBS plot (channel 2), and travel time overlays for the *horizon* model. (B) Velocity model and ray paths, with horizon names indicated.

A sediment containing substantial amounts of gas hydrate would display an abnormally high velocity gradient, which would return to a normal gradient at depths deeper than the BGHSZ. Sediments that contain gas hydrates, and have a free gas zone beneath them will display an anomalously low velocity beneath the BGHSZ, due to the effect of the free gas. These velocities can be close to the velocities of water, which contrast greatly with the high velocities seen in the overlying hydrated sediment, and are lower than the equivalent value from the regional gradient. The velocity of a free gas zone studied at the Blake Ridge indicates velocities near 1500 m/s (Holbrook et al., 1996).

Reflector	Two way travel time below seafloor (s)	Depth below seafloor (m)	Interval velocity (m/s)
Seafloor	0.000	0	1550
Light Red	0.072	50	1550 – 1585
Brown	0.182	147	1585 – 1750
Carmine	0.234	191	1790 – 1800
Flesh	0.309	255	1800 –1810
Rose	0.428	370	1820 – 1830
Grey	0.467	404	1840 – 1850
Magenta	0.625	559	1870 – 1950

Table 5.1: Summary of 2 way travel times, depth below seafloor, and interval velocity based on the wide−angle Reflection model.

5.4.1 Velocity Structure

The regional velocity of the area has been estimated using vertical seismic profile data from Acadia, Tantallon deep water wells, and wide−angle velocities from the Sohm Abyssal plain (East Coast Basin Atlas), to obtain an average velocity gradient. A linear trend has been applied to these data, to approximate the velocity gradient of local sediments (Fig. 5.9). This velocity gradient is also included on the local velocity−depth plot, as a comparison to estimated velocities.

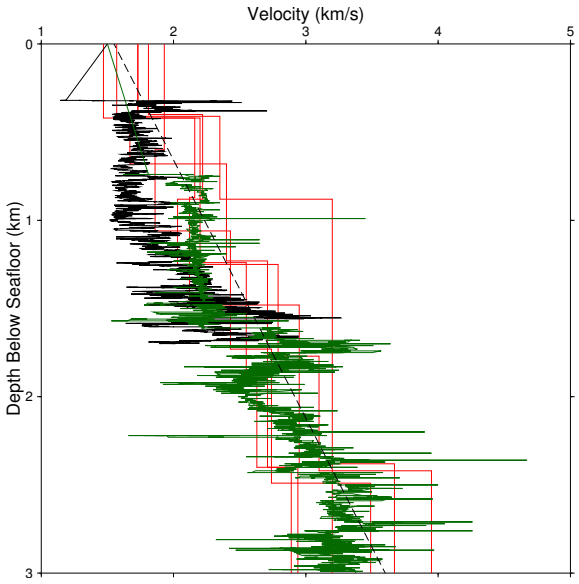

Figure 5.9: Regional velocity depth plot. The green line is vertical seismic profile data (VSP) from the Tantallon deep water well, the black is from the Acadia K–62 well, the red lines are wide–angle data from the Sohm Abyssal plain, and the dashed line is the regional trend

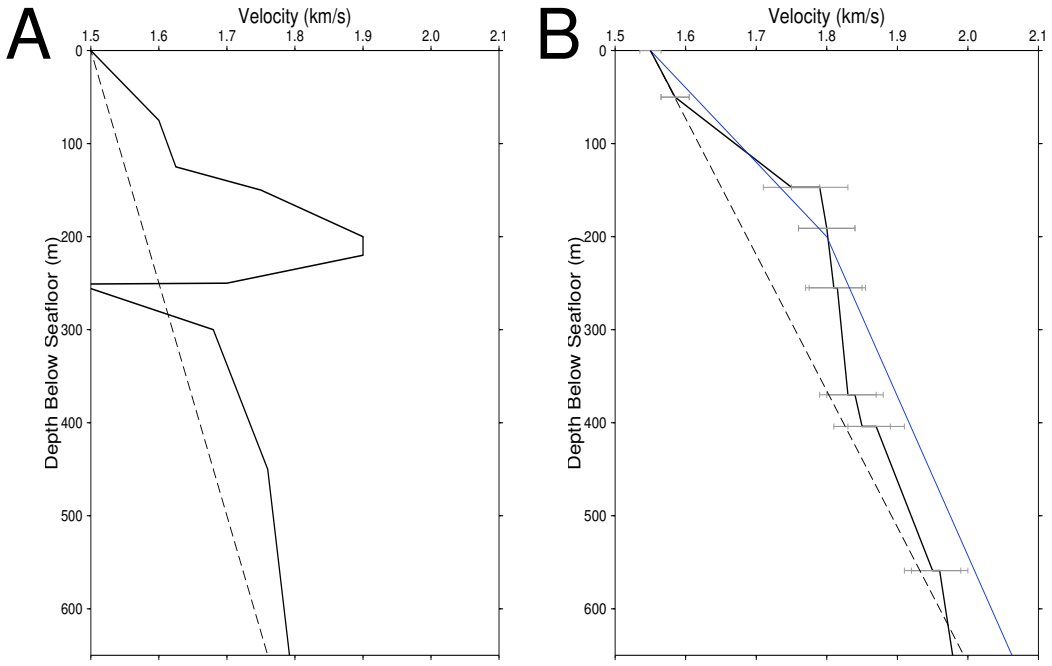

Figure 5.10: (A) The velocity vs. depth profile for the sediments studied by Yuan et al. on the Cascadia margin (1996), as a comparison to the local velocity structure . The solid black line is the approximate velocity structure of the sediments, while the dashed line is the regional trend. This plot displays a high gradient from the seafloor to approximately 230 m, then a large velocity inversion to approximately 1480 m/s, followed by a trend similar to the regional gradient. (B) Plot of velocity vs. depth (below sea level) from the *reflection* model of the study area. The blue line is the refraction data, the solid line is the reflection data (with error bars of approximately ±40 m/s), and the dashed line is the regional trend.

The velocity–depth profile for the OBS location displays the reflection velocity estimates and the velocities estimated from the 2 layer refraction model. The reflection data is the highest resolution data available for this region. The reflection and refraction data display a high velocity gradient in the first 200 mbsf, followed by a lower velocity gradient. The reflection model shows the velocity returning to a gradient similar to the regional gradient at approximately 380 mbsf. The refraction model displays a gradient deeper than 200 mbsf that slowly converges with the regional velocity gradient, but is almost parallel to it.

Sediments on the northern Cascadia continental slope containing high concentrations of gas hydrates have been studied by Yuan et al. (1996). The Blake Ridge is another location that has been studied to examine the relationship between seismic velocities and gas hydrate concentrations. The Cascadia site is a better analogy, because the water and BGHSZ depths are closer to that of the study area. Yuan et al. (1996) propose that the sediments reach a maximum gas hydrate concentration of 20 – 30% of pore space. The BSR (assumed to be coincident with the BGHSZ) occurs at approximately 230 mbsf, which is similar to the theoretical BGHSZ studied in this report (Fig. 5.10A).

The sediments that Yuan et al. (1996) discuss reach a maximum measured velocity of 1900 m/s, which is approximately 100 m/s greater than the sediments studied on the Scotian slope. The data required to quantify the percentage of pore space occupied by gas hydrate described by Lee et al. (1993B), such as porosity, compression velocity of the matrix, compression velocity of hydrated sediment, is not yet available for the BGHSZ in the study area. Therefore a first approximation model was used, assuming

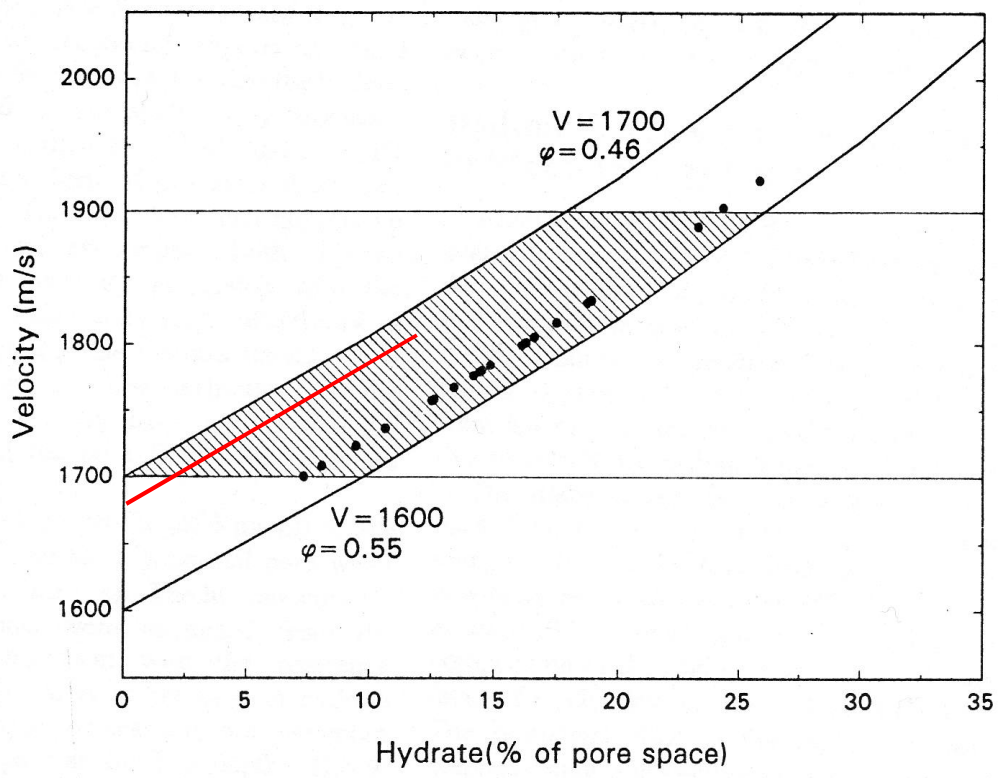

Figure 5.11: Plot of sediment velocity versus hydrate percentage of pore space, produced for the Cascadia area (after Yuan et al., 1996). The velocity anomaly for the Verrill canyon area is shown in red.

the same parameters as for the Cascadia site. A non–hydrated sediment velocity of 1650 m/s for estimated sediment near the BGHSZ from the regional gradient (Fig. 5.10). An increase of 100 m/s would require approximately 13% of the pore space to be occupied by gas hydrate, as seen in Figure 5.11 (Yuan et al., 1996). The uncertainty involved in this calculation is high, and an accurate estimate of gas hydrate in the pore space certainly requires parameters that are better constrained.

CHAPTER 6: DISCUSSION

The head scarps of the mass−failures near 500 mbsl are apparent on the multibeam bathymetry image (Fig. 5.2). These occur in close proximity to the depth at which the BGHSZ intersects the seafloor (near 500 mbsl). These failures also occur close to the downslope limit of the till tongues. Booth et al. (1994) describe slide head scarps on the US Atlantic Continental margin that seem to occur very close to the intersection of the BGHSZ with the seafloor. This is cited as circumstantial evidence for a relationship between slumps and gas hydrate processes.

The 6 slump failures seen on the upper slope of the study area all occur in similar water depth, and share apparently similar structures. The seismic lines did not cross the upper slope failures, so the structure cannot be discussed in detail. Upper slope failures are more likely to have been influenced by hydrate dissociation than deeper failures, especially at the intersection of the seafloor with the BGHSZ (Paull et al, 2000). Therefore the upper slope sediment (near the intersection of the BGHSZ with the seafloor) would be more influenced by an increase in pore pressure, compared to the lower slope. The similarity of the failures near 500 mbsl with the failures discussed by Booth et al. (2001) indicate that the failures may have been caused by similar processes.

Gauley (2001) describes the upper slope rotational failures as occurring near the downslope extend of the till tongues. Piper (2001) states that the failures near 500 mbsl may be due to (a) overconsolidation of sediment shallower than 500 mbsl, as a result of ice or iceberg loading, (b) silty sediment prone to liquefaction is most common at this depth, or (c) failure due to gas hydrate dissociation at a "gas hydrate cap". At this time there is not enough information to determine which of these three factors is dominant.

The head scarps on the middle and lower slope reach as much as 80 m vertical height (Mosher, 1987). The BGHSZ at 1500 mbsl is approximately 320 mbsf (using the pressure, and temperature parameters of the OBS location). This BGHSZ is where the gas hydrate becomes unstable and therefore where it will probably dissociate first, increasing pore pressure near the BGHSZ. Gas beneath the BGHSZ that migrates up through the sediment would most likely form gas hydrate once it re–enters the GHSZ, but a pore pressure increase in sediments above the BGHSZ due to dissociation of gas hydrates cannot be dismissed as a possible mechanism of pore pressure increase. The head scarps of 80 m height are probably too shallow in the sediment to have been *greatly* influenced by gas hydrate dissociation, compared to the upper slope rotational failures. Therefore the middle and lower slope failures were probably influenced little by possible gas hydrate dissociation events.

Much of this thesis relies on the velocity structure defined from the wide–angle data. Therefore the reliability of the velocity data is important to the findings of this report. The largest problem encountered with this data is the ringy nature. Much of the data for the shallow reflectors is obscured by reverberations. Higher quality data would yield a higher resolution velocity model.

The velocity depth model (Fig. 6.1) indicates that there is a high velocity gradient in the first 200 m of sediment, followed by a lower velocity gradient beneath this depth. This is supported by modelling of the reflectors, and refractor modelling using a simple 2 sediment layer model. The velocity of the sediment near 200 mbsf appears to be approximately 100 – 150 m/s greater than the regional velocity gradient at that depth. The velocity of 1800 m/s is consistent with hydrated sediments at this depth, such as the

sediments seen at ODP site 889 on the Cascadia margin (Spence et al., 2000). The velocity gradient seen at ODP site 889 increases from close to 1500 m/s at the seafloor, to approximately 1900 m/s near 210 mbsf. Near 230 mbsf, the velocity sharply decreases to approximately 1480 m/s, and at 300 mbsf appears to follow the reference velocity gradient. This site has a high concentration of gas hydrate and a free gas layer, resulting in a high velocity in the hydrated sediment and a low velocity in the free gas bearing sediment.

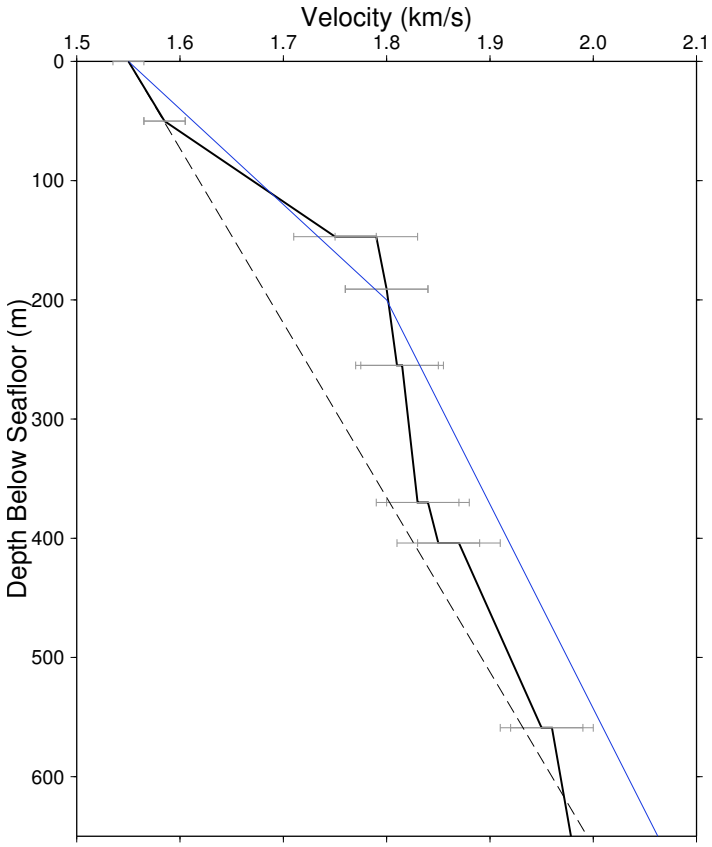

Figure 6.1: Velocity vs. depth profile for the OBS location, displaying an anomaly of approximately 100 m/s near 200 mbsf. The blue line is the velocity profile from the refraction analysis, the solid black line is the reflection analysis data, and the dashed line is the regional trend. The error bars correspond to ±40 m/s.

The area studied by Spence et al. (2000) displays a strong BSR, and likely has a much higher concentration of hydrate and free gas than the study area discussed in this

report. The region show a similar velocity gradient to the one produced for the study area. Site 889 does display a sharp decrease in velocity beneath the BSR, which is not seen at the OBS location studied in this report. This is likely due to a lack of free gas in the sediments beneath the BGHSZ.

The lack of free gas beneath the theoretical BGHSZ is indicated by the 2 layer refractor model. If a low velocity zone existed, it would cause the refractor to terminate. The refractor does not terminate in the OBS data, therefore it is unlikely that a low velocity zone exists in the sediments studied. The absence of a low velocity zone in the sediments indicates that a substantial free gas zone is probably not present under the BGHSZ.

The high velocity anomaly, which may indicate gas hydrate, appears coincident with the Carmine horizon. This horizon represents the start of glacial sedimentation at 0.45 Ma (Piper and Normark, 1989). It is possible that the velocity anomaly could be explained in terms of either lithology or the presence of gas hydrate. The porosity of a shallow sediment is related to its depth of burial, as discussed in relation to sediments on the Cascadia margin (Yuan et al., 1996). Therefore glacial sediments should display similar velocities to non−glacial sediments. There is currently not enough information to differentiate between the cause of this velocity increase.

The most effective way to determine whether the velocity profile is due to lithology or the presence of hydrate would be to obtain OBS data from a location in deeper water. According to the stability model, the BGHSZ should be much deeper while the depth to the Carmine reflector should remain constant or decrease in depth below the seafloor. If the high velocity gradient was maintained until the BGHSZ, it

would support the gas hydrate theory. If the velocity gradient was similar to the OBS location used in this report, it would support the lithological explanation.

The velocity structure below approximately 200 mbsf slowly returns to the reference value, and is possibly explained better by the lithological model. If the cause of the velocity anomaly were gas hydrate, the velocity of sediments below the BGHSZ should sharply decrease to a value similar to the reference gradient, which it does not.

The lack of a bottom simulating reflector does not necessarily indicate the lack of gas hydrate. The sediments of the study area are highly reflective, which often poses a significant problem to the detection of BSRs (Chapman, 2001). Another common factor that accounts for the lack of a BSR is the lack of free gas beneath the BGHSZ. This is a documented phenomenon, and it commonly observed adjacent to areas that display pronounced BSR features, such as the Blake Ridge (Holbrook et al., 1996). The probable lack of free gas beneath a hydrate deposit is likely related to the flux, and mass fraction of methane. The lack of free gas beneath the approximate BGSZ is probably the most important factor in absence of a BSR.

The abundance of pockmarks from 500 to 1100 mbsl is a good indication for the presence of gas, and possibly gas hydrates. However, the relationship of pockmarks to deeper structures has not been studied in depth on the Scotian Slope, and it is not apparent if the pockmarks are simply gas escape features, or if they are related to gas hydrate processes. However, it does indicate that methane gas is present in sufficient amounts to create these features, and therefore hydrate *could* be forming in the GHSZ.

The iterative process of determining sediment layer velocities is subjective, and likely to yield different results by different individuals. It is therefore necessary to have

a method which can be used to confidently confirm or discount the presence of a high velocity layer in the region of gas hydrate stability. Constraining the upper and lower velocity limits of the layers near the BGHSZ is a useful exercise for this purpose, and indicates that the velocity near 200 mbsl is approximately 100 – 150 m/s higher than a normal velocity gradient would permit, therefore indicating the possible presence of gas hydrate.

On the basis of wide–angle seismic evidence it is proposed that there are gas hydrates present in the sediment, to a depth of approximately 200 mbsf, while an underlying free gas layer appears to be absent. Other circumstantial evidence such as the location and close proximity of several head scarps, the BSR feature (90 km from the study area), pockmarks, and the stability calculations indicate that gas hydrate is possibly present.

CHAPTER 7: CONCLUSIONS AND FUTURE WORK

7.1 Conclusion

The presence of hydrate in the sediments of the study area is supported by the location of sediment failure head scarps, style and age of failures, presence and distribution of pockmarks, and favourable conditions for the formation of gas hydrate. The proximity of a BSR to the study area suggests that hydrates may also be present in the study area. Despite the lack of evidence of hydrate in the single channel reflection seismic data, the anomalously high velocity structure of the sediment in the gas hydrate stability zone indicates that gas hydrates may be present, but an underlying free gas zone is probably not. Further work is required to better determine the possible concentration and extent of gas hydrate in this area.

The possible presence of gas hydrate suggests that pore pressures may have been affected by the dissociation of gas hydrate during periods when the BGHSZ decreased in depth, either from an increase in bottom water temperature or a drop in sea level. It is therefore proposed that the failures in the study area, near 500 mbsl may have been influenced by elevated pore pressures at least partially resulting from the dissociation of gas hydrates.

7.2 Future work

Future wide−angle seismic work in the study area should use a better acoustic source, perhaps in similar water depths to the BSR found on industry seismic data. Coupling the wide−angle data with gas hydrate stability measurements is important, therefore direct measurements of seafloor temperature, geothermal gradient and possibly *in situ* pore pressure are important.

It is possible that analysis of other locations, using a similar seismic approach could discover different conditions. The BSR found within 90 km of the study area is in waters that are significantly deeper than the location the OBS was deployed in. An investigation using several OBSs in various locations on the slope would yield a more reliable conclusion. Determining the velocity structure of the sediment near the BSR may be useful for study of the area, and as an analogue for other locations.

The close proximity of the carmine horizon to the BGHSZ is a problem, but the deployment of an OBS in deeper water would resolve whether the velocity profile can be explained either by lithology or the presence of gas hydrate. This would also yield additional data about the shallow sediment velocity structure.

There have been indications of BSR features in industry seismic data, and some of this information has been shared. The use of shallow industry data, especially 3d seismic would be an excellent tool for mapping the extent and character of a BSR. Mapping the extent of the BSR (within 90 km of the study area) is a clear method of estimating the distribution of gas hydrate near the area.

Direct proof of gas hydrate existence in the sediment of the study area would have to be performed by drilling. The likelihood of obtaining a core that contains intact hydrate is very small, but geochemical analysis (eg: Cl^-analysis from cores) can yield important information about possible hydrate concentrations. *In situ* measurement of sediment velocity can be performed by use of vertical seismic profiling (Holbrook et al., 1996; Yuan et al., 1996). This procedure would yield detailed information about the velocity structure of the sediment.

References

Adams, T., 2001. Sediment Slope Stability of a Small Region of the Scotian Slope off Nova Scotia, Canada. Unpublished work term report, Dalhousie University.

Baltzer, A., Cochonat, P., and Piper, D.J.W. 1994. In situ geotechnical characterisation of sediments on the Nova Scotian Slope, eastern Canadian continental margin. Marine Geology 120, p.291–308.

Booth, J.S., Winter, W.J., and Dillon, W.P., 1994. Circumstantial Evidence of Gas Hydrate and Slope Failure Association on the United States Atlantic Continental Margin, in: Natural Gas Hydrates, Sloan, E.D., Annals of the New York Academy of Sciences 715, p. 487–489.

Campbell, D.C, 2000. Relationship of Sediment Properties to Failure Horizons for a Small Area of the Scotian Slope, Geological Survey of Canada (Atlantic) Current Research, 2000–D8.

Chapman, R., 2001. Submarine Gas Hydrates in the Cascadia Accretionary Margin. From University of Victoria. Notes from seminar, Dalhousie Oceanography Departmental Seminar.

Dillon, W.P., and Max, M.D., 2000. Oceanic Gas Hydrate, in: Max, M.D. (ed.), Natural Gas Hydrate in Oceanic and Permafrost Environments, Kluwer academic publishers, p.61–76.

Dillon, W.P., and Max, M.D., 2000. The U.S. Atlantic Continental Margin; the Best–known Gas Hydrate Locality, in: Max, M.D.(ed.), Natural Gas Hydrate in Oceanic and Permafrost Environments, Kluwer academic publishers, p.157–170.

Fjeldskaar, W., Lindholm, C., Dehls, J.F., Fjeldskaar, I., 2000. Postglacial Uplift, Neotectonics and Seismicity in Fennoscandia. Quaternary Science Reviews, 19 p. 1413 – 1422.

French, J. 1998. Velocity Structure of a Methane Hydrate Stability Zone, Offshore Vancouver Island: unpublished BSc thesis, Dalhousie University.

Gauley, B.J.L. 2001. Lithostratigraphy and Sediment Failure on the Central Scotian Slope. Unpublished MSc thesis, Dalhousie University.

Hampton, M.A., and Lee, H.J. 1996. Submarine Landslides. Reviews of Geophysics, 34:1, p.33–59.

Haq, B.U., 2000. Climatic impact of Natural Gas Hydrate, in: Max, M.D. (ed.), Natural Gas Hydrate in Oceanic and Permafrost Environments, Kluwer academic

publishers, p.137–148.

Henriet, J.P., and Mienert, J. 1998. Gas Hydrates *relevance to world margin stability and climatic change.* Geological Society of London Special Publication No. 137.

Holbrook, W.S., Hoskins, H., Wood, W.T., Stephen, R.A., Lizarralde, D., 1996. Methane Hydrate and Free Gas on the Blake Ridge from Vertical Seismic Profiling. Science, 273, p. 1840 – 1843.

Hyndman, R.D. and E.E. Davis, 1992. A Mechanism for the Formation of Methane Hydrate and Sea floor Bottom Simulating Reflectors by Vertical Fluid Expulsion, Journal of Geophysical Research, 97, p. 7025 – 7041.

Issler D.R., and Beaumont, C., 1986. Estimates of Terrestrial Heatflow in Offshore Eastern Canada: reply, Canadian Journal of Earth Sciences, v. 23, p. 2083.

Keen, M.J., Adams, J., Moran, K., Piper, D.J.W., and Reid, I., 1990. Earthquakes and Seismicity, in Geology of the Continental Margin off Eastern Canada. Geological Survey of Canada, Geology of Canada, no. 2, p. 793–798.

Kvenvolden, K.A., 2000. Natural Gas Hydrate: Introduction and History of Discovery, in: Max, M.D. (ed.), Natural Gas Hydrate in Oceanic and Permafrost Environments, Kluwer academic publishers, p.9–16.

Kvenvolden, K.A., and Barnard, L.A., 1983. Gas hydrates of the Blake Outer Ridge, Site 533, Deep Sea Drilling Project Leg 76. In Sheridan, R.E., Gradstein, F.M., et al., Initial Reports. DSDP, 76: Washington (U.S. Govt. Printing Office), p. 353 – 365.

Lee, H.J., Schwab, W.C., and Booth, J.S. 1993. Submarine Landslides: An Introduction. In Submarine Landslides: selected studies in the U.S. exclusive economic zone,US Geological Survey, p.1–10.

Lee, M.W., Hutchinson, D.R., Dillon, W.P., Miller, J.J., Agena, W.F., and Swift, B.A., 1993B. Method of Estimating the Amount of *in situ* Gas Hydrates in Deep Marine Sediments, Marine and Petroleum Geology, v. 10, p. 493 – 506.

Lee, M.W., and Collett, T.S., 2001. Comparison of Elastic Velocity Models for Gas–Hydrate Bearing Sediments. Geophysical Monograph, v. 124, p.179–187.

Locat, J., and Lee, H.J. 2000. Submarine Landslides:Advances and Challenges. From Proceedings of the 8th International Symposium on Landslides, Cardiff, U.K., June 2000. p.1–30.

Locat, J. 2001. Instabilities along margins: a geomorphological and geotechnical perspective. Marine and Petroleum Geology, 18, p.503–512.

Majorowicz, J.A., Osadetz, K., 2002. Natural Gas Hydrate Potential in the Atlantic Margin of Canada, Geological Survey of Canada (Calgary) report.

Max, M.D., 2000. Hydrate as a Future Energy Resource for Japan, in: Max, M.D. (ed.), natural Gas Hydrate in Oceanic and Permafrost Environments, Kluwer academic publishers, p.225−238, 361−370.

Max, M.D. 2000. Natural Gas Hydrate, *in Oceanic and Permafrost Environments,* in: Max, M.D. (ed.), Natural Gas Hydrate in Oceanic and Permafrost Environments, Kluwer academic publishers, p. 225 – 239.

Mello, U.T., Pratson, L.F., 1999. Regional Slope Stability and Slope−Failure Mechanics from the Two−Dimensional State of Stress in an Infinite Slope, Marine Geology, 154 p. 339 – 356.

Miles, P.R., 2000. Geophysical Sensing and Hydrate, in: Max, M.D. (ed.), Natural Gas Hydrate in Oceanic and Permafrost Environments, Kluwer academic publishers, p.261−275.

Moran, K., Piper, D.J.W., Mosher, D.C., 2001. Gas hydrate: a Potential Slope Failure Trigger on the Scotian Slope (abstract), Eos. Trans. AGU, 82(20), Spring Meeting Supplement.

Mosher, D.C., Piper, D.J.W., Campbell, D.C., and Jenner, K.A. 2002. Near Surface Geology and Sediment Failure Geohazards of the Central Scotian Slope. AAPG bulletin (submitted but not published at time of writing).

Mosher, D.C., 2001. Cruise Report HUDSON 2001−048A. Geological Survey of Canada (Atlantic).

Mosher, D.C., 1987. Late Quaternary Sedimentology and Sediment instability of a Small Area on the Scotian Slope. Unpublished M.Sc. Thesis, Memorial University of Newfoundland, St. John's, Newfoundland.

Mosher, D.C., Moran, K., and Hiscott, R.N. 1994. Late Quaternary sediment, sediment mass flow processes and slope stability on the Scotian Slope, Canada. Sedimentology, 41, p. 1039−1061.

Mosher, D.C. 2000. Cruise Report Hudson 2000−042. Geological Survey of Canada (Atlantic).

Mulder, T., and Moran, K. 1995. Relationship among submarine instabilities, sea level variations, and the presence of an ice sheet on the continental shelf: An example from the Verrill Canyon Area, Scotian Shelf. Pleoceanography, 10:1, p.137−154.

Mulder, T., Cochonat, P. 1996. Classification of Offshore Mass Movements. Journal of Sedimentary Research, 66:1, p.43–57.

Paull, C.K., and Dillon W.P. 2001. Natural Gas Hydrates, *Occurrence, Distribution, and Detection.* American Geophysical Union, Washington, DC.

Paull, C.K., Buelow, W.J., Ussler, and W., Borowski, W.S. 1996. Increased continental–margin slumping frequency during sea–level lowstands above gas hydrate–bearing sediments. Geology, v. 24, no. 2, p. 143–146.

Paull, C.K., Ussler, W., Dillon, W.P., 2000. Potential Role of Gas Hydrate Decomposition in generating Submarine Slope Failures, in: Max, M.D. (ed.), Natural Gas Hydrate in Oceanic and Permafrost Environments, Kluwer academic publishers, p.149–156.

Paull, C.K., Ussler, W. III, and Dillon, W.P., 2000. Potential Role of Gas Hydrate Decomposition in Generating Submarine Slope Failures, in: Max, M.D. (ed.), Natural Gas Hydrate in Oceanic and Permafrost Environments, Kluwer academic publishers, p.149–156.

Pecher, I.A., and Holbrook, W.S., 2000. Seismic Methods for Detecting and Quantifying Marine Methane Hydrate/Free Gas Reservoirs, in: Max, M.D. (ed.), Natural Gas Hydrate in Oceanic and Permafrost Environments, Kluwer academic publishers, p.275–294.

Pellenbarg, R.E., and Max, D., 2000. Introduction Physical Properties, and Natural Occurrences of Hydrate, in: Max, M.D. (ed.), Natural Gas Hydrate in Oceanic and Permafrost Environments, Kluwer academic publishers, p.1–8.

Peltzer, E.T., and Brewer, P.G., 2000. Practical Physical Chemistry and Empirical Predictions of Methane Hydrate Stability, in: Max, M.D. (ed.), Natural Gas Hydrate in Oceanic and Permafrost Environments, Kluwer academic publishers, p.17–20.

Piper, D.J.W., and Normark, W.R., 1989. Late Cenozoic Sea–Level Changes and the Onset of Glaciation: Impact on Continental Slope Progradation off Eastern Canada. Marine and Petroleum Geology, v. 6, 336–348.

Piper, D.J.W., Skene, K.I., and Morash, N. 1999. History of major debris flows on the Scotian Rise, offshore Nova Scotia. Geological Survey of Canada, current research, 1999–E, p. 203–212.

Piper, D.J.W. 2001. The Geological Framework of Sediment Instability on the Scotian Slope: Studies to 1999. Geological Survey of Canada Open File 3920.

Popenoe, P., Schmuck, E.A., and Dillon, W.P., 1993. The Cape Fear LandSlide: Slope

Failure Associated with Salt Diapirism and Gas Hydrate Decomposition. In Schwab, W.C., Lee, H.J. and Twichell, D.C., (Eds.), Submarine Landslides: Selective Studies in the U.S. Exclusive Economic Zone. U.S. Geological Survey Bulletin, 2002, p. 40 – 53.

Reiter, M., and Jessop, A.M., 1985. Estimates of Terrestrial Heat Flow in Offshore Eastern Canada. Canadian Journal of Earth Science, 22, p. 1503 – 1517.

Reynolds, J.M., 1997. An Introduction to Applied and Environmental Geophysics. John Wiley and Sons Inc., New York, p. 360.

Sloan, E.D. 1998. Clathrate Hydrates of Natural Gases, Marcel Bekker Inc., New York.

Spence, G.D., Hyndman, R.D., Chapman, N.R., Riedel, M., Edwards, N., Yuan, J., 2000. Cascadia Margin, Northwest Pacific Ocean: Hydrate Distribution from Geophysical Investigations, in: Max, M.D. (ed.), Natural Gas Hydrate in Oceanic and Permafrost Environments, Kluwer academic publishers, p.323–348.

Stea, R.R., Piper, D.J.W., Fader, G.B.J., and Boyd, R. 1998. Wisconsinan glacial and sea–level history of Maritime Canada and the adjacent continental shelf: A correlation of land and sea events. GSA Bulletin, v. 110, no. 7, p. 821–845.

Stern, L.A., Kirby, S.H., Durham, W.B., Circone, S., and Waite, W.F., 2000. Laboratory synthesis of pure methane hydrate suitable for measurement of physical properties and decomposition behaviour, in: Max, M.D. (ed.), Natural Gas Hydrate in Oceanic and Permafrost Environments, Kluwer academic publishers, p.323–348.

Xu, W., and Ruppel, C., 1999. Predicting the Occurrence, Distribution, and Evolution of Methane Gas Hydrate in Porous Marine Sediments. Journal of Geophysical Research, 18, p. 5081 – 5095.

Yuan, T., Hyndman, R.D., Spence, G.D., and Desmos, B., 1996. Seismic Velocity Increase and Deep–Sea Gas Hydrate Concentration Above a Bottom–Simulating Reflector on the Northern Cascadia Continental Slope, Journal of Geophysical Research, v. 101, p. 13655 – 13671.

Zelt, C. A., and Smith, R.B., 1992. Seismic Traveltime Inversion for 2–D Crustal Velocity Structure, Geophysical Journal International, 108, p. 16 – 34.

APPENDIX A – OBS DATA

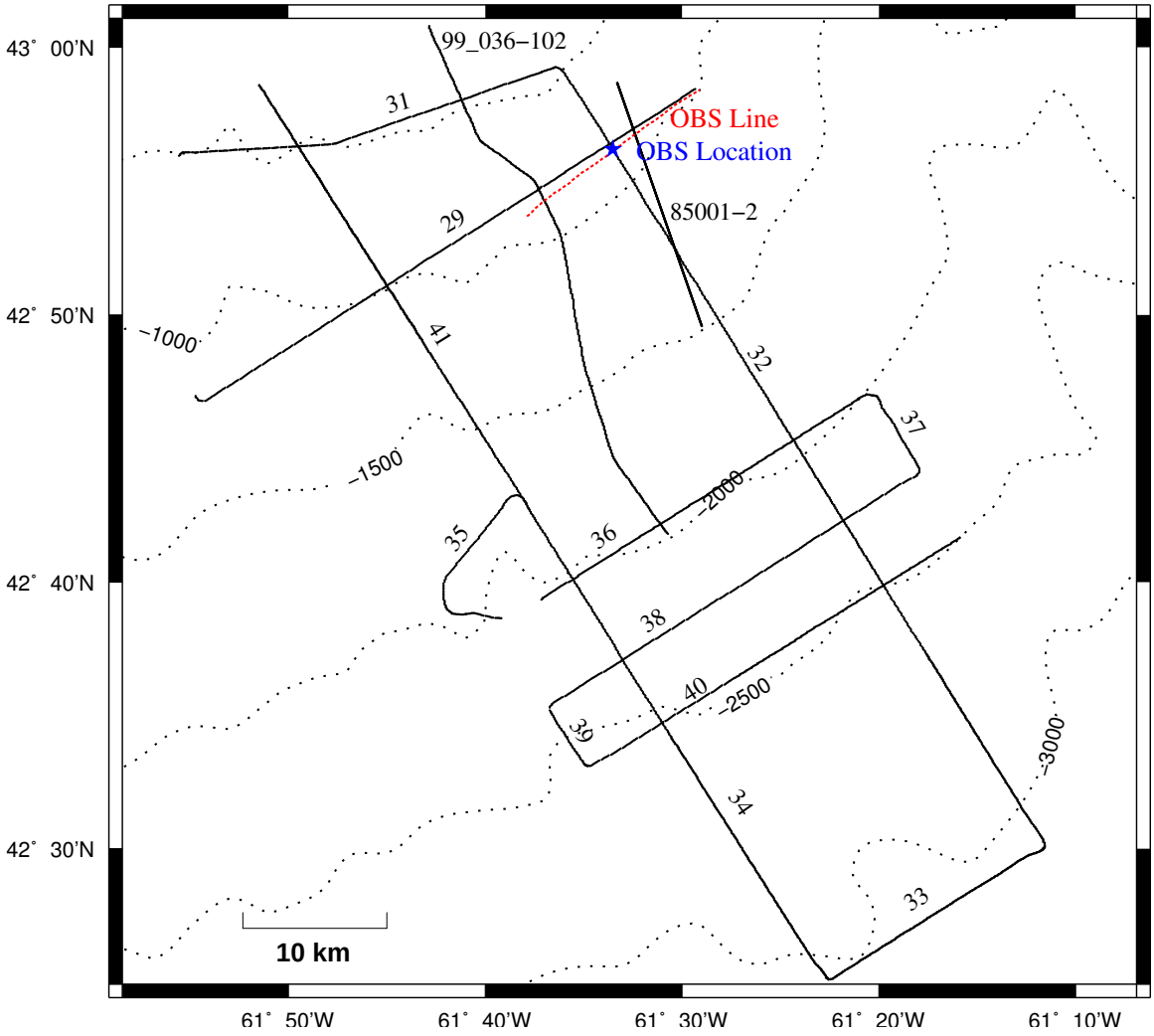

Figure A1: Detailed location map, including all line numbers and locations (line numbers 29 – 41 are from Hudson cruise 2001–048A). Depth contours are dotted lines, the OBS shot line is a red dashed line, the OBS location is a blue star, and the single channel reflection lines are solid black.

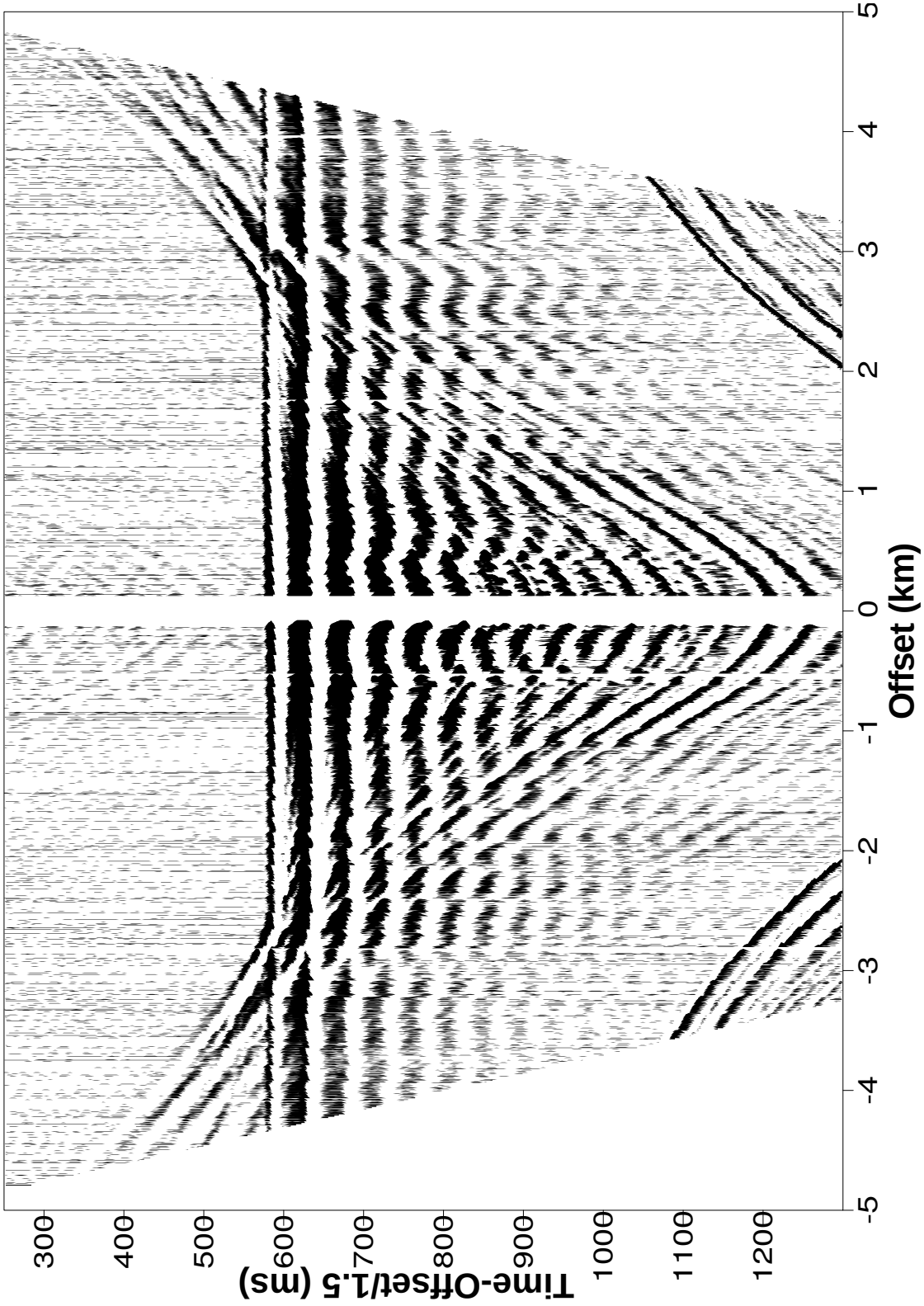

Figure A2: NMO corrected OBS data, channel 1.

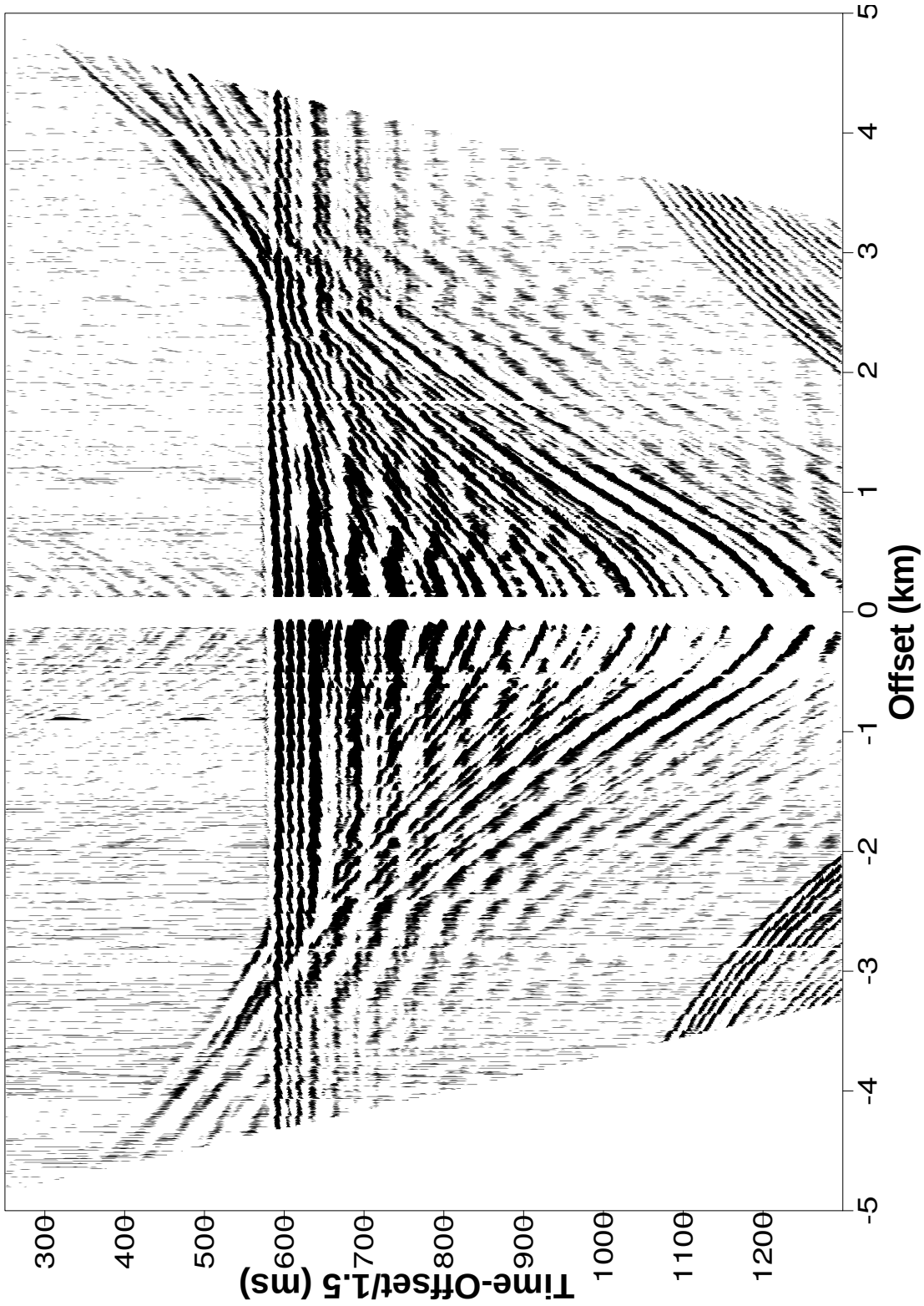

Figure A3: NMO corrected OBS plot, channel 2.

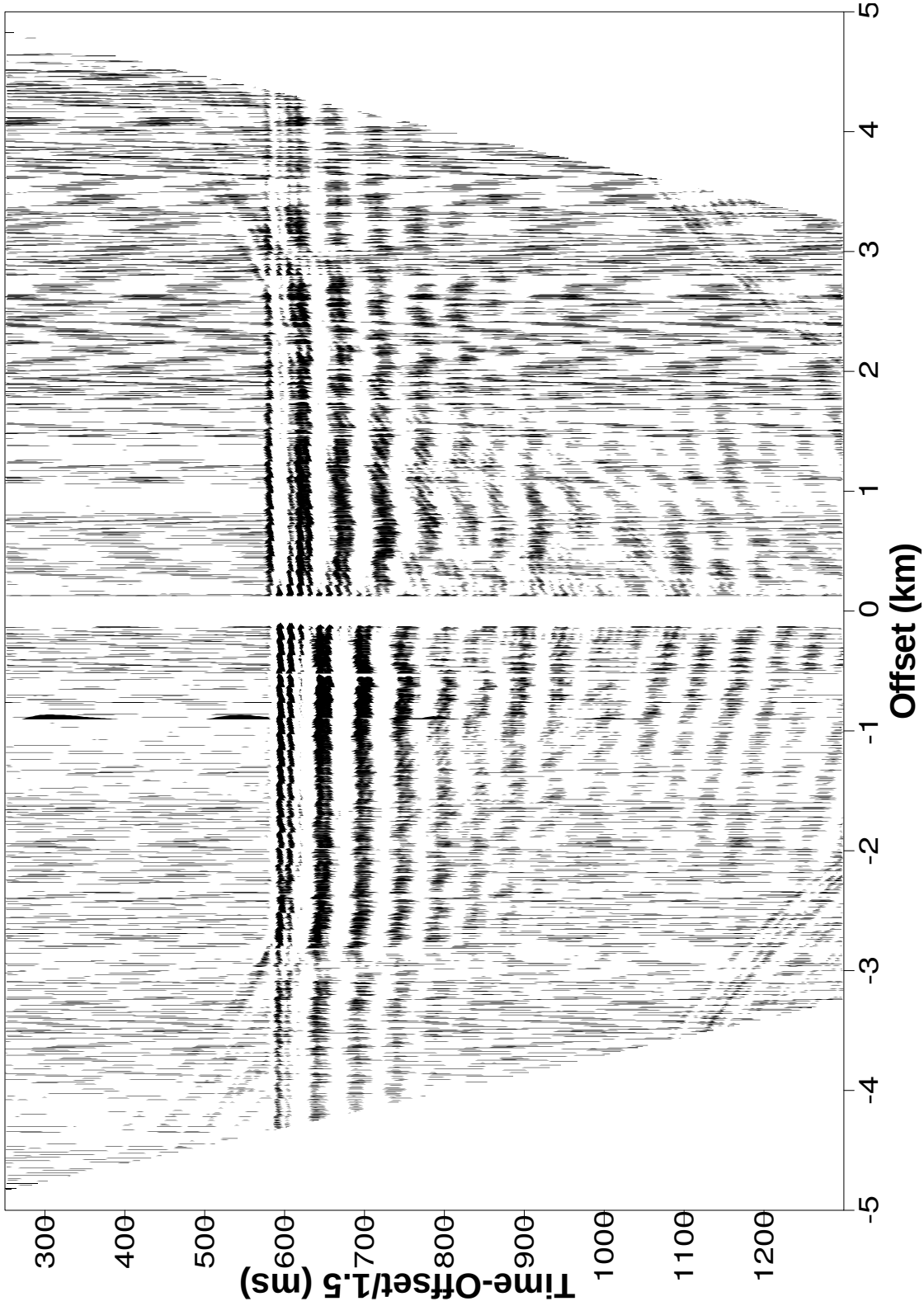

Figure A4: NMO corrected OBS plot, channel 3.

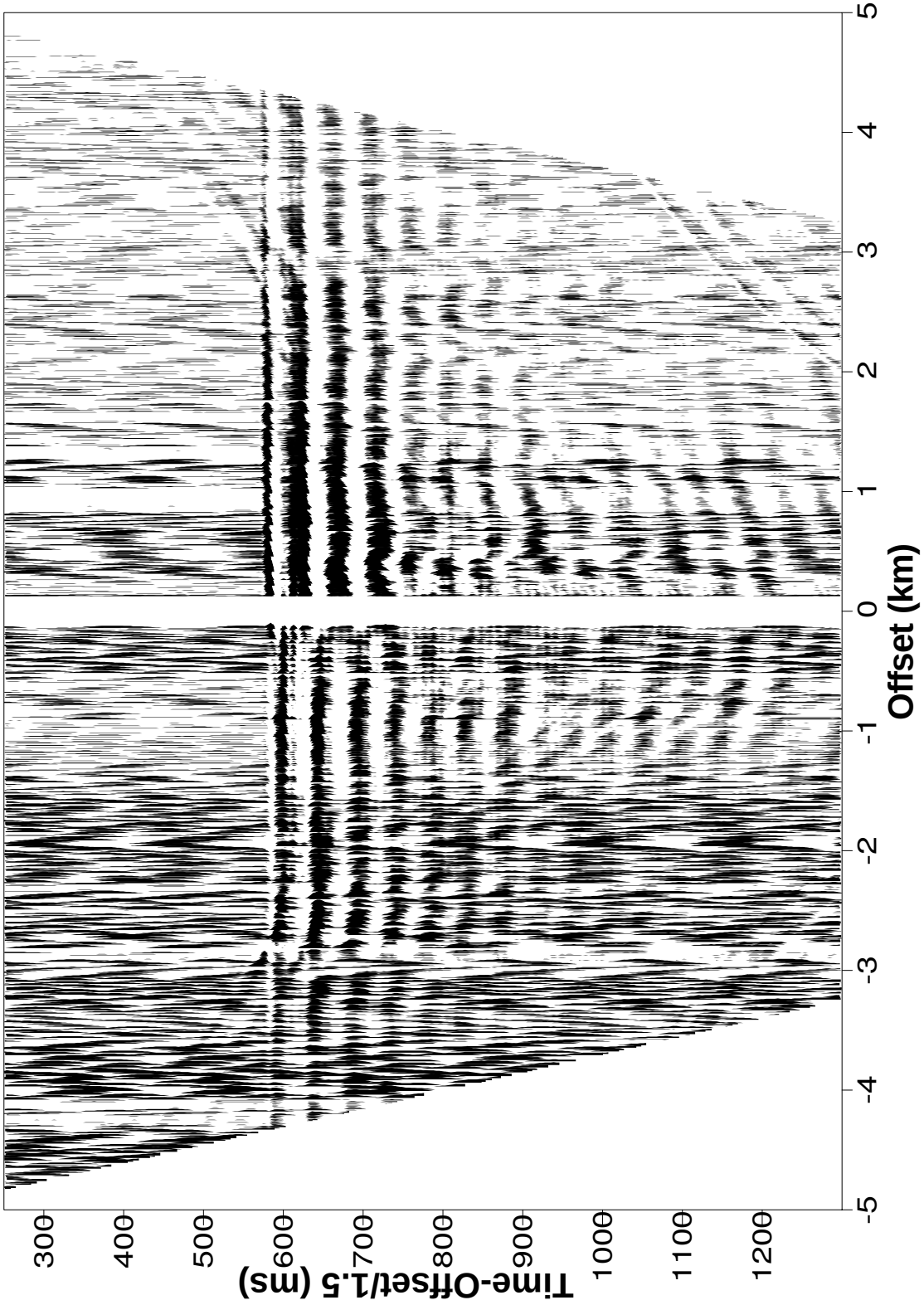

Figure A5: NMO corrected OBS plot, channel 4.

APPENDIX B – SINGLE CHANNEL SEISMIC SECTIONS

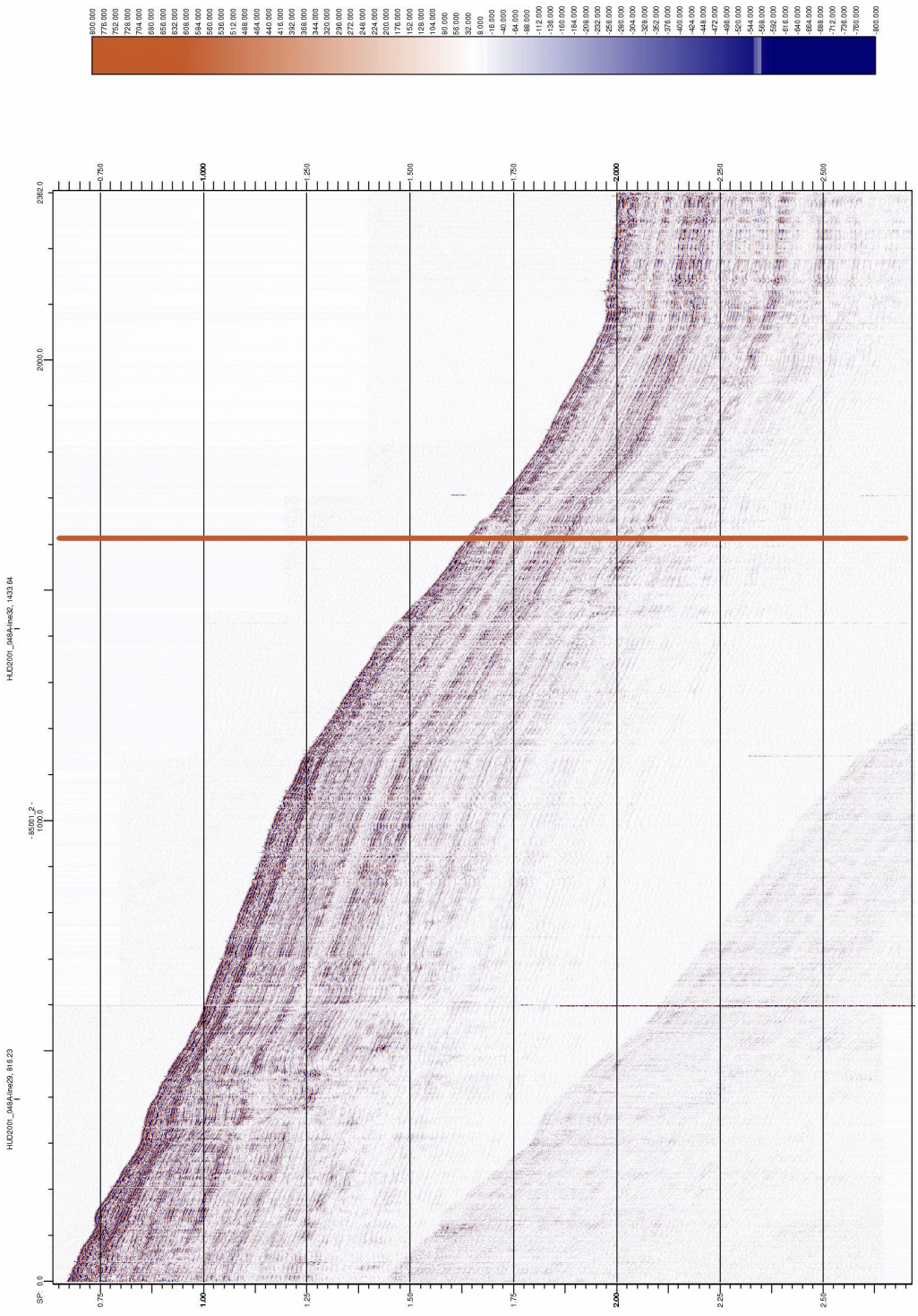

Figure B1: Seismic section 85001–2. This section was used to digitise the horizons.

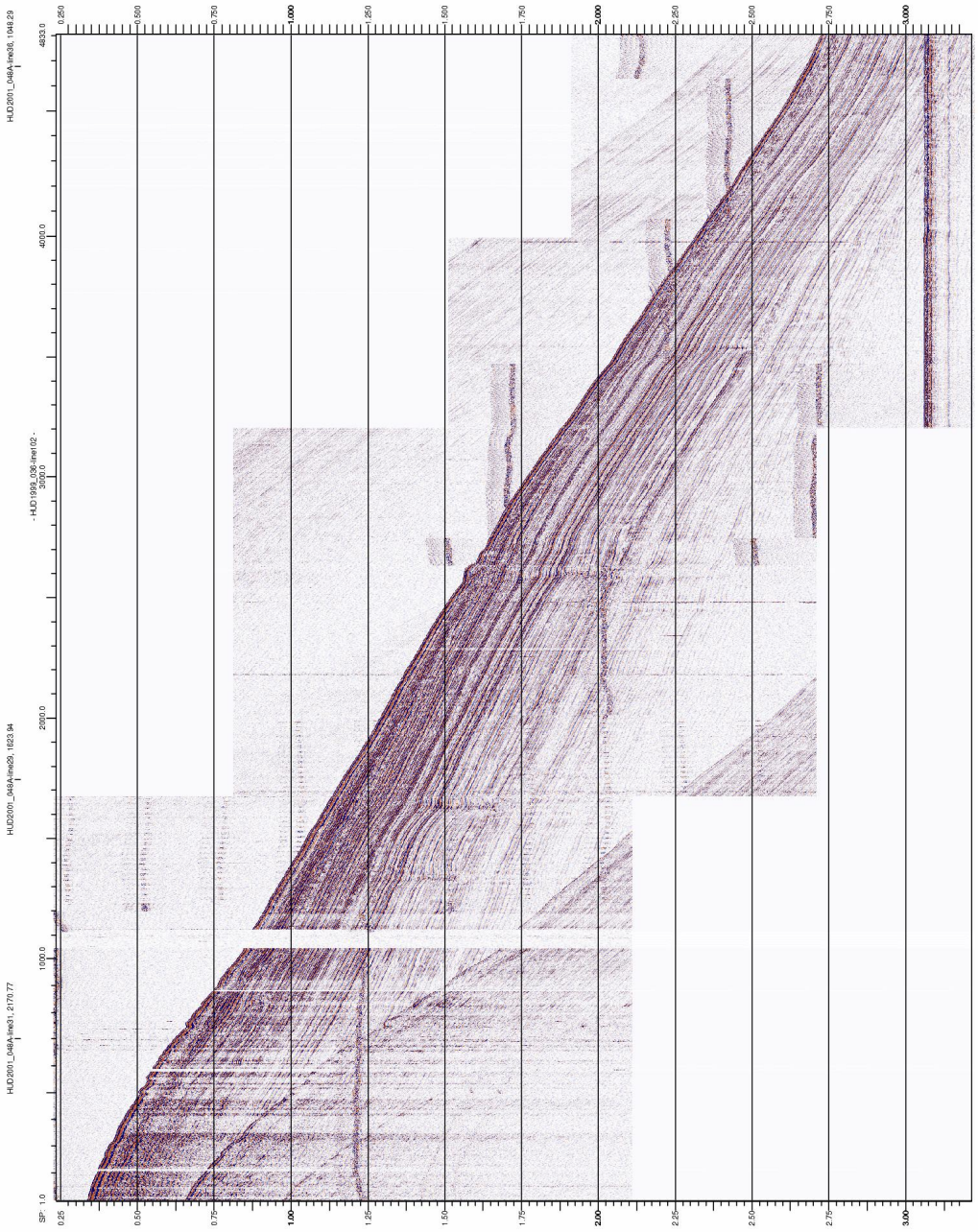

Figure B2: Seismic line HUD1999−036−102. This line was used to compare to the horizons picked by Gauley (2001).

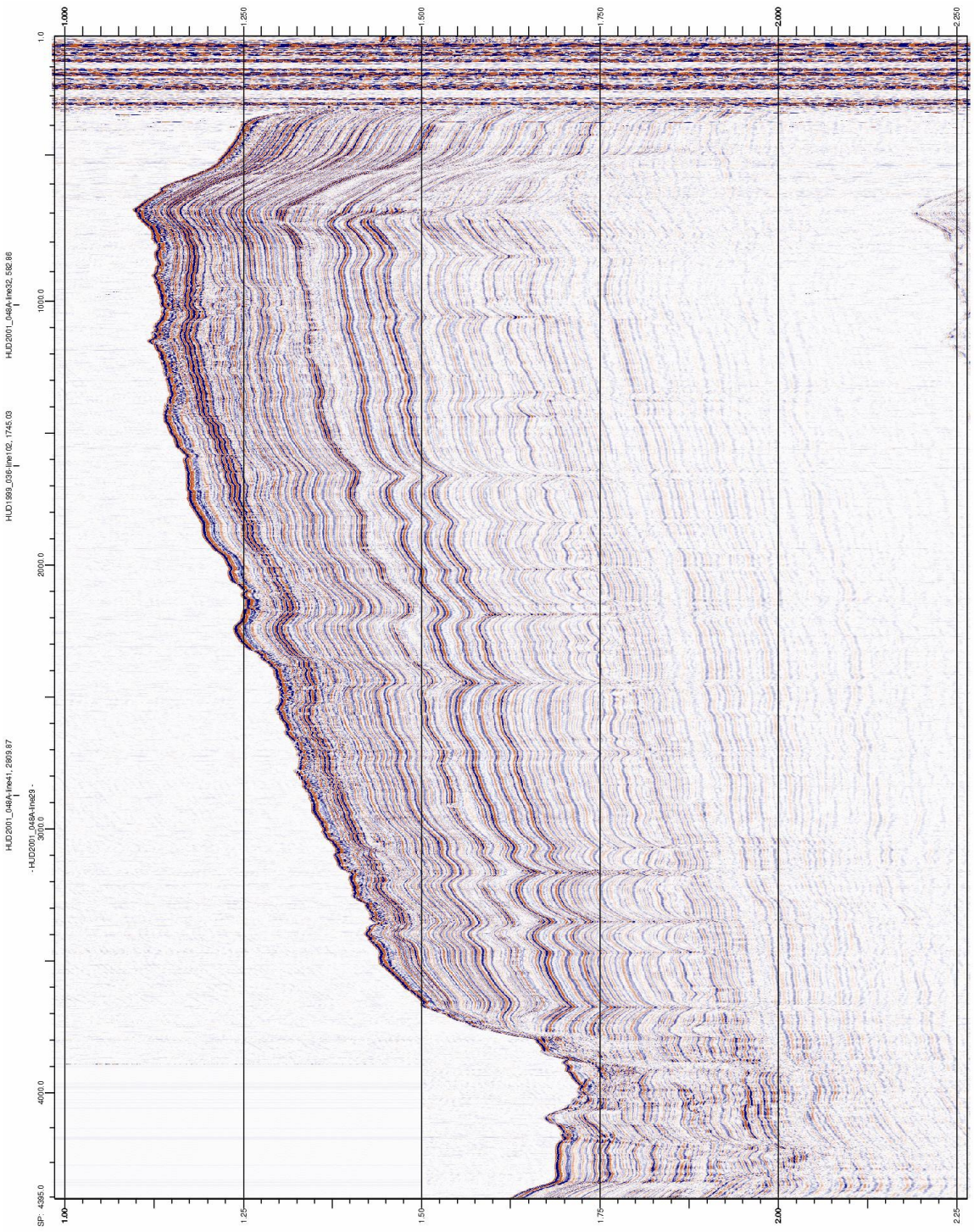

Figure B3: Seismic line HUD2001_048A line 29.

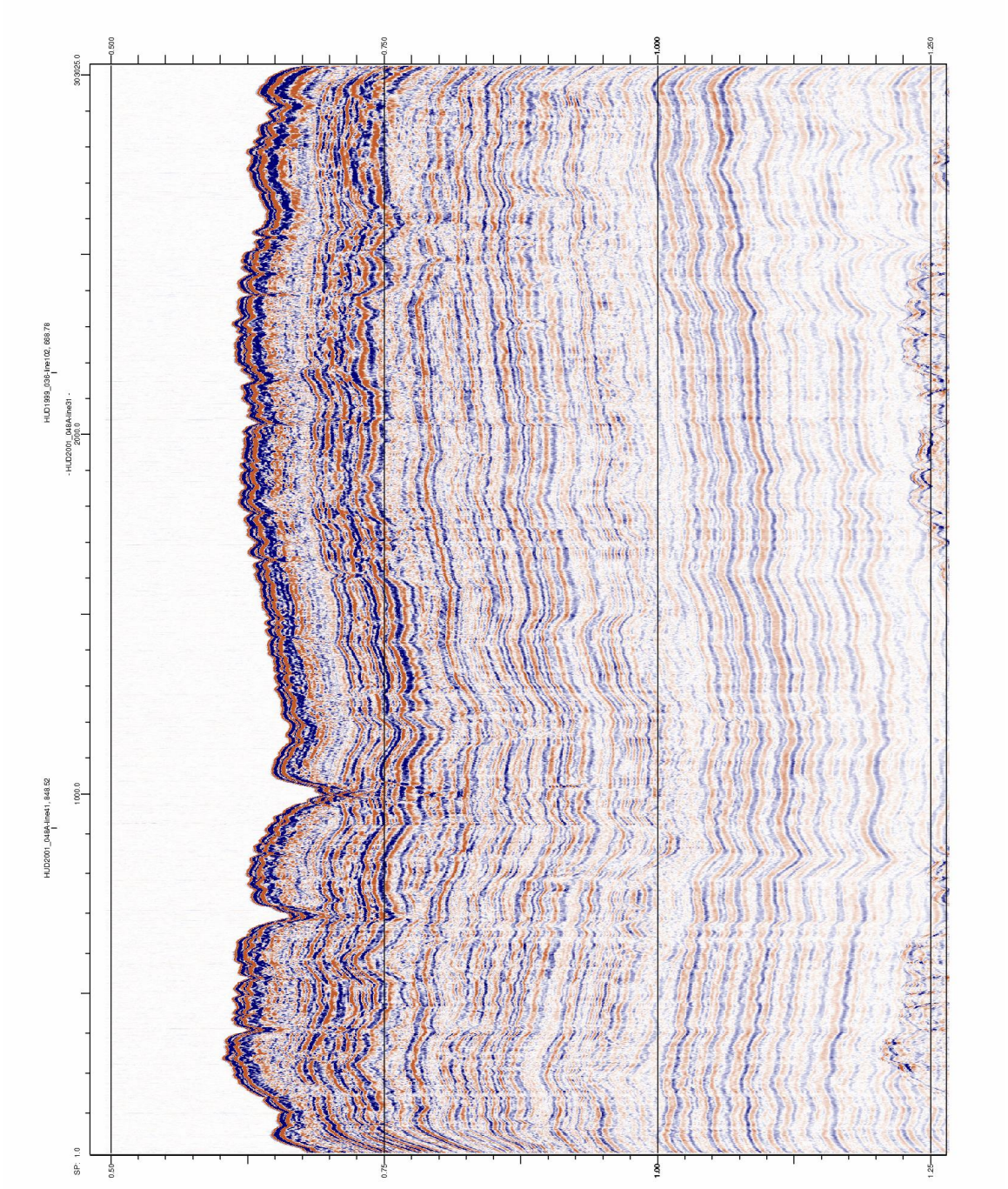

Figure B4: Seismic line HUD2001_048A line 31.

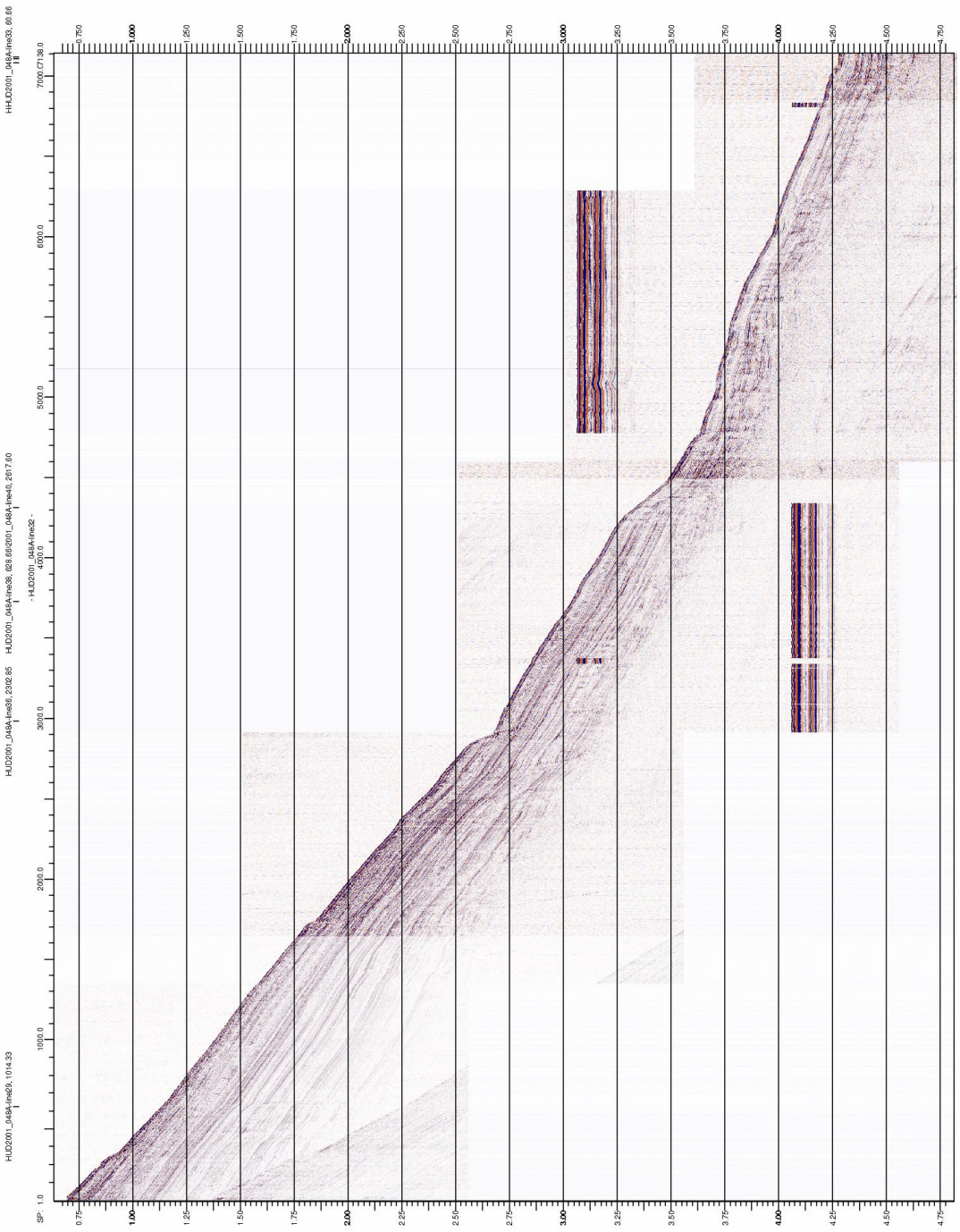

Figure B5: Seismic line HUD2001_048A line 32.

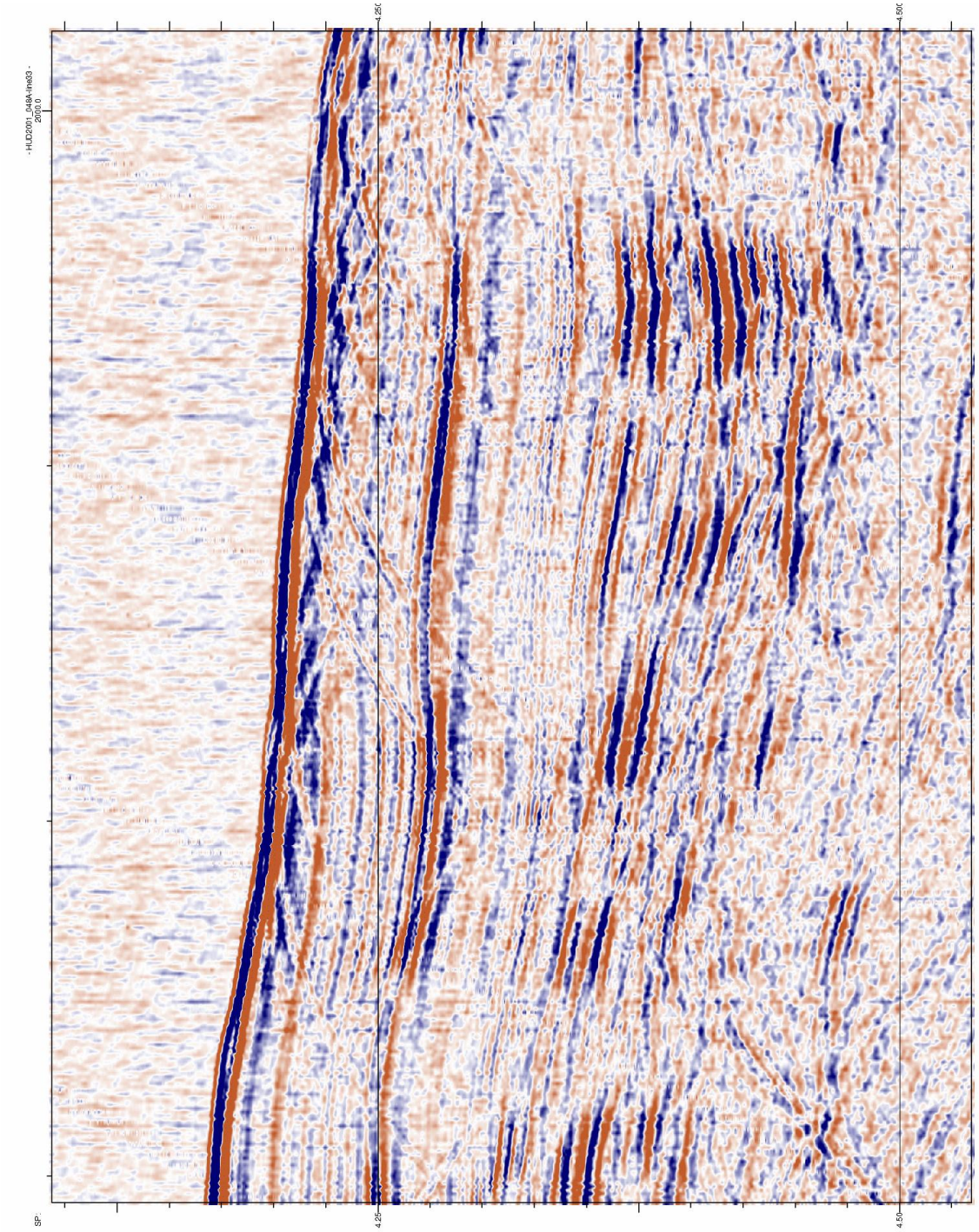

Figure B6: Seismic line HUD2001_048A line 33.

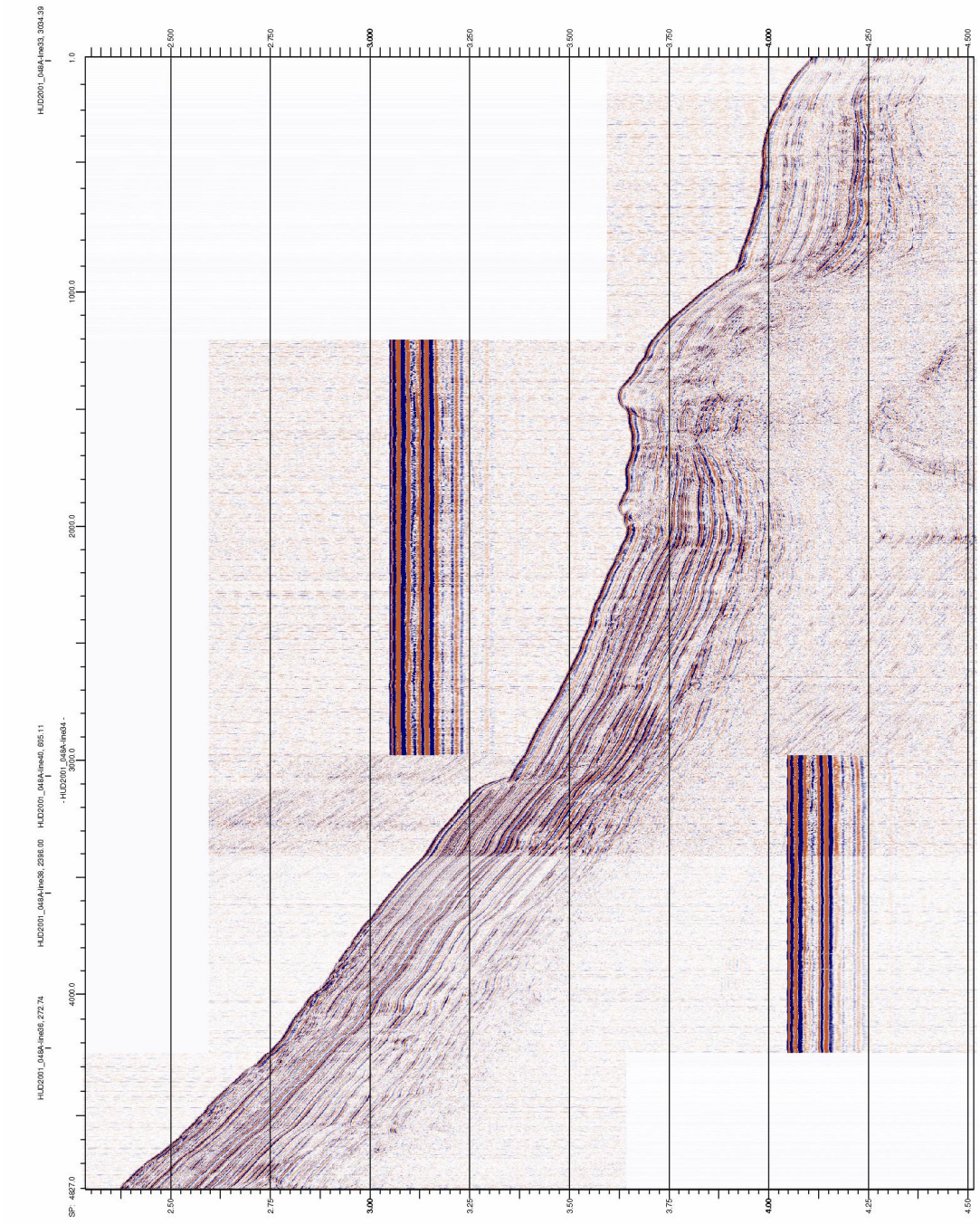

Figure B7: Seismic line HUD2001_048A line 34.

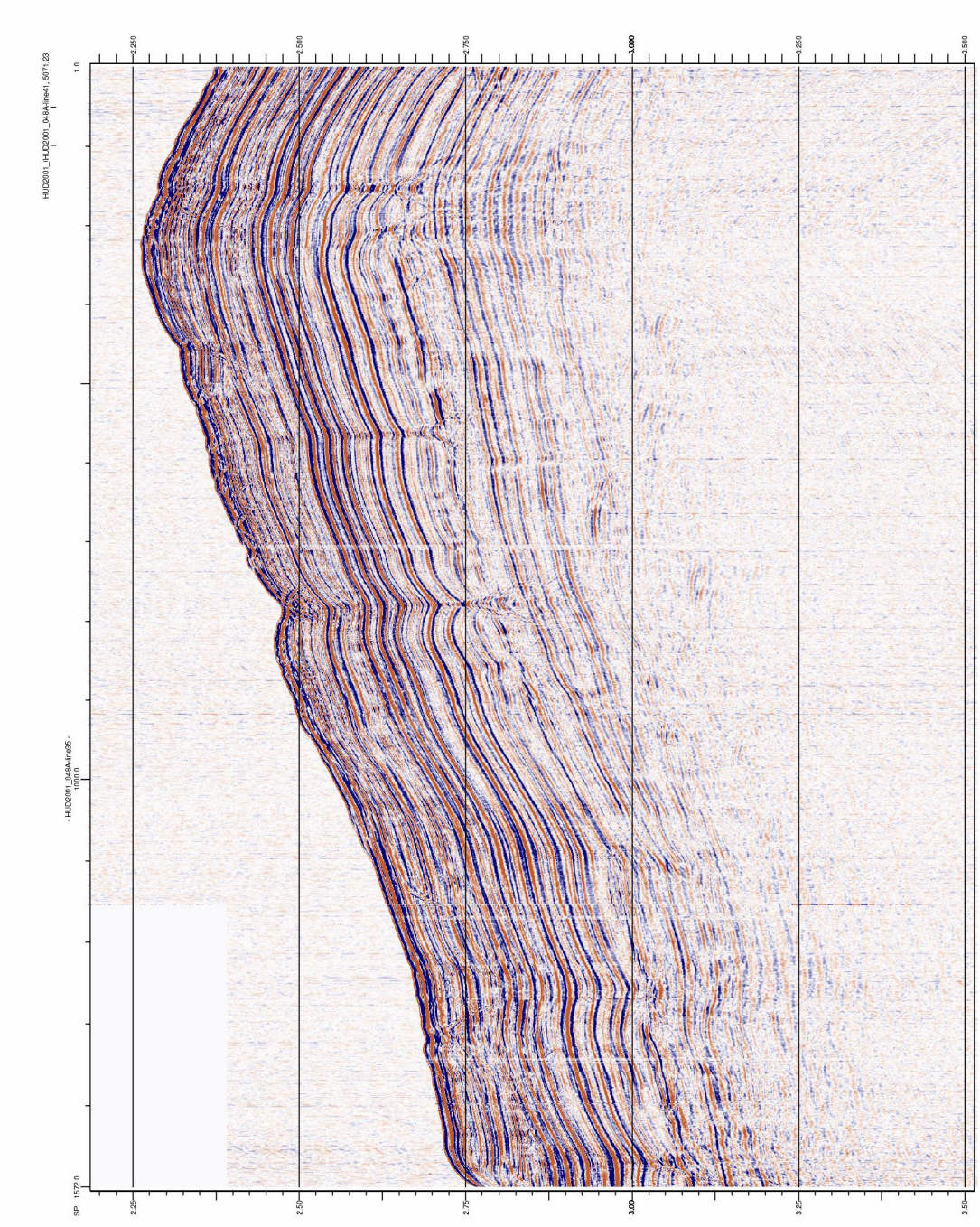

Figure B8: Seismic line HUD2001_048A line 35.

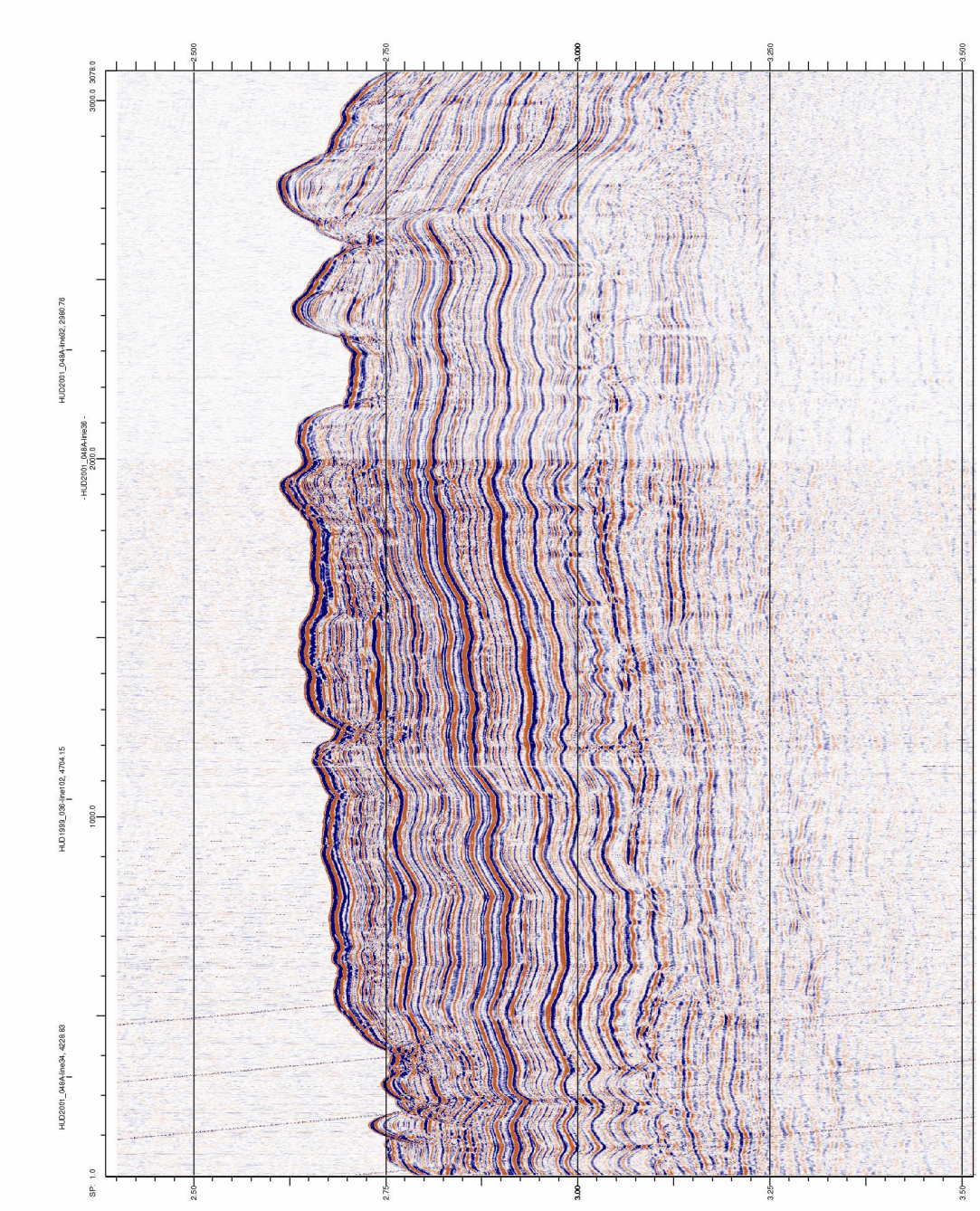

Figure B9: Seismic line HUD2001_048A line 36.

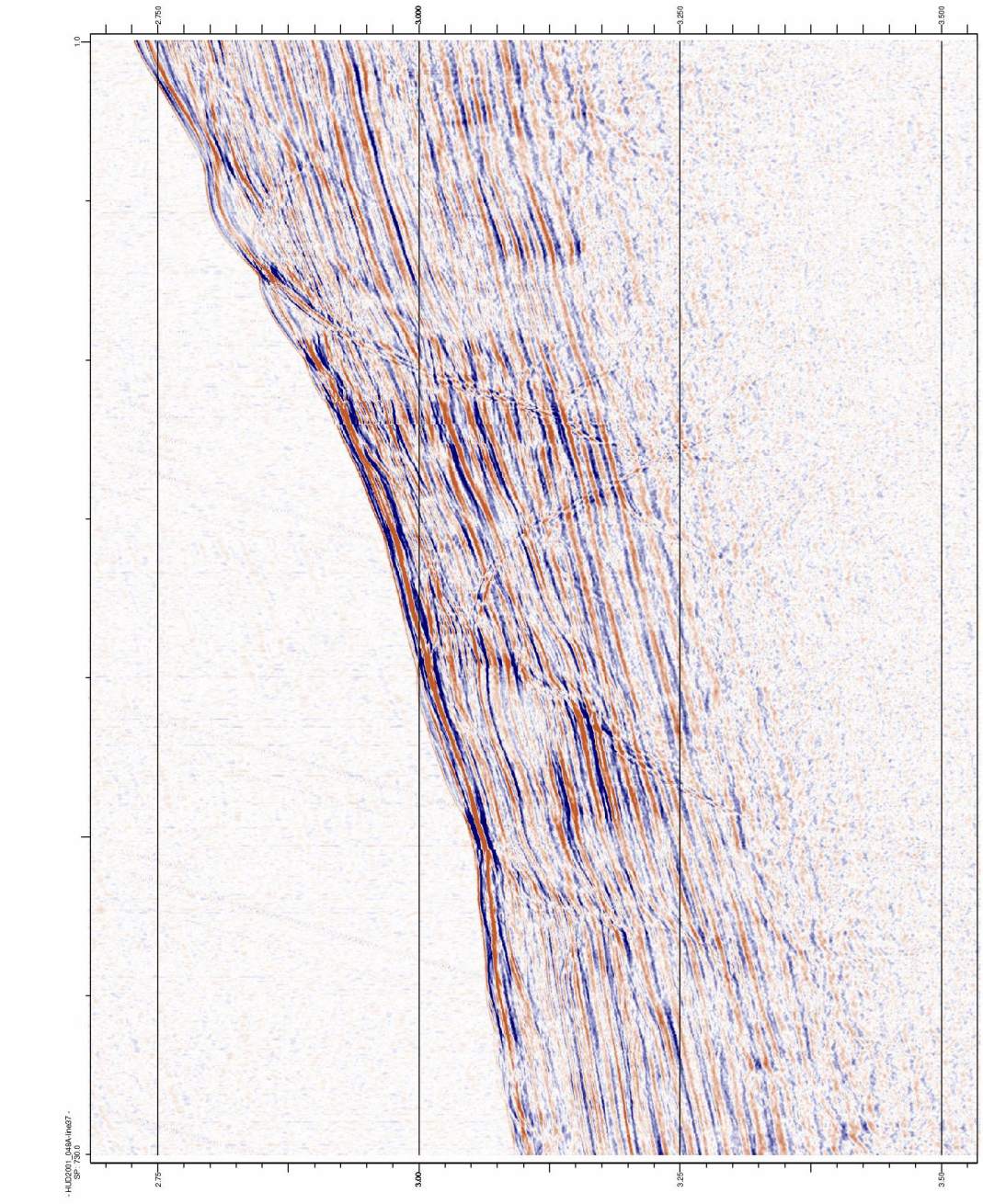

Figure B10: Seismic line HUD2001_048A line 37.

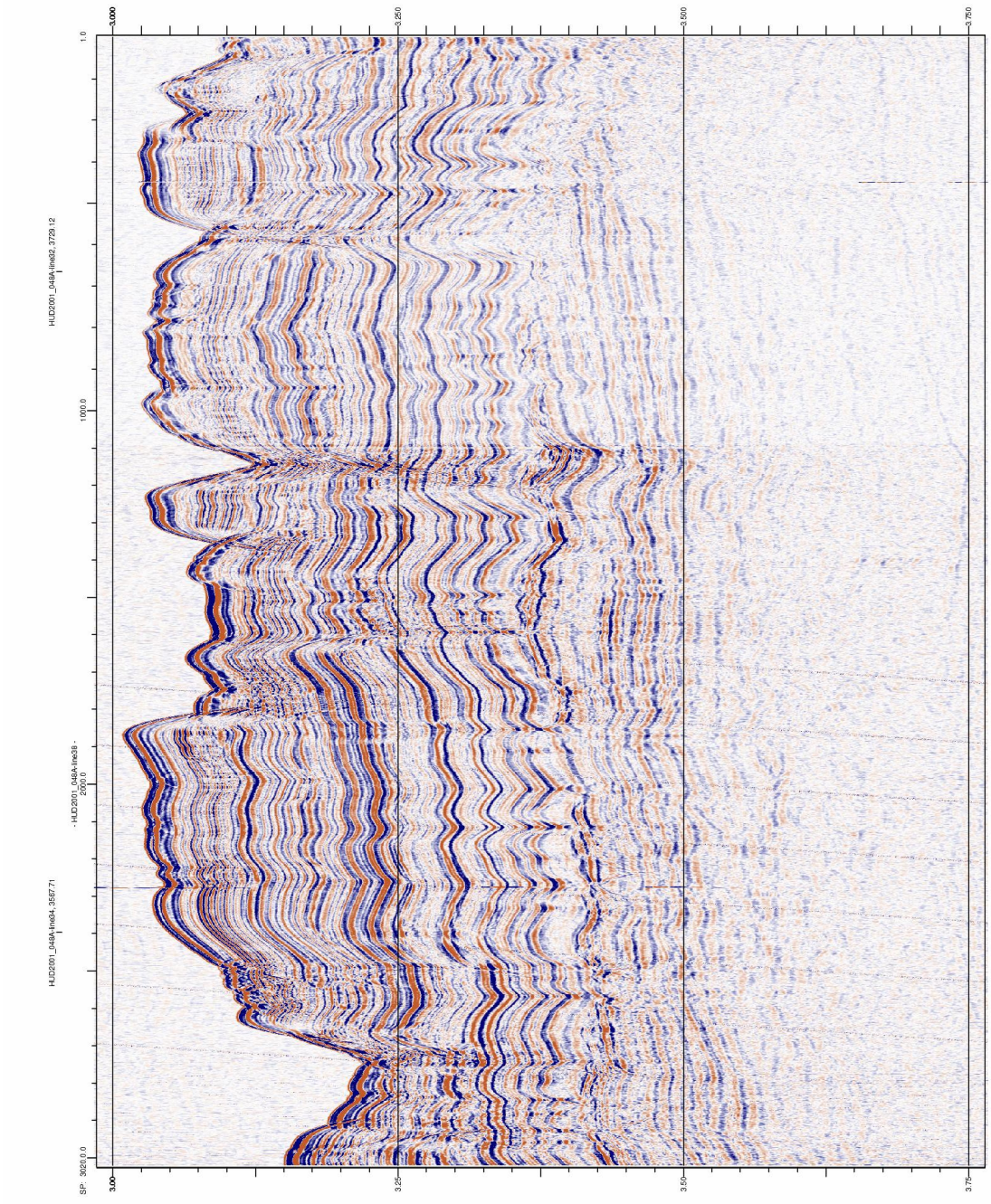

Figure B11: Seismic line HUD2001_048A line 38.

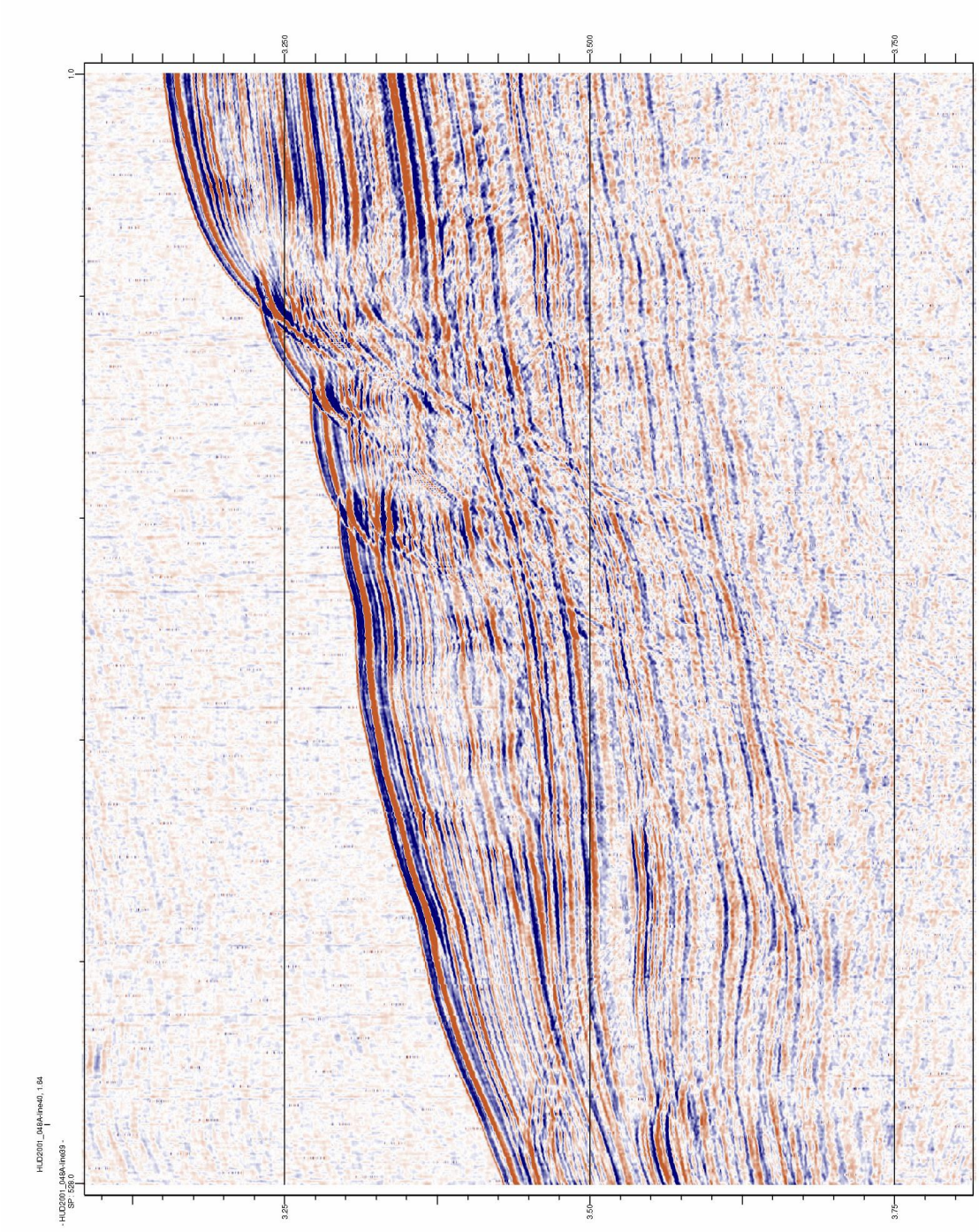

Figure B12: Seismic line HUD2001_048A line 39.

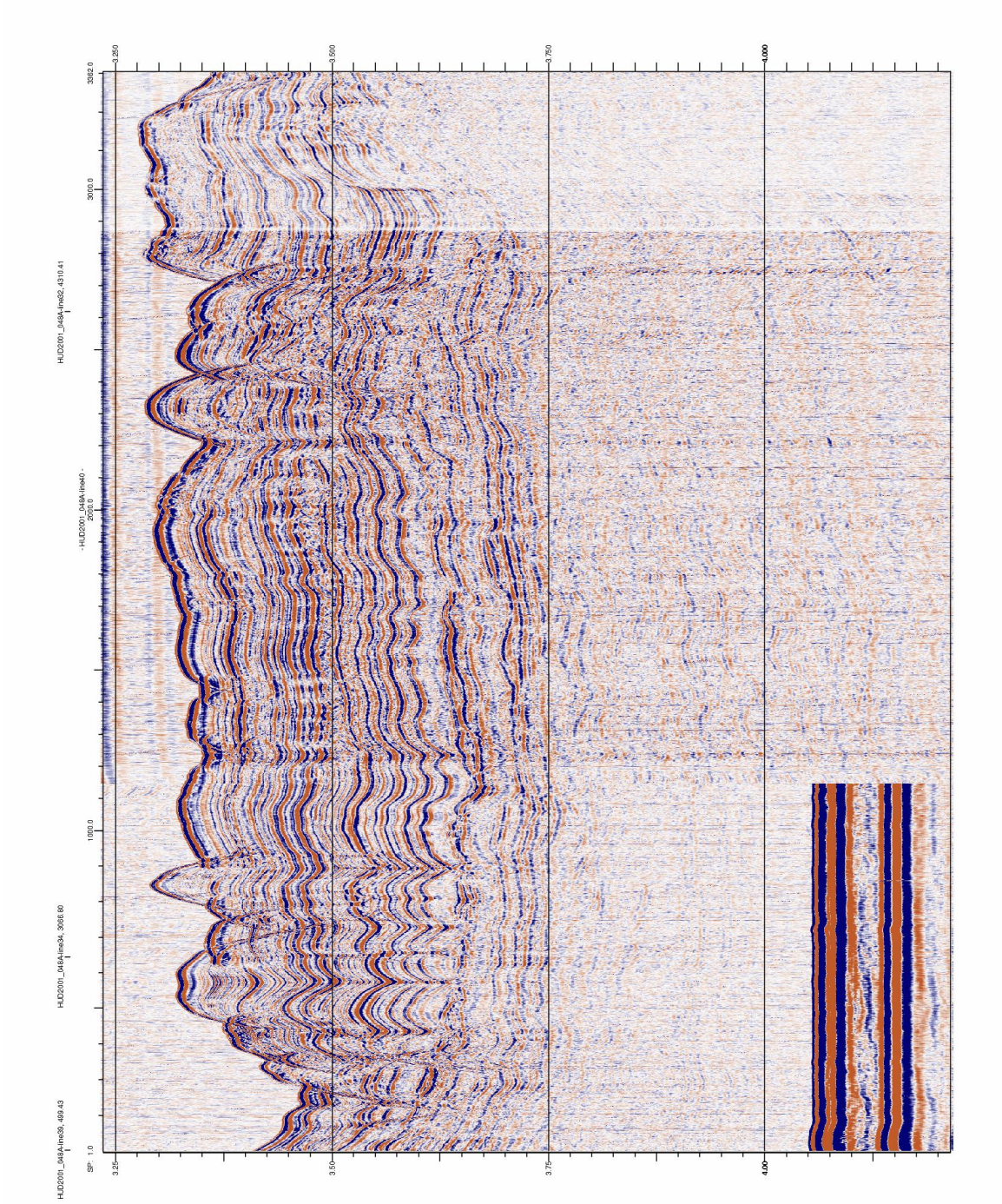

Figure B13: Seismic line HUD2001_048A line 40.